Zeitschrift: IABSE reports of the working commissions = Rapports des commissions de travail AIPC = IVBH Berichte der Arbeitskommissionen

Band: 29 (1979)

Rubrik: Session III: Slabs

SESSION III

Slabs

Dalles

Platten

Chairman: Prof. Ch. Massonnet, Belgium

Introductory Lectures: „The Theory of Plasticity for Reinforced Concrete Slabs"
Prof. M.P. Nielsen, Denmark

„Punching Shear in Concrete Slabs"
M.W. Braestrup, Denmark

(The Introductory Lectures are published in the Introductory Report, Volume AK 28)

Leere Seite
Blank page
Page vide

III

Complete Limit Analysis Solutions and Yield Line Theory

La solution exacte de l'analyse limite et la théorie des lignes de rupture

Vollständige Lösungen nach Traglastverfahren und Fliessgelenklinientheorie

J. SOKOL-SUPEL
Research Associate
Polish Academy of Sciences
Warsaw, Poland

A. SAWCZUK
Professor of Structural Mechanics
Polish Academy of Sciences
Warsaw, Poland

SUMMARY
Yield line theory solutions for a circular plate subjected to point loads are compared with the exact solutions obtained by integration of the plastic plate equations for parabolic stress regimes. Differences between the approaches are discussed.

RESUME
Des solutions obtenues selon la théorie des lignes de rupture pour une plaque circulaire soumise aux forces concentrées sont comparées avec la solution exacte provenant de l'intégration des équations des plaques plastiques en régime parabolique. Les différences entre ces deux méthodes sont présentées.

ZUSAMMENFASSUNG
Fliessgelenklinienlösungen für eine Kreisplatte unter Einzellasten werden mit den vollständigen Lösungen verglichen, welche durch Integration der für parabolische Spannungsfelder plastischer Platten geltender Gleichungen erhalten werden. Unterschiede zwischen den beiden Betrachtungsweisen werden erörtert.

1. INTRODUCTION

For plates obeying the Johansen yield criterion the complete limit analysis solutions are available in several cases, [1]. This criterion is usually employed in the yield line theory to obtain an upper bound to the collapse load since the respective calculations concern solely the mechanism of motion under the limit load, [2].

We intend to show on a simple example similarities and differences between the yield line theory solutions and those which give for the Johansen criterion the full information about the collapse load, the collapse mode, and the stress field at collapse, [4], [5].

For the maximum principal moment yield criterion the complete solutions can be obtained for various cases of loading of simply supported plates. A perfectly plastic plate whenever it goes plastic, is totally or partially in the parabolic, isotropic or hyperbolic stress regime or its stress field remains below the yield point, whenever the respective part of the plate remains rigid [4]. The type of stress regime depends on the equation of the yield surface [5], [6].

Stress discontinuities may occur across the line separating different stress regimes, [4], [5], [7]. Discontinuities of the tangent to the deflected surface are admitted by the maximum principal moment yield criterion. This property is used in the yield line theory to generate collapse mechanisms with hinge lines, [2], [8], [9].

The complete solution of a limit analysis problem for a plate consists in finding the collapse load intensity and the associated field of moments and shear forces satisfying
- the internal equilibrium requirements and the prescribed stress boundary conditions
- not violating the yield condition

The complete solution also contains
- the displacement velocity field specifying a kinematically admissible collapse mechanism associated with positive energy dissipation at the plate collapse, [4].

Complete solutions may differ from the results obtained employing the yield line theory both in the collapse load multiplier and in the yield pattern because of the difference in the set of equations used. A yield line solution does not specify the stress field in the plate at collapse as it disregards the differential equations of equilibrium, which are taken into account in any complete solution. It is known that the yield line theory gives upper bounds to the collapse load. In the yield line theory any collapse mode consists of developable surfaces which, in fact, correspond to parabolic stress regimes of the method giving complete solutions, [3], [4].

A circular simply supported plate subjected to two point loads furnishes the case when the yield line theory results differ in comparison with the complete solution.

2. GENERALITIES

We consider a perfectly plastic plate, isotropic both in "positive" and "negative" bending, with the yield moments M_o and M'_o respect-

ively. We shall refer the field variables either to the cartesian or to the polar coordinate systems.

The comparison of the exact and yield line solutions will be made for a simply supported plate, Fig. 1a. The point loads Q_1 and Q_2 are applied at the equal distances A from the plate center. The following dimensionless quantities will be used.

$$\varrho = \frac{r}{R}, \quad a = \frac{A}{R}, \quad \Lambda = \frac{M_o}{M_o}, \quad w = \frac{W}{R}, \tag{2.1}$$

$$m_i = \frac{M_i}{M_o}, \quad t_i = \frac{T_i R}{M_o}, \quad i = x, y, xy, r, \theta, r\theta \tag{2.2}$$

$$q_1 = \frac{Q_1}{M_o}, \quad q_2 = \frac{Q_2}{M_o}, \quad \alpha = \frac{q_2}{q_1}, \quad 0 \leqslant \alpha \leqslant 1 \tag{2.3}$$

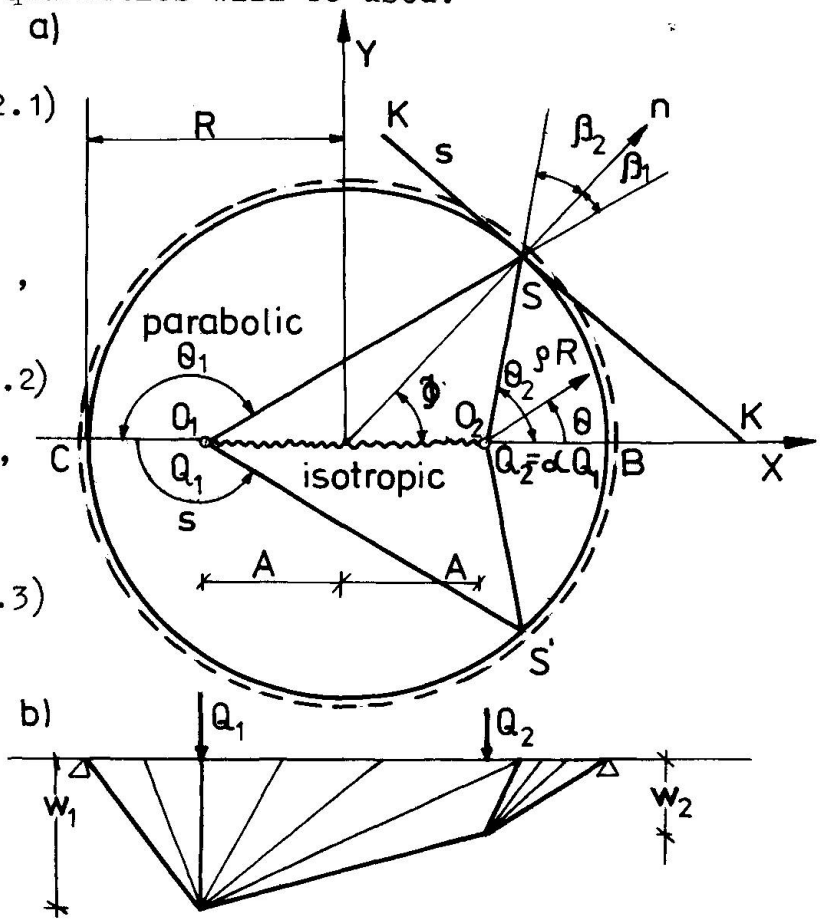

Fig. 1

where W, M_i, T_i denote the deflection velocity, the bending moments and the shear forces respectively whereas R stands for the reference length which equals to the plate radius.

Moreover,

$$q = (1 + \alpha)\, q_1 \tag{2.4}$$

denotes the dimensionless total collapse load of the plate. The q_+, q_{1+}, q_{2+} will stand for dimensionless limit loads corresponding to yield line theory solutions. The ratio of the deflection velocities of the points of load application, Fig. 1b, is $\beta = w_2/w_1$.

The maximum principal moment yield condition of the Johansen criterion represents a square yield locus in the plane of principal bending moments

$$\frac{m_2 - m_1}{2} \pm \frac{m_1 + m_2}{2} \mp 1 = 0, \quad \frac{m_2 - m_1}{2} \pm \frac{m_1 + m_2}{2} \pm \Lambda = 0 \tag{2.5}$$

or a pair of intersecting cones in the moment space m_x, m_y, m_{xy}.

3. COMPLETE SOLUTION

The complete solution of the considered plate under the criterion (2.5) consists of the parabolic zones $SCS'O_1$ and $S'BSO_2$ joined by the isotropic regime $SO_1S'O_2$. In the isotropic zone the dimensionless stress field is

$$m_x = m_y = m_r = m_\theta = 1, \quad t_x = t_y = t_r = t_\theta = 0 \tag{3.1}$$

Thus any direction is principal and the zone caries no transverse loading. The velocity field is arbitrary and is subjected to the condition that the Gaussian curvature of the deflected surface is non-negative there [3], [4].

In the parabolic zones $SCS'O_1$ and $S'BSO_2$ the bending moments and the shear forces expressed in the polar coordinates with origin each time at the point of loading, Fig. 1a, are respectively

$$m_\theta = 1, \quad m_r = -\frac{a^2\sin^2\theta}{1-a^2\sin^2\theta}, \quad t = 0, \quad t_r = -\frac{1}{\rho}\frac{1}{1-a^2\sin^2\theta} \tag{3.2}$$

The velocity of deflection in a parabolic zone is bounded by a developable surface, [4]. For the point loading considered two conical surfaces $SCS'O_1$ and $S'BSO_2$ are obtained. The vertices of the cones are at the points of the load application, Fig. 1b.

Along the lines O_1S, O_2S, and symmetrically, discontinuities in the radial moment appear, as it can be seen when comparing the results (3.1) and (3.2). Between the parabolic and the isotropic regimes on the lines SO_1 and SO_2 in Fig. 1a, there is a continuous transition of the circumferential derivative of the deflection velocity. The triangular part AO_1O_2 of the isotropic range rotates with respect to the axis K-K, Fig. 1a, which is tangent to the plate boundary at S. Geometrical considerations lead to the conclusion that the flat element O_1SO_2 is tangent to the sectors of cones SO_1S' and SO_2S'. The points of load application have the vertical velocities related as follows

$$\beta = \frac{w_2}{w_1} = \frac{1 - a\cos\phi}{1 + a\cos\phi} \tag{3.3}$$

The collapse loads are calculated considering the shear force along a circumferential trajectory [4], [7].

$$q_1 = 2\int_0^S (-t)\,ds = 2\int_0^{\gamma} (-t)\rho\,d\theta \tag{3.4}$$

and the results are respectively

$$q_1 = \frac{2}{\sqrt{1-a^2}}\left[\pi - \arctan\sqrt{1-a^2}\,\frac{\sin\phi}{a+\cos\phi}\right] \tag{3.5}$$

$\gamma = 0$ if $\phi \leqslant \arccos a$ $\quad \gamma = \pi$ if $\phi > \arccos a$

$$q_2 = \frac{2}{\sqrt{1-a^2}}\left[\gamma - \arctan\sqrt{1-a^2}\,\frac{\sin\phi}{a+\cos\phi}\right] \tag{3.6}$$

The obtained parabolic solutions are valid for the following positions of the load application points

$$0 \leqslant a \leqslant k\sqrt{\frac{\Lambda}{1+\Lambda}} \tag{3.7}$$

where $k = \sec\theta_i$, $\theta_i < \pi/2$, $k = 1$, $\theta_i > \pi/2$, $i = 1,2$. The angle specifying the meeting point S of the parabolic regimes is given by the equation

$$\alpha = \frac{\gamma - \arctan\left(\sqrt{1-a^2}\cdot\frac{\sin\phi}{a-\cos\phi}\right)}{\pi - \arctan\left(\sqrt{1-a^2}\cdot\frac{\sin\phi}{a+\cos\phi}\right)} \tag{3.8}$$

In Fig. 2 this angle is specified in terms of the ratio of the loads applied. This allows to derive the shape of the central isotropic zone for the given α and the load application point a.

The deflection rates at the points of loading are not equal if the loads are not equal, $\alpha \neq 1$. The shape of the deflected surface is indicated in Fig. 1b. It is seen that for the load ratio $\alpha = 1$ is for any position of the loading $\beta = 1$.

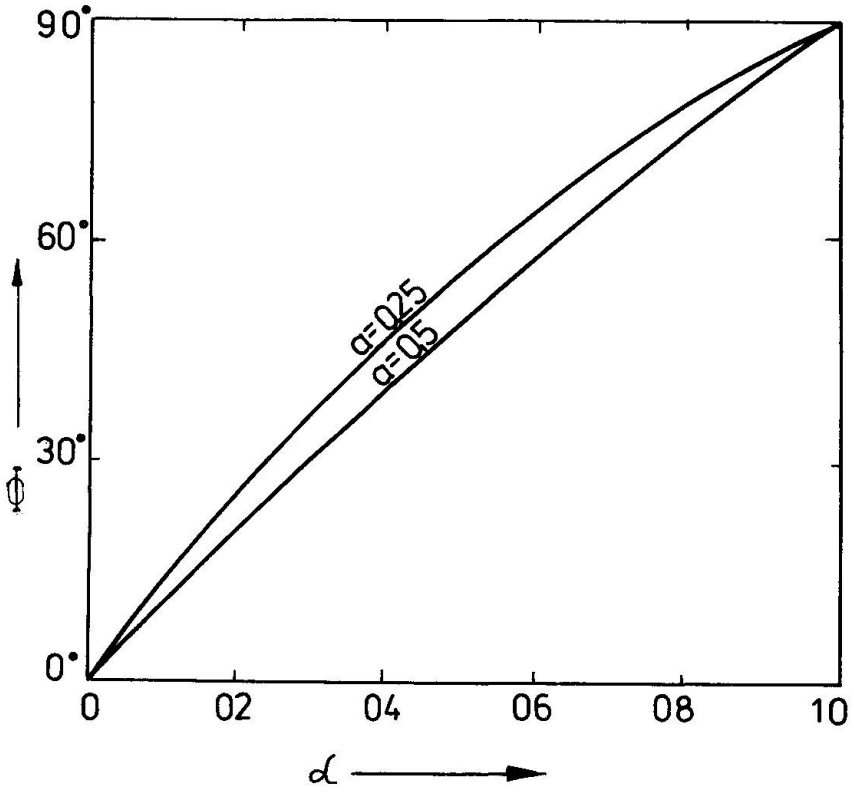

Fig. 2

At the point S a concentrated reaction appears, namely

$$V = \tan\beta_1 + \tan\beta_2 = \frac{2a\sin\phi}{1 - a^2\cos^2\phi} \tag{3.9}$$

and the reaction on the boundary is $t = t_n + \partial m_{ns}/\partial s$ where m_{ns} denotes the twisting moment appearing along the simply supported edge.

4. YIELD LINE SOLUTION

To this end a kinematically admissible deformation mode is assumed

first. For the considered plate and the loading the deflected surface consists of conical elements Fig. 3. The zones SO_1S and $S'O_2S'$ are sectors of cones with the vertices at the points of load application. The zone SKS corresponds to a cone with the vertex on the plate boundary. There is a ridge O_1O_2 on the deflected surface, consisting of intersection of the cone SKS with the symmetric one.

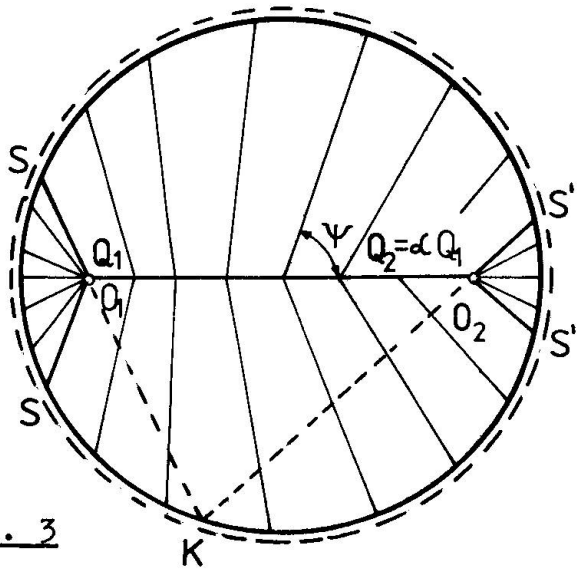

Fig. 3

In the yield line theory, when a continuous field of yield lines is considered, the dissipations due to the internal forces is expressed as follows

$$D = M_o w_o \int_A \varkappa_\theta \, dA = M_o w_o \left\{ \int_{\theta_1}^{\theta_2} \left[1 + \left(\frac{\varrho'}{\varrho} \right)^2 \right] d\theta - \left[\frac{\varrho'}{\varrho} \right]_{\theta_1}^{\theta_2} \right\} \tag{4.1}$$

or

$$D = M_o w_o \left\{ \int_{\theta_1}^{\theta_2} \left[1 + \left(\frac{z'}{z} \right)^2 \right] d\theta - \left[\left(1 - \frac{z_1}{z} \right) \frac{z}{z} \right]_{\theta_1}^{\theta_2} \right. \tag{4.2}$$

respectively to the situations shown in Figs 4a and 4 b. The results concern the collapse mechanism of Fig. 3. The solution (4.1) concerns the cones with vertices at O_1 and O_2, whereas (4.2), [10], gives the dissipations on the collapse mode in the form of a conical surface with its vertex on the plate boundary as shown in Fig.3.

For a given ratio of the loads a bound to the load carrying capacity is

$$q_+ = \min \frac{2(1+\alpha)}{\sqrt{1-a^2}(C+\alpha D)} \left\{ C\left(\Omega + \arctan \frac{\sqrt{1-a^2}\sin\psi}{a-\cos\psi} \right) + \right.$$

$$\left. + D\left(\arctan \frac{\sqrt{1-a^2}\sin\psi}{a+\cos\psi} \right) + \frac{4a\sin\psi}{\sqrt{1-a^2}} \right\}, \quad 0 \leqslant \alpha \leqslant 1 \tag{4.3}$$

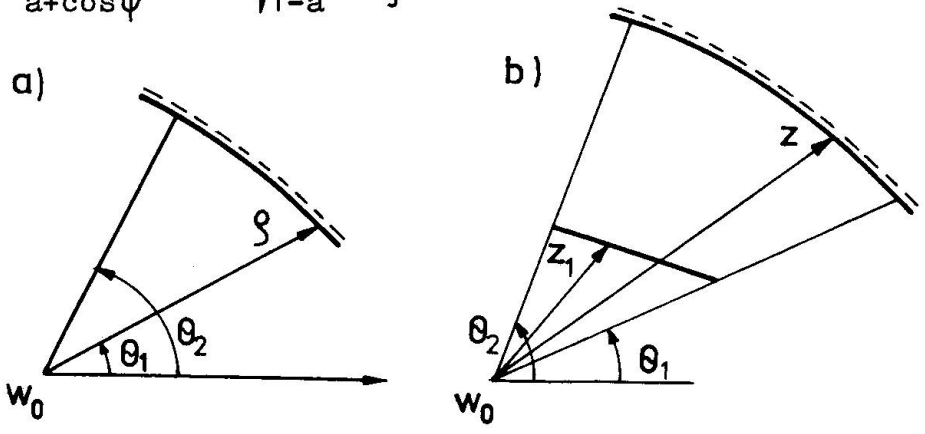

Fig. 4

where $C = 1 + a\cos\psi$, $D = 1 - a\cos\psi$
and $\Omega = 0$ if $\arccos a < \psi \leqslant \pi/2$, $\Omega = \pi$ if $\psi < \arccos a$

Another collapse mode consisting of conical parts SO_1S and $S'O_2S'$ joined by the cylindrical surfaces can be conceived. The vertices of the cones SKS' are at the infinity, [10]. The respective results are in [11].

In Fig. 5 the collapse load intensities are shown for the considered collapse mode as well as the exact result.

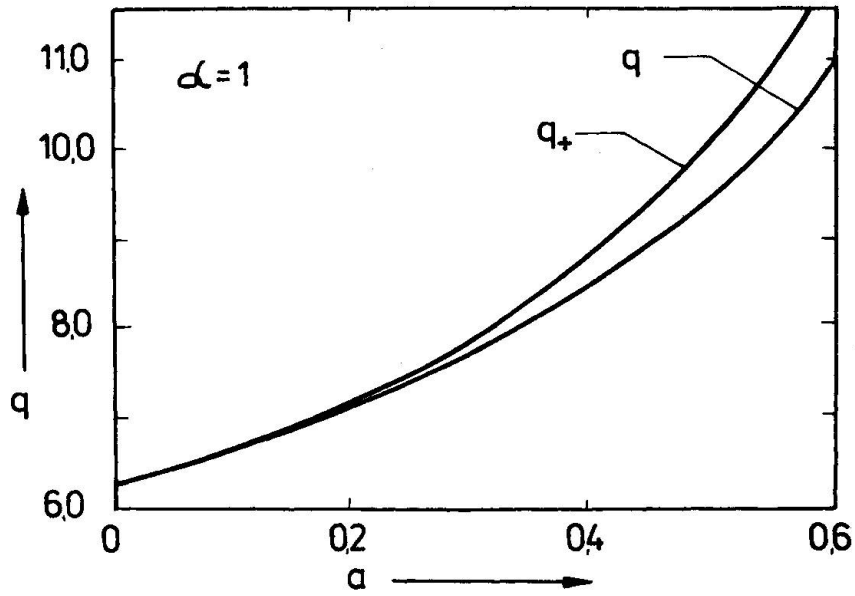

Fig. 5

5. COMPARISONS

Comparing the complete solution with the considered kinematical solutions one can conclude that for the load ratio $0 < \alpha < 0.5$ the differences between the solutions is of order of few per cent only. The largest admissible excentricity for the studied complete solution involving parabolic and isotropic regimes is for $\alpha = 1$, Fig. 6. The results are given in the table. The considered kinematically admissible collapse modes of the yield line theory and the velocity field corresponding to the exact limit analysis solution of a rigid-perfectly plastic plate are compared in Fig. 7 at $\alpha = 1$ for the load excentricity $a = 0.5$.

The analysis of complete and kinematically admissible solutions of the considered plate problem suggests that experiments should be made regarding the existence of an isotropic zone as well as to its extent, and regarding the data concerning the limit load and the largest differences should appear for the load excentricity $a = 0.7$, close to the limiting case of applicability of the parabolic-isotropic solution. For $\alpha > \sqrt{\Lambda}/(1+\Lambda)$ a hyperbolic zone must appear and the exact solution is not known. In the considered case of "layered isotropy", $\Lambda = 1$, the hyperbolic zone appears for $a > 0.707$.

The exact solution allows to assess the reaction distribution along the support. A concentrated force V appears at the point S, where two parabolic zones meet the isotropic region.

Load carrying capacity q at $\alpha = 1$

a	exact	yield line theory
0	6.283	6.283
0.5	9.674	10.170
0.7	13.141	14.760

Acknowledgement. The work is related to the joint research task on application of the mechanics of plastic structures in engineering

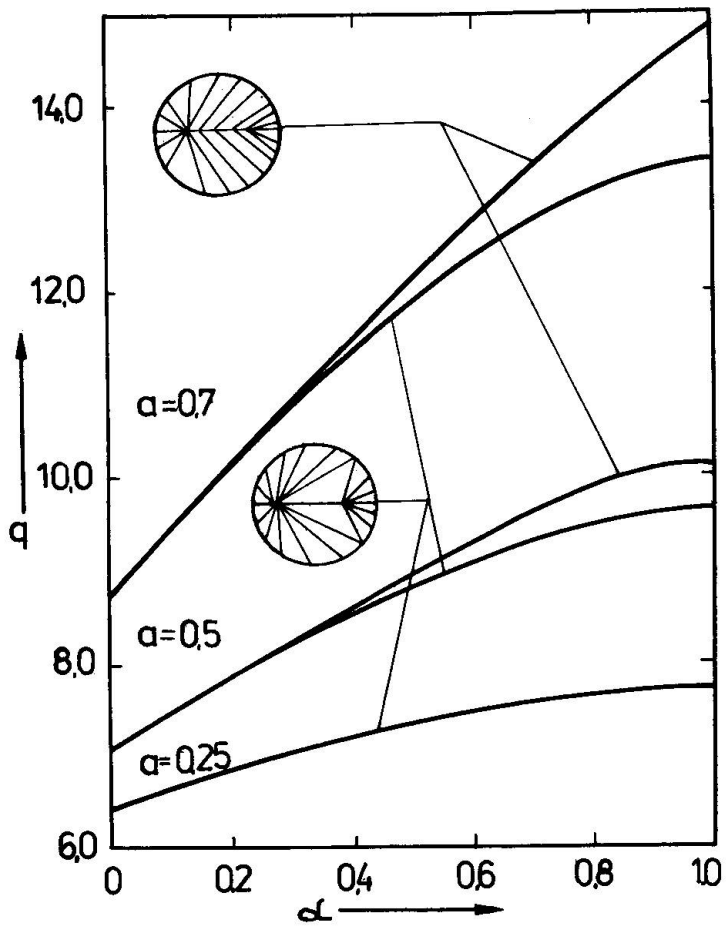

Fig. 6

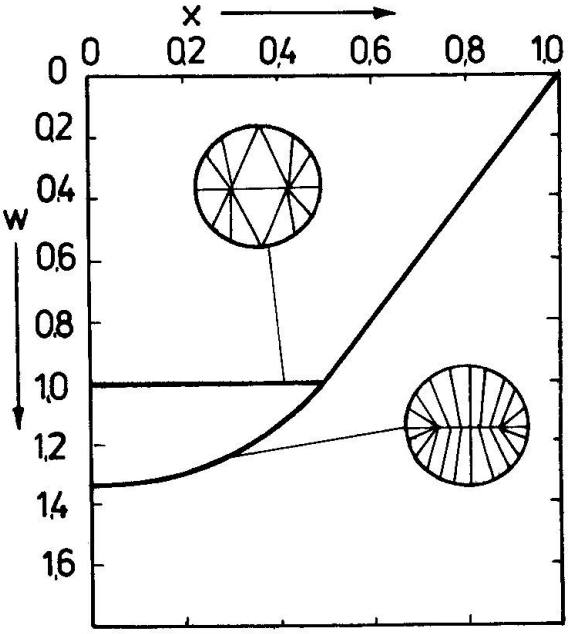

Fig. 7

practice and operating between the Faculte Polytechnique de Mons and the Institute of Fundamental Technological Research, Warsaw.

REFERENCES

[1]. NIELSEN,M.P. The theory of plasticity for reinforced concrete slabs, "Plasticity in Reinforced Concrete" /Copenhagen 1979/, Introductory Report, IABSE, Zürich 1978, pp. 93-114
[2]. JOHANSEN,K.W. Yield-line Theory, cement and concrete, London1962
[3]. SAWCZUK,A. Introduction a la flexion plastique des plaques "Elasticite et Plasticite" Eyrolles, Paris, 1979 /in press/
[4]. SAWCZUK, A., HODGE,P.G.Jr. Limit analysis and yield line theory, J.Appl.Mech. 35, 1968
[5]. SAWCZUK,A. Contribution a l'analyse limite des plaques "Problemes de Rheologie et des Mecanique des Sols", PWN, Warsaw 1977
[6]. MASSONNET,Ch. Complete solutions describing the limit state of reinforced concrete slabs, Mag.Concr.Res. 19, 58, 1967
[7]. SAWCZUK,A., SOKOŁ-SUPEL,J. Bending of plates obeying maximum principal moment yield criterion, Bull.Acad.Pol.Sci.Ser.Sci.Tech. 23, 1975
[8]. SAVE,M.A. A consistent limit-analysis theory for reinforced concrete slabs, Mag.Concr.Res., 19, 58, 1967
[9]. SAVE,M.A., MASSONNET,C.E. Plastic Analysis and Design of Plates, Shells and Disks, North-Holland, Amsterdam 1972
[10]. JANAS,M. Kinematical compatibility problems in yield line theory, Mag.Concr.Res. 19, 58, 1967
[11]. SOKOŁ-SUPEL,J., SAWCZUK,A. Comparison of the complete limit analysis and yield line theory solutions for plates. An outline of experimental studies. IPPT Reports 8, 1979

III

Circular Slabs with Limited Plastic Flow Capacity

Dalles circulaires à capacité d'écoulement plastique limitée

Kreisplatten mit begrenzter plastischer Verformbarkeit

K. SONODA
Professor of Civil Engineering
Osaka City University
Osaka, Japan

SUMMARY
A method of elasto-plastic analysis for reinforced concrete circular slabs with a limited plastic rotation capacity is presented. The procedure used is numerical, but analytical elastic solutions already known are utilized as much as possible here. Examples show the relationships between ultimate bending strengths and plastic flow abilities for such slabs.

RESUME
Une méthode d'analyse élasto-plastique est présentée pour des dalles circulaires en béton armé et à capacité de rotation plastique limitée. Il s'agit d'une méthode numérique, mais des solutions analytiques connues pour des plaques élastiques sont utilisées autant que possible. Les relations entre la résistance ultime à la flexion et la capacité de rotation plastique sont illustrées par quelques exemples.

ZUSAMMENFASSUNG
Eine Methode zur elastisch-plastischen Berechnung von Kreisplatten aus Stahlbeton mit einer begrenzten plastischen Rotationsfähigkeit wird dargestellt. Das verwendete Verfahren ist numerisch, doch wird soweit wie möglich auf bekannte analytische Lösungen für elastische Platten zurückgegriffen. Mit Beispielen werden die Beziehungen zwischen den Biegebruchlasten und der plastischen Verformbarkeit solcher Platten erläutert.

1. INTRODUCTION

The classical plastic design method has been developed on the assumption that a structural material or element consists of a perfectly plastic substance which can flow plastically under a constant yield stress until a whole or a part of structure becomes unstable by forming a collapse mechanism. The plastic flow capacity of a concrete being a significant structural material, however, is not unlimited. It is well known that the stress-strain curve of a concrete undergoing a uniaxial compression rises to a strain of about 0.25% and afterward falls gradually to a strain of about 0.35% when a crushing failure occurs. Then, the maximum plastic strain can not be anticipated to exceed 0.3% in uniaxial compression.

On the other hand, the plastic rotation capacity of a reinforced concrete beam is predominated by the plastic extension of the reinforcing steel bars when its reinforcement is very small but by the plastic contraction of the concrete when the reinforcement is rather large. Hence, the plastic rotation capacity becomes smaller as a reinforcing steel ratio becomes larger.

A similar circumstance is naturally supposed to exist in a reinforced concrete slab. This paper is intended to investigate on the effect of the limited plastic flow capacity on the ultimate load carrying capacity for a reinforced concrete circular slab. The rectangular yield curve in the bending moment plane is used here as the initial plastic flow condition of the slab-section, and the subsequent yield curves in an unstable plastic region after a considerable plastic flow are determined according to a piecewise linear strain softening theory. The stress-rate *versus* strain-rate relations in both stable and unstable plastic regions are derived by using the associated flow rule of the plasticity, and consequently the fundamental differential equation concerning load-rate and deflection-rate is obtained.

On the other hand, this paper also presents a new method for the numerical solution of the fundamental differential equation, which is different from the well-known finite element method and finite difference one. The method is developed under the idea that the effect of plastic flow can be replaced with an addition of the self-equilibrating virtual loads resulting from the deviatoric part from the moment distribution given by the linear elastic solution, and the elasto-plastic solution, therefore, can be given by the superposition of the elastic solutions for both the actual and the virtual load distributions.

2. DEFLECTION-RATE EQUATION

A circular slab subjected to axially symmetric loads is dealt with here. Idealizing the moment-curvature relation of the slab section, the curve including linear elastic, perfectly plastic and strain softening parts will be obtained as Fig. 1. Assuming a rectangular yield curve which is based upon the shear fracture of concrete by the Mohr-Coulomb's theory and the tensile plastic flow of steel bars and, using the normality law on plastic strain-rates postulated by A.C.Palmer *et al.* [1], the loading surfaces after a plastic flow are supposed as Fig. 2. Namely, when yielding at the line A B, the yield surface diminishes to A'B', A"B", ·····, and when yielding at the line A C, to E'C', E"C", ·····, and when yielding at the corner A, to D', D", ·····. Hence, the expression of the loading function can be written as

$$\max \left[\, | M_r | - M_{or}(e_r) \, , \, | M_\theta | - M_{o\theta}(e_\theta) \, \right] = 0 \qquad (1)$$

where M_r, M_θ, $M_{or}(e_r)$, and $M_{o\theta}(e_\theta)$ are radial and circumferential moments and those bending strengths in the polar coordinates (r, θ), respectively and e_r and e_θ are parameters representing plastic curvatures. The Hooke's law and the associated flow rule of the plasticity give the following relations of moment-rates and curvature-rates :

$$\begin{Bmatrix} \dot{M}_r \\ \dot{M}_\theta \end{Bmatrix} = D \begin{bmatrix} 1 & \nu \\ \nu & 1 \end{bmatrix} \begin{Bmatrix} \dot{\kappa}_r - d\mu_r \cdot \partial F_r / \partial M_r \\ \dot{\kappa}_\theta - d\mu_\theta \cdot \partial F_\theta / \partial M_\theta \end{Bmatrix} \tag{2}$$

where ν = Poisson's ratio, D = flexural rigidity, $\dot{\kappa}_r$, $\dot{\kappa}_\theta$ = curvature-rates, and $d\mu_r$, $d\mu_\theta$ = plastic flow coefficients ; and

$$F_r = | M_r | - M_{or}(e_r) \ , \quad F_\theta = | M_\theta | - M_{o\theta}(e_\theta) \ ,$$

$$M_{or}(e_r) = \bar{M}_{or} - \beta_r D e_r \ , \quad M_{o\theta}(e_\theta) = \bar{M}_{o\theta} - \beta_\theta D e_\theta \ ,$$

$$e_r = \int_0^t d\mu_r \ , \quad e_\theta = \int_0^t d\mu_\theta \ ,$$

where β_r, β_θ = strain softening rates which may be related to the coefficient $\bar{\beta}/(1-\bar{\beta})$ indicated in Fig. 1. The plastic flow coefficients are expressed as follows :

for the corners A, D', D", ····· ;

$$\begin{Bmatrix} d\mu_r \\ d\mu_\theta \end{Bmatrix} = \frac{1}{(1-\beta_r)(1-\beta_\theta) - \nu^2} \begin{bmatrix} 1-\beta_\theta-\nu^2 & -\nu\beta_\theta \\ -\nu\beta_r & 1-\beta_r-\nu^2 \end{bmatrix} \begin{Bmatrix} \dot{\kappa}_r \\ \dot{\kappa}_\theta \end{Bmatrix} ; \tag{3}$$

for the lines A B, A'B', A"B", ····· ;

$$F_\theta = 0, \quad d\mu_\theta = (\dot{\kappa}_\theta + \nu\dot{\kappa}_r)/(1-\beta_\theta), \quad d\mu_r = 0 \ ; \tag{4}$$

for the lines A C, E'C', E"C", ····· ;

$$F_r = 0, \quad d\mu_r = (\dot{\kappa}_r + \nu\dot{\kappa}_\theta)/(1-\beta_r), \quad d\mu_\theta = 0 \ ; \tag{5}$$

and the expressions for the other lines and corners will easily be obtained by exchanging appropriately the signs of the coefficients in the above expressions. Eqs. (3), (4), (5) and others will be represented for simplification as

$$\begin{aligned} d\mu_r &= \phi_{11}\dot{\kappa}_r + \phi_{12}\dot{\kappa}_\theta \\ d\mu_\theta &= \phi_{21}\dot{\kappa}_r + \phi_{22}\dot{\kappa}_\theta \end{aligned} \tag{6}$$

Using the relation between curvature-rates and deflection-rate in an axially symmetric bending, namely

$$\begin{aligned} \dot{\kappa}_r &= -\partial^2\dot{w}/\partial r^2 \\ \dot{\kappa}_\theta &= -\partial\dot{w}/r\partial r \end{aligned} \tag{7}$$

and substituting Eq. (2) into the following equilibrium equation :

$$\frac{\partial^2 \dot{M}_r}{\partial r^2} + \frac{1}{r}\frac{\partial}{\partial r}(2\dot{M}_r - \dot{M}_\theta) = -\dot{p}(r) \tag{8}$$

where $\dot{p}(r)$ = a load-rate distribution, the fundamental differential equation about deflection-rate can be derived as follows :

$$D\left(\frac{\partial^2}{\partial r^2} + \frac{1}{r}\frac{\partial}{\partial r}\right)^2 \dot{w} = \dot{p}(r) + \frac{\partial^2}{\partial r^2}\dot{X}_1 + \frac{1}{r}\frac{\partial}{\partial r}\dot{X}_2 \tag{9}$$

where

$$\left.\begin{aligned} \frac{\dot{X}_1}{D} &= (\phi_{11}\phi_a + \nu\phi_{21}\phi_b)\frac{\partial^2 \dot{w}}{\partial r^2} + (\phi_{12}\phi_a + \nu\phi_{22}\phi_b)\frac{1}{r}\frac{\partial \dot{w}}{\partial r} \\ \frac{\dot{X}_2}{D} &= \left[(2-\nu)\phi_{11}\phi_a + (2\nu-1)\phi_{21}\phi_b\right]\frac{\partial^2 \dot{w}}{\partial r^2} + \\ &\quad + \left[(2-\nu)\phi_{12}\phi_a + (2\nu-1)\phi_{22}\phi_b\right]\frac{1}{r}\frac{\partial \dot{w}}{\partial r} \end{aligned}\right\} \tag{10}$$

in which $\phi_a = \partial F_r/\partial M_r$ and $\phi_b = \partial F_\theta/\partial M_\theta$.

The second and the third terms in the right side of Eq. (9) mean the addition of the self-equilibrating virtual load-rate distributions resulting from a deviatoric part from a linear elastic moment distribution, namely the moment redistributions due to plastic flow.

3. METHOD OF SOLUTION

The differential operator of the left side in Eq. (9) is the same as an elastic problem, and the unknown moment-rate redistributions ($\dot{X}_1$, $\dot{X}_2$) in a plastic region, therefore, are determined by the solution of the following simultaneous integro-differential equation :

$$\left[(\phi_{11}\phi_a + \nu\phi_{21}\phi_b)\frac{\partial^2}{\partial r^2} + (\phi_{12}\phi_a + \nu\phi_{22}\phi_b)\frac{1}{r}\frac{\partial}{\partial r}\right] \times$$
$$\times \left[\dot{p}w_o + \int_{R_p}\frac{\partial^2}{\partial \xi^2}\dot{X}_1\bar{w}(r,\xi)d\xi + \int_{R_p}\frac{1}{\xi}\frac{\partial}{\partial \xi}\dot{X}_2\bar{w}(r,\xi)d\xi\right] = \frac{\dot{X}_1}{D} \tag{11}$$

$$\left\{\left[(2-\nu)\phi_{11}\phi_a + (2\nu-1)\phi_{21}\phi_b\right]\frac{\partial^2}{\partial r^2} + \right.$$
$$\left. + \left[(2-\nu)\phi_{12}\phi_a + (2\nu-1)\phi_{22}\phi_b\right]\frac{1}{r}\frac{\partial}{\partial r}\right\} \times$$
$$\times \left[\dot{p}w_o + \int_{R_p}\frac{\partial^2}{\partial \xi^2}\dot{X}_1\bar{w}(r,\xi)d\xi + \int_{R_p}\frac{1}{\xi}\frac{\partial}{\partial \xi}\dot{X}_2\bar{w}(r,\xi)d\xi\right] = \frac{\dot{X}_2}{D} \tag{12}$$

where $\dot{p}$ = an actual load-rate intensity, w_o = the elastic solution for the actual load-rate distribution with the unit intensity, $\bar{w}(r,\xi)$ = the elastic solution for a circular line load with the unit intensity at the position r = ξ within a plastic region, and R_p = the plastic region.

Now consider a method of numerical solution for Eqs. (11) and (12). Dividing the radial region of a circular slab by a net of sufficiently fine meshes and considering the case when only the part of one mesh becomes of plasticity, the distributions of the $\dot{X}_1$ and $\dot{X}_2$ within the mesh may be assumed to consist of the continuous three parabolic curves as shown in Fig. 3, because equilibrium conditions require that both the moment redistributions and their first derivatives related to shearing forces must be continuous within a whole plastic region and at an elastic-plastic boundary. Thus the virtual load-rate distributions being equivalent to these moment-rate redistributions are given from Eq. (9) as Fig. 3, which are naturally self-equilibrating. When a region including a number of meshes is plasticized, therefore, the deflection-rate of the slab is obtained by the superposition of the elastic solutions for both the actual load-rate distributions and the virtual load-rate ones mentioned above. Namely,

$$\left.\begin{aligned}
\dot{w} &= \dot{p}w_o + \sum_i \dot{Z}_{1i}\bar{w}_{1i} + \sum_i \dot{Z}_{2i}\bar{w}_{2i} \\
\dot{\kappa}_r &= -\frac{\partial^2 \dot{w}}{\partial r^2} = -\dot{p}\frac{\partial^2 w_o}{\partial r^2} - \sum_i \dot{Z}_{1i}\frac{\partial^2 \bar{w}_{1i}}{\partial r^2} - \sum_i \dot{Z}_{2i}\frac{\partial^2 \bar{w}_{2i}}{\partial r^2} \\
\dot{\kappa}_\theta &= -\frac{1}{r}\frac{\partial \dot{w}}{\partial r} = -\frac{\dot{p}}{r}\frac{\partial w_o}{\partial r} - \sum_i \dot{Z}_{1i}\frac{1}{r_i}\frac{\partial \bar{w}_{1i}}{\partial r} - \sum_i \dot{Z}_{2i}\frac{1}{r_i}\frac{\partial \bar{w}_{2i}}{\partial r}
\end{aligned}\right\} \qquad (13)$$

where $\bar{w}_{1i}$ and $\bar{w}_{2i}$ represent the elastic deflections due to the virtual load-rate distributions with the unit intensity, $\dot{Z}_{1i} = 1$ and $\dot{Z}_{2i} = 1$, at the mesh point, i, which will easily be obtained by the integration of the solution for a circular line load given by the well-known literatures, e.g., Timoshenko's book [2], and the summation is executed over all meshes in plastic regions. Substituting the rate-equation (13) into Eq. (10) and using the relations, $\dot{Z}_{1i} = 4\dot{X}_1/\Delta r^2$ and $\dot{Z}_{2i} = 4\dot{X}_2/[\Delta r(2r_i - \Delta r)]$, shown in Fig. 3, a simultaneous equation about the unknowns, $\dot{Z}_{1i}$, $\dot{Z}_{2i}$, $i = 1,2,\cdots\cdots$, are obtained, and the substitution of its solution into Eq. (13) consequently determines the deflection-rate and the curvature-rates resulting from the actual load-rate, $\dot{p}$. Finally, the total deflection, the total curvatures, and the total moments are obtained from the integration of Eqs. (13) and (2) by making use of the forward difference method of sufficiently short intervals about load increment or central deflection-increment, which may be familiar in the elasto-plastic numerical analysis for a solid [3].

4. RELATIONSHIP BETWEEN PLASTIC FLOW CAPACITIES AND ULTIMATE BENDING STRENGTHS

Numerical calculations for the load *versus* central deflection curves for circular slabs subjected to partially or entirely uniform loads are carried out by setting the following material constants :

yield stress of steel, $f_s = 275$ N/mm^2; compressive strength of concrete, $f_c = 27.5$ N/mm^2; secant modulus of elasticity of concrete, $E_c = 1.4 \times 10^4$ N/mm^2; reinforcing steel ratio, $p = 0.008$; $\nu = 1/6$; $d/a = 0.1$, d = effective depth, a = radius; strain softening rates, $\beta_r = \beta_\theta = \bar{\beta}/(1-\bar{\beta})$; $D = E_c d^3/12(1-\nu^2)$; $\bar{M}_{or}/E_c d^2 = \bar{M}_{o\theta}/E_c d^2 = \bar{M}_o/E_c d^2 = 1.5 \times 10^{-4}$(isotropic

reinforcements); and $\bar{M}_o = f_s d^2 p \cdot (1 - 3p \cdot f_s / 4f_c)$;

and by taking the 11 dividing net points along the radius.

Fig. 4 shows the relationships between the plastic flow ability and the ultimate load in which K_e = limit elastic curvature, θ_e (=dK_e) = a standardized rotation at the built-in edge, K_p = limit plastic curvature, θ_p = limit plastic rotation at the built-in edge, and P/P_o = the ratio of the ultimate load of the slab to that of the perfectly plastic slab. On the curves for the clamped slabs in Fig. 4, the dotted lines indicate that the limitation of plastic rotation at the built-in edge is more dominant than that of plastic curvature at the center for reducing their ultimate loads. From the figure it can be observed that the influence of plastic flow ability upon the ultimate load carrying capacities becomes larger as the loaded area becomes smaller. Figs. 5 and 6 indicate the relationship between the magnitude of plastic curvature or rotation and the load *versus* deflection curves obtained for the uniformly loaded slabs, and Fig. 7 shows the variations of moment distributions along the radius for the simply supported and uniformly loaded slab with $\bar{\alpha}$ = 0.25 and $\bar{\beta}$ = 0.1, in which the numerals within circles indicate the correspondence to those in Fig. 5. It can be seen that the load *versus* deflection curves for the clamped slab are sensitively influenced by a limit rotation capacity in the built-in edge, and after the built-in edge plastically fails, they follow those for the simply supported slabs.

5. CONCLUSIONS

An elasto-plastic analysis for reinforced concrete circular slabs with limited plastic curvature or rotation abilities due to the restriction of compressive plastic flow of concrete has been carried out by using the associated plastic flow rule of the plasticity which is related to the loading functions considering a strain softening effect. Here, a fundamental differential equation concerning load-rate and deflection-rate has been derived, and a new solution method being different from the finite difference method for this equation has been presented, in which elastic analytical solutions previously known can be utilized as possible. Numerical calculations have revealed the relationships between the load carrying capacities and the plastic flow abilities for reinforced concrete circular slabs with typical material constants.

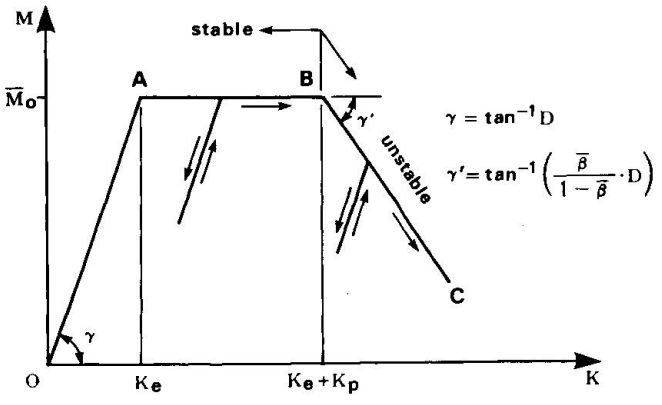

Fig. 1 Idealized Moment-curvature Curve.

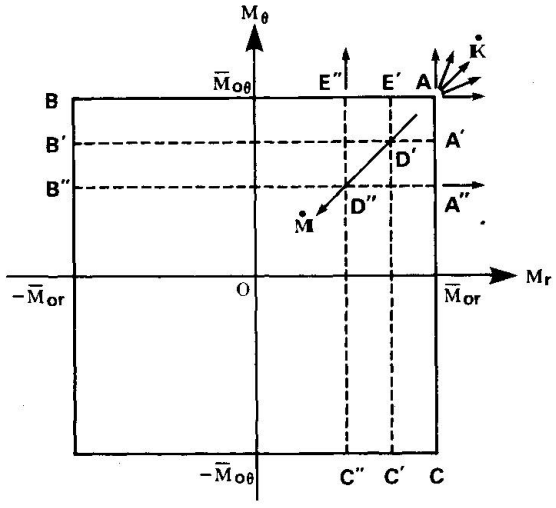

Fig. 2 Loading Surfaces.

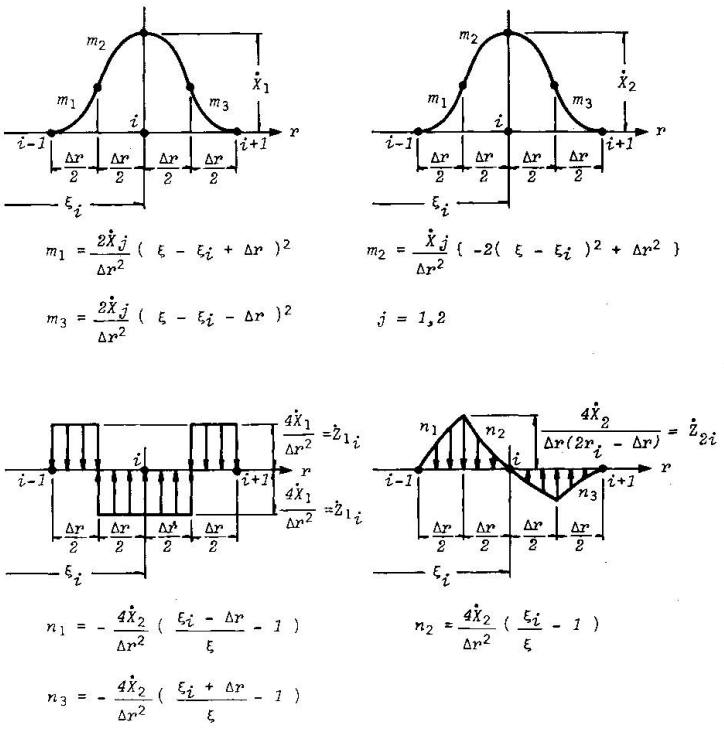

Fig. 3 Moment Redistributions and Virtual Load Distributions Corresponding to Them.

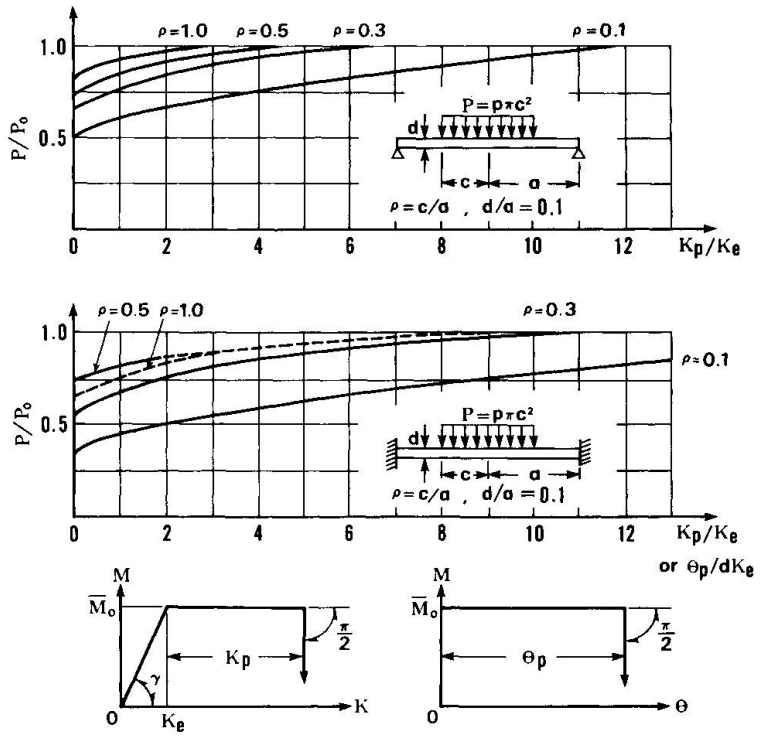

Fig. 4 Relationships Between Ultimate Loads and Limit Plastic Curvature or Limit Plastic Rotation.

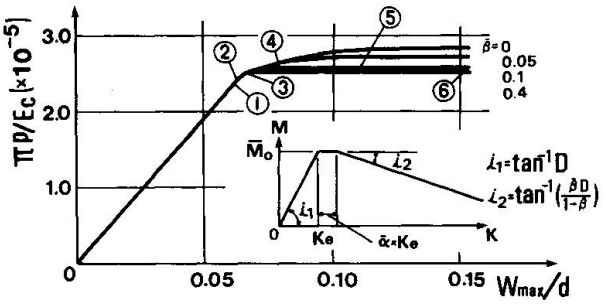

Fig. 5 Load-deflection Curves for the Simply Supported Slab under a Uniform Load, Where $\bar{\alpha}$ = 0.25 is set.

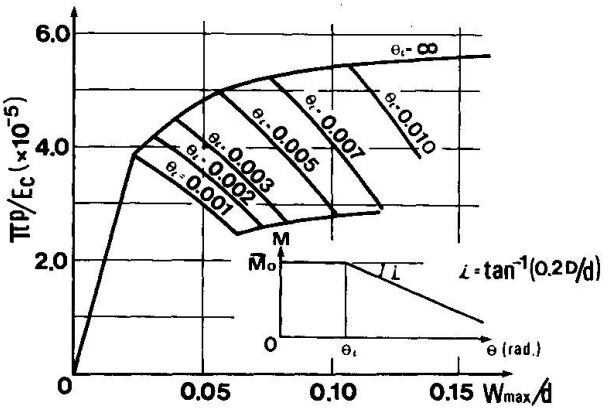

Fig. 6 Load-deflection Curves for the Clamped Slab under a Uniform Load.

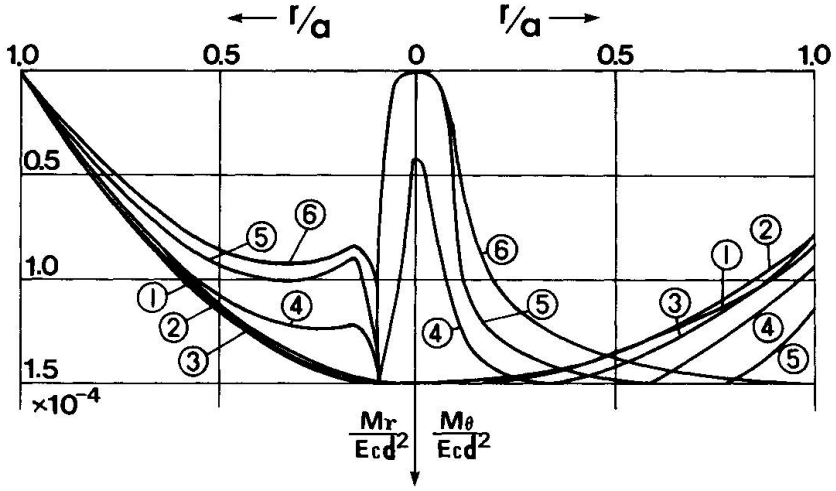

Fig. 7 Variations of Bending Moments along the Radius for the Simply Supported and Uniformly Loaded Slab with $\bar{\alpha}$ = 0.25 and $\bar{\beta}$ = 0.1 in Fig. 5.

REFERENCES

1. Palmer, A.C., Maier, G. and Drucker, D.C.: " Normality Relations and Convexity of Yield Surfaces for Unstable Materials or Structural Elements ", Journal of Applied Mechanics, Vol. 42, 1967, pp. 464-470.

2. Timoshenko, S.P. and Krieger, S.W.: " Theory of Plates and Shells ", 2nd Edition, McGraw-Hill Book Company, INC., 1959, pp. 51-67.

3. Zienkiewicz, O.C., Valliappan, S. and King, I.P.: " Elasto-Plastic Solutions of Engineering Problems 'Initial Stress', Finite Element Approach ", Int. J. Numerical Methods in Engineering, Vol. 1, 1969, pp. 75-100.

III

The Bimoment Method for Hillerborg Slabs

La méthode du bimoment pour les dalles-Hillerborg

Die Bimomentsmethode für Hillerborg-Platten

C.R. GURLEY
Partner
Wargon Chapman & Gurley, Consulting Engineers
Auckland, New Zealand

SUMMARY
This contribution introduces a new macroscopic principle of static equilibrium for segments of Hillerborg plate of large size. These elements can then be seen to be more nearly statically determinate than had been realized. Exact plastic design of Hillerborg plates is often a practical routine design-office activity.

RESUME
L'article présente un nouveau principe macroscopique d'équilibre statique pour des éléments de grande dimensions de dalles-Hillerborg. Le degré d'indétermination statique est plus petit que celui auquel on pouvait s'attendre. L'analyse plastique exacte de dalles-Hillerborg fait souvent partie de l'activité de routine d'un bureau d'ingénieurs.

ZUSAMMENFASSUNG
Ein neues makroskopisches Gleichgewichtsprinzip für Elemente von Hillerborg-Platten wird eingeführt, und es wird gezeigt, dass der Grad der statischen Unbestimmtheit dieser Elemente geringer ist als erwartet. Die plastizitätstheoretisch vollständige Bemessung von Hillerborg-Platten ist oft ein praktisches Handwerkszeug für die übliche Bemessungstätigkeit.

The papers by Morley and by Nielsen in the Introductory Report provide excellent statements of the current research situation in regard to plastic behaviour of slabs. The subject is certainly a difficult one - one has only to reflect that we are now approaching a half-century of work since Johansen began his pioneering efforts and to consider the number of eminent engineers who have contributed in that time. It is satisfying then that worthwhile progress is being made into matters of quite basic and fundamental importance.

Nevertheless it does seem that it will be some time yet before the more advanced matters considered in this session are fully resolved and reduced to routine design-office procedures. The present situation in design practice is not entirely satisfactory and it seems then that designers will need to seek some interim approach of a rather more pragmatic character until these more basic issues are resolved. It cannot be assumed that all designers will have easy access to computer facilities at all times. Neither is it desirable that designers become totally reliant on such facilities. We seek then "here-and-now" design procedures which will provide for straight-forward design with no more equipment than a pocket calculator.

The purpose of this contribution is to suggest that there is a good deal of unrealised potential in Hillerborg's Simple Strip Method and to show how that Method can be improved a more satisfactory design procedure. This can be done by re-examining the equilibrium conditions for a rectangular segment of Hillerborg plate of finite (non-differential) size.

Consider then a small (differential) element of Hillerborg plate as sketched in Fig. 1. The coordinate axes and the element edges are to be taken parallel to the directions of the reinforcing mesh. We assume here that these are perpendicular although the extension to skew reinforcement would not seem to be difficult so long as there are just two reinforcement directions. Following Hillerborg it is assmed that the local twisting moments 'm_{xy}' and 'm_{yx}' are zero everywhere. It follows that there are only local distributed shear forces and local distributed bending moments on each edge. The variation of these stesses across the width 'dx' of the element involves expressions like:

$$m_x + dm_x$$

We do not record these here because the equilibrium conditions for a differential element are already well-known and our present interest is to formulate the equilibrium conditions for a large element.

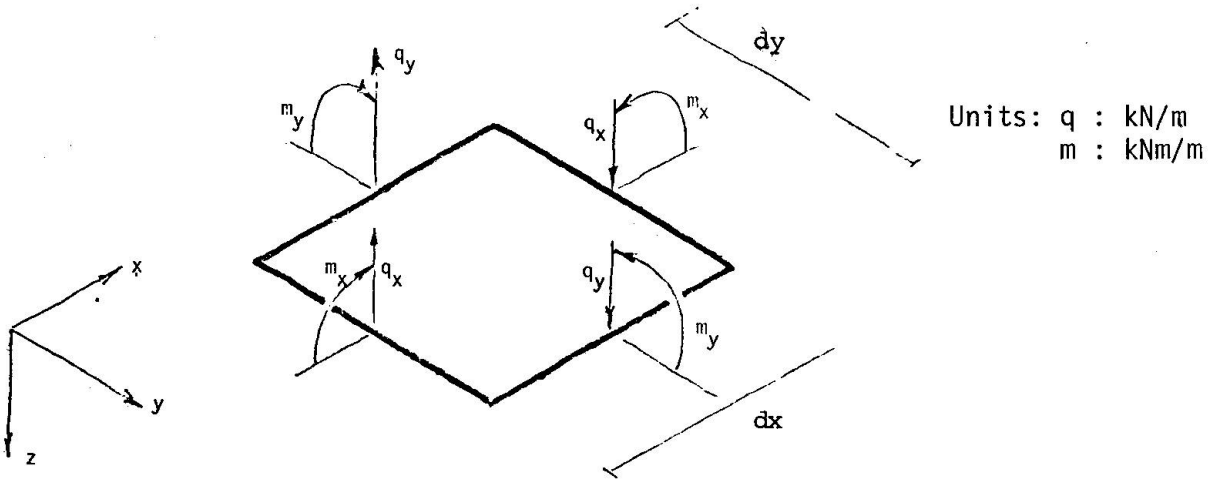

Fig. 1 Local Distributed Stress-Resultants on a Small Element

Consider then a typical large element shown in Fig. 2. The scale of this element may be of the order of several metres on each edge and it may incorporate several Hillerborg strips in each direction. The external equilibrium conditions for this element involve the 8 independent stress-resultants shown together with a further 8 independent coordinates specifying the position of action of each of these stress-resultants measured along the relevant edge. Thus there are, in total, 16 indpendent stress-resultant variables involved in the overall equilibrium of the segment. The conventional state-of-the-art would suggest that these are subject to 3 independent overall equilibrium conditions so that, the large element is 13 times hyperstatic externally. The proposition of this contribution is that there are, in fact, 4 independent overall equilibrium conditions so that the element is only 12 times hyperstatic externally. And, of course, this proposition applies to any and every sub-element resulting from sub-division of the element. It turns out that, while the degree of reduction in hyperstasy appears slight it is, combined with the usual yield conditions, often sufficient to permit exact plastic design as a matter of practical routine in many common design-office situations.

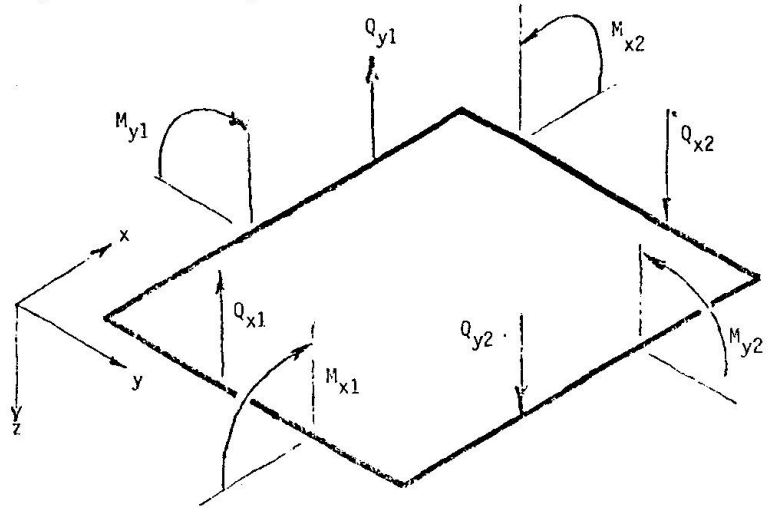

Units: Q : kN
M : kNm

Fig.2 Stress-Resultants on a Large Element

We consider now a virtual displacement in the form of a small unit hyperbolic paraboloid (Fig. 3):

$$z = xy$$

The position of the origin 'O' is arbitrary except only that it is in the plane of the element. Under this displacement, the generators of the hypar remain straight so there is no curvature in the directions of the reinforcing mesh and so no virtual work is done by the bending moments except on the perimeter. In this sense then the above is a virtual rigid body displacement.

All of the quantities involved in the virtual work equation will have dimensions of force times two distinct leverarms e.g. kNm^2. It may be somewhat misleading to reuse Vlasov's term "bimoment" in this context but it does have a certain logical inevitability.

We define then the "Restoring Bimoment" of the above plate about origin 'O' as the virtual work done by the perimeter moments under the above virtual displacement. Similarly we define the "Overturning Bimoment" about origin 'O' as the virtual work done by the loads. It is usually more convenient to include the virtual work done by the perimeter shears in the overturning bimoment as if they were perimeter line-loads. On this basis the virtual work equation becomes, very simply:

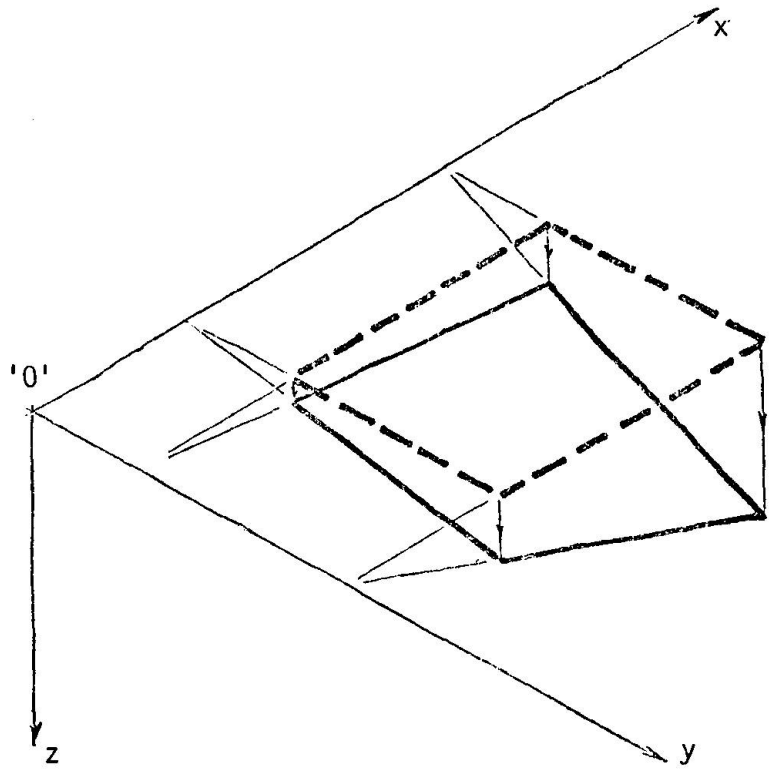

Fig. 3

Overturning Bimoment = Restoring Bimoment

This result can be expressed in mathematical terms using double integrals. Indeed it can be proved by integrating the local (differential) equilibrium equation with the aid of Green's theorem (two-dimensional integration by parts). To do so would obscure the simplicity of the result. In a routine design calculation the quantities concerned can, almost invariably be evaluated from direct, simple physical considerations. It is not necessary either to become pre-occupied with matters of sign convention. The correct sign is usually quite obvious and can, in any case, always be resolved by sketching out the virtual displacement.

For any particular segment it is always possible to find four independent bimoment equilibrium equations. These include the known three equilibrium equations e.g. moments about each of two axes and equilibrium of total load with perimeter shears. Indeed these known conditions can be regarded as bimoment conditions in which the origin has been pushed to infinity in one or other or both directions. In any case it is clear that we now have available a good deal more equilibrium information than we had expected. This is surely significant.

The author has developed the above approach and used it in many actual routine design calculations since mid 1977. The principal advantage is that it provides simple direct relationships between moment-fields and total loads. It is possible then to avoid the initial arbitrary assignment of strip-widths and strip-loads as suggested in the original Hillerborg proposals. This makes it possible to produce "practical optimum" designs every time and to do so within the constraints of Code minimum reinforcement content, reasonable simplicity of construction etc.

However the author does conclude all designs with a Hillerborg solution showing the strip-loads calculated from the assigned moment-fields. Whether or not such a solution is theoretically essential, it provides an independent check against gross errors of calculation and this is always desirable.

Is the Bimoment Method a Lower Bound approach? It uses a macroscopic form of the equilibrium conditions but, theoretically at least, it can be applied to progressively smaller elements and, in the limit, this process amounts to differentiation and necessarily re-establishes the local (differential) equilibrium conditions. In practice the author only uses bimoment methods to assign sufficient of the moment-field to determine reinforcement (including, sometimes, cut-off and curtailment positions) and then uses Hillerborg methods to complete and check the statical solution. This combination seems to work very well.

In many cases it is possible to do exact plastic design of slabs regarded as Hillerborg plates. It would seem that such designs are necessarily very efficient lower bound designs for slabs regarded as Johansen plates. In practice the steel in quite extensive areas of slabs is determined by Code rules on minimum reinforcement content. It is usually possible to ensure that this steel is fully utilised at yield strength under design load.

In other cases, particularly those involving a re-entrant or near-point load or support acting integrally with the slab, it is not possible to find an exact plastic solution even when the slab is regarded as a Hillerborg plate. These situations seem synonymous with those in which the, usually, "secondary" effects of shear and strain-hardening have substantial significant. It is not reasonable to expect rigid plastic thin plate theory to provide "exact" solutions in such complex 3-dimensional situations. Design in such situations is a linear programming "game". Success in such situations does depend on the judgement and intuition of the designer but, then, these are the skills possessed by experienced designers and the bimoment approach does provide equilibrium information in a form most easily assimilated and used. Safety is not an issue, because all designs can be checked by Hillerborg procedures, but economy and suitability will still depend on the individual approach. In this matter then Engineering remains an art as well as a science.

A longer paper [Ref. 1] expected soon attempts to cover many of the points omitted because of the limited length of this contribution.

REFERENCES

1. GURLEY, C.R., "Bimoment Equilibrium of Finite Segements of Hillerborg Plate", Publication pending, Magazine of Concrete Research, London

Leere Seite
Blank page
Page vide

III

Nodal Forces as Real Forces

Les forces nodales en tant que forces réelles

Knotenkräfte als wirkliche Kräfte

D.H. CLYDE
Professor of Civil Engineering
University of Western Australia
Nedlands, W. Australia

SUMMARY
The conventional approach to nodal forces in yield line theory is re-examined because it leads to breakdown cases and other anomalies. It is shown that the true nodal forces are vertical shears at and parallel to strength discontinuities. The existence of these forces was demonstrated for elastic plates by Thomson and Tait but is now shown to be a general statical requirement of shear flow closure. The resulting insight enables the fundamental errors associated with invalid and breakdown cases to be demonstrated.

RESUME
La méthode traditionnelle des forces nodales de la théorie des lignes de rupture est réexaminée parce qu'on obtient dans certains cas des contradictions et d'autres anomalies. On montre que les forces nodales vraies sont des forces de cisaillement existant le long des lignes de discontinuité de la résistance. L'existence de ces forces a été démontrée par Thomson et Tait pour les plaques élastiques. Dans le présent article, on montre que ces forces correspondent à une condition statique générale d'après laquelle les forces de cisaillement doivent être continues. Les conclusions obtenues permettent de montrer les erreurs fondamentales associées aux cas contradictoires de l'application de la méthode des forces nodales.

ZUSAMMENFASSUNG
Die herkömmliche Methode der Knotenkräfte innerhalb der Fliessgelenklinientheorie wird neu betrachtet, da sie in gewissen Fällen zu Widersprüchen und anderen Unregelmässigkeiten führen kann. Es wird gezeigt, dass die wahren Knotenkräfte Querkräften entsprechen, die entlang von Widerstands-Diskontinuitätslinien auftreten. Das Vorhandensein solcher Kräfte wurde für elastische Platten durch Thomson und Tait nachgewiesen. Hier wird gezeigt, dass sie der allgemeinen statischen Forderung nach einem geschlossenen Schubfluss entsprechen. Die grundlegenden Fehler, welche mit Fällen widersprüchlicher Ergebnisse bei der Anwendung der Methode der Knotenkräfte verbunden sind, können mit Hilfe der neu gewonnenen Erkenntnisse aufgezeigt werden.

1. INTRODUCTION

Nodal forces arise in the equilibrium method of yield line theory. A nodal force is a concentrated internal transverse force which, under special circumstances, must be inserted at an end of a straight internal section. Johannsen [1] established the existence of such forces and formulated rules for their determination. Later workers have attempted to improve the rigour of the rules but have, nevertheless, found that breakdown cases exist for which solutions using these rules do not agree with solutions using the alternative work method.

Conflict in the results of different solution methods for properly posed problems in structural mechanics indicates a lack of rigour in setting up one or both of the methods. Fox [2,3] demonstrated that the assumptions of yield line theory can provide the basis of a rigorous rigid-plastic analysis. He constructed coincident upper and lower bound solutions for certain problems whose intractability had earlier suggested an inconsistency between the failure criterion of yield line theory and rigorous plasticity theory [4]. It should be noted that Fox's solutions include zones of finite curvature within which the slabs deform into general developable surfaces whereas in yield line theory only one such surface, the cone, is used. Given the conflict mentioned above and the evidence that a properly formulated solution method has demonstrated the essentially well-posed nature of the problems one must examine the basis of the methods which produce the conflicting solutions. The equilibrium method is so named because a separate equilibrium equation is written for each rigid slab element. The following requirements are satisfied as well as equilibrium :

(i) The forces on the internal boundaries satisfy the failure criterion which in force space [5] is given by

$$M_{xy}^2 - (M^x - M_x)(M^y - M_y) \leqslant 0 \qquad M_{xy}^2 - (M_x - \bar{M}^x)(M_y - \bar{M}^y) \leqslant 0 \qquad (1)$$

(ii) Application of the flow rule to (1) defines associated curvature rates [5]. It may readily be shown that the relative rotations about the yield line of the two rigid segments abutting the yield line correspond to concentrations of one class of curvature rates which satisfy the flow rule.

(iii) The layout of yield lines is such that these relative rotations taken in conjunction with the boundary conditions form a compatible mechanism.

2. NODAL FORCES

Johannsen established that simultaneous solution of the equilibrium equations is theoretically equivalent to the extremised solution of a global equilibrium equation most conveniently written using virtual work.

The most readily demonstrated justification for nodal forces is that there are cases where the two methods give different results and that these can be reconciled by inserting nodal forces of such a magnitude as to cause the equilibrium method solution to co-incide with the work method solution. This method is inferential and has been used by some [6] as a de facto basis for establishment for their magnitude. Johannsen's analysis which established rules for their determination is also inferential and is based on small perturbations of the layout from which it can be shown that nodal forces are required for stationariness.

Despite the indirect determination of nodal forces Johannsen also gave a physical explanation, i.e. "In addition (to the normal moment) a torsional moment and shear stress act on the yield line. These can be resolved into two single forces, one at each end of the section". A counter-example to refute Johannsen's physical

explanation is readily found.

Criterion (1) is in the form containing only force variables. Implicit in its derivation is the requirement that the applied normal moment M_n does not exceed the normal moment capacity M^n i.e.

$$M_x \cos^2\alpha + M_y \sin^2\alpha + 2M_{xy} \sin\alpha\cos\alpha \leq M^x\cos^2\alpha + M^y \sin^2\alpha \qquad (2)$$

The limit of the inequality may be shown to lead to :

$$M_{nt} = (M^x - M^y) \sin\alpha\cos\alpha \qquad (2a)$$

Since for isotropic reinforcement $M^x = M^y$, M_{nt} must be zero everywhere on an isotropic yield line and $\frac{\partial M_{nt}}{\partial t}$ will thus also be zero. Furthermore translation of the yield line should not lead to violation of (2) so that $\frac{\partial M_n}{\partial n} = 0$ on the yield line. Hence neither twisting moment nor shear force may exist on an isotropic yield line. Nevertheless a classic example of a nodal force occurs where an isotropic yield line meets a free edge and has magnitude $M \cot\alpha$ [5]. Thus Johannsen's explanation breaks down. Direct application along the yield line of Thomson-Tait [7] statical equivalence [6] must also fail where there are no forces to which the nodal force can be statically equivalent. Somewhat surprisingly, however, the author has found that the physical basis of the nodal force can be found in other portions of Thomson and Tait's work by examination, not of the yield line which being internal must satisfy conditions of continuity, but of the boundary itself.

3. BOUNDARY CONDITIONS AT AN EDGE

Thomson and Tait utilised equivalence as a mathematical device to reduce three boundary conditions at a free edge to two. Considering a free edge x = a (Fig.1) the apparent consequences of the absence of surface tractions $M_x = 0$, $M_{xy} = 0$, $Q_x = 0$ may be reduced to two namely $M_x = 0$ and $Q_x - \frac{\partial M_{xy}}{\partial y} = 0$. Although Thomson and Tait used statics to derive this result subsequently they showed that there is a local disturbance due to twisting moment at the free edge of an elastic plate which dies out rapidly as one moves away from the edge. They invoked this solution to confirm that St.Venant's principle applies to the statically equivalent forces.

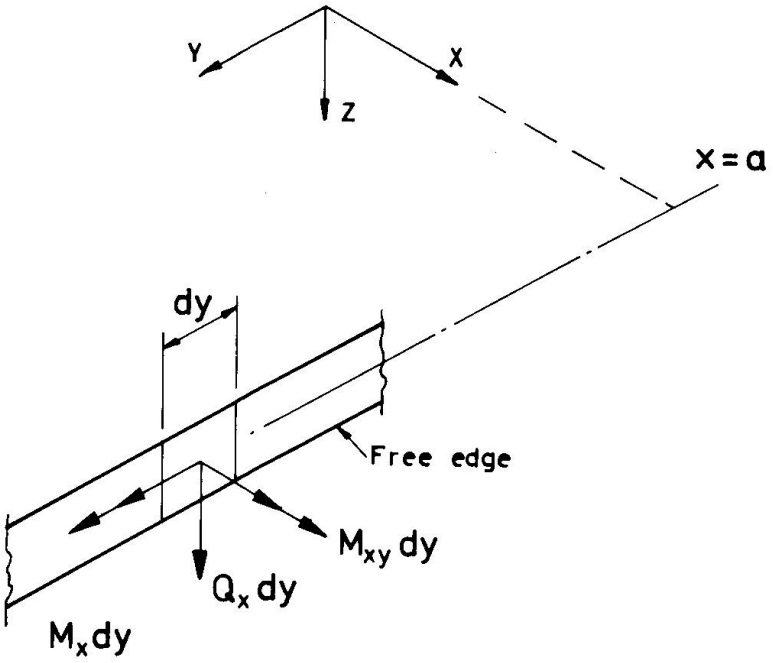

Figure 1. Apparent vanishing forces at free edge.

The analysis which demonstrates the rapid decay provides further insight. It is the treatment of anticlastic curvature produced by alternating upward and downward

corner loads on a square plate as a limiting case of St. Venant torsion. They observed that only one half of the total torsional moment arises from the M_{xy} stresses, the other half being due to "two tangential tractions distributed over areas of the edge infinitely near the ends acting perpendicularly to the plate towards opposite parts". These transverse forces exist because the opposing horizontal shear flows which constitute the M_{xy} couple require closure at a stress free edge (Fig.2). Popov [8] has added clarification to this requirement.

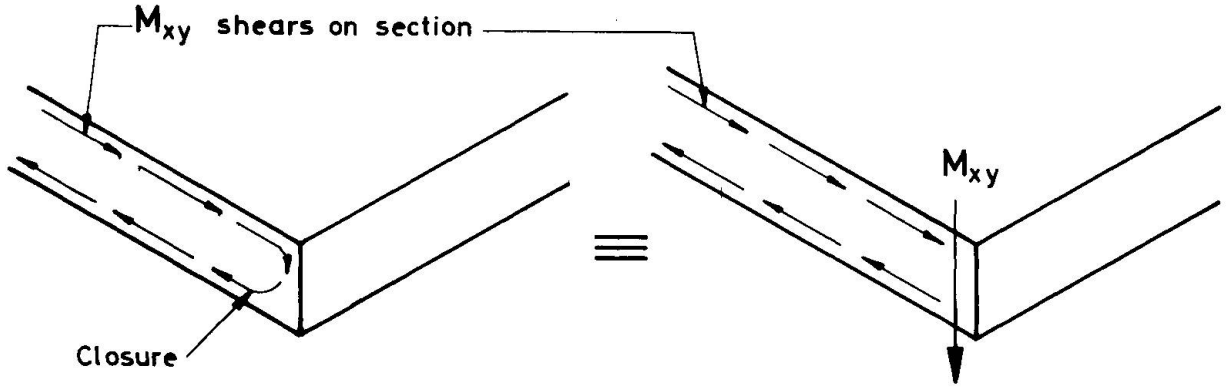

Figure 2. Equivalence of shear flow closure.

While Thomson and Tait's conclusions were based on an elastic solution, the requirement is one of statics and is independent of the nature of the stress distribution which goes to make up M_{xy}. This will now be demonstrated. A twisting moment M_{xy} on a section normal to the free edge is associated with a conjugate M_{xy} on a section parallel to the edge. Assume that the limits of this ideal flexural behaviour occur on a face Δx inside the free edge and parallel to it (Figure 3).

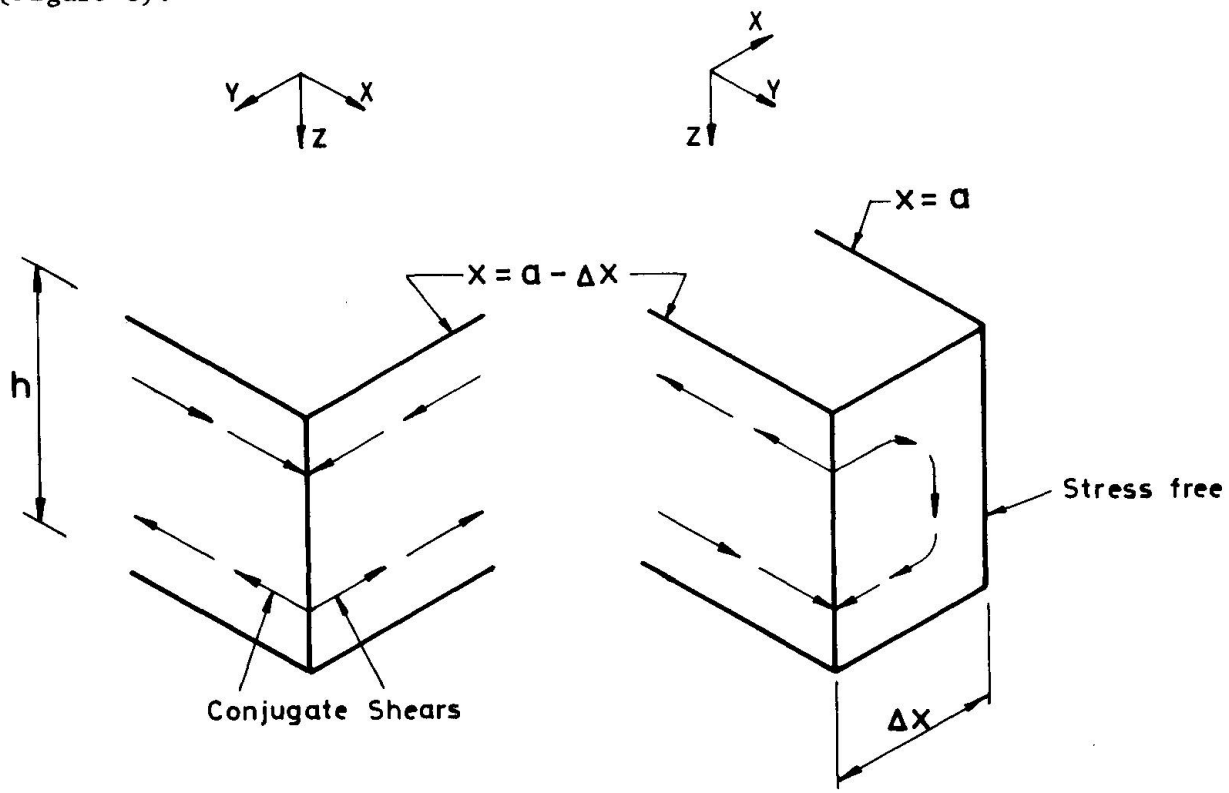

Figure 3. Isolation of Edge Strip.

In the strip Δx wide by h deep the transition from M_{xy} stresses to the stress-free edge state must occur, i.e. over this interval :

$$\int_0^{\Delta x} \frac{\partial \tau_{xy}}{\partial x}\, dx = \tau_{xy}\Big|_{\Delta x} \qquad (4) \qquad \text{where } M_{xy}\Big|_{\Delta x} = \int_{-\frac{h}{2}}^{+\frac{h}{2}} \tau_{xy}\Big|_{\Delta x}\, z\, dz \qquad (5)$$

hence
$$M_{xy} = \int_{-\frac{h}{2}}^{+\frac{h}{2}} \int_0^{\Delta x} \frac{\partial \tau_{xy}}{\partial x}\, z\, dx\, dz \qquad (6)$$

In order to maintain equilibrium parallel to the edge, the differential equation of equilibrium :-

$$\frac{\partial \sigma_y}{\partial y} + \frac{\partial \tau_{xy}}{\partial x} + \frac{\partial \tau_{yz}}{\partial z} = 0 \qquad (7)$$

must be satisfied everywhere. If $\sigma_y = 0$ (i.e. ignoring bending which may be superposed later) this reduces to

$$\frac{\partial \tau_{xy}}{\partial x} = -\frac{\partial \tau_{yz}}{\partial z} \qquad (8)$$

Thus the rate of change of horizontal shear τ_{xy} over the width Δx generates vertical shears τ_{yz} which integrate to yield a vertical force Z_y as follows:-

$$Z_y = \int_0^{\Delta x} \int_{-\frac{h}{2}}^{+\frac{h}{2}} \tau_{yz}\, dz\, dx = \int_0^{\Delta x} \Big[\tau_{yz}\, z\Big]_{-\frac{h}{2}}^{+\frac{h}{2}} dx - \int_0^{\Delta x} \int_{-\frac{h}{2}}^{+\frac{h}{2}} z\, \frac{\partial \tau_{yz}}{\partial z}\, dz\, dx \qquad (9)$$

Since $\tau_{yz} = 0$ at $z = \pm \frac{h}{2}$ the first term is zero and substituting (8) in the second yields :-

$$Z_y = \int_0^{\Delta x} \int_{-\frac{h}{2}}^{+\frac{h}{2}} z\, \frac{\partial \tau_{xy}}{\partial x}\, dz\, dx = M_{xy}\Big|_{\Delta x}. \qquad (10)$$

This vertical shear force in the edge strip is a physical reality which transcends mere statical equivalence. Because it is a force and not a stress it is invariant under change of angle of the cutting section relative to the edge. Thus for any but the normal section it is not related to the twisting moment on the internal face and it is quite possible to have zero twisting moment in a skew face but to have an edge shear force. This somewhat surprising result clarifies the vertical equilibrium of a 45° corner triangle of the square plate case placed in a state of pure torsion by upward and downward corner forces [9].

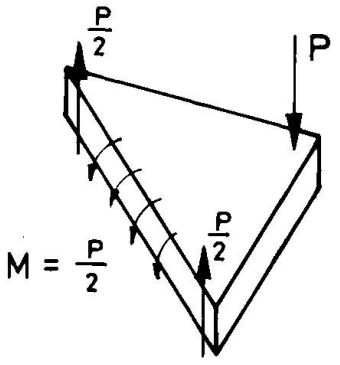

Figure 4. Vertical equilibrium in pure torsion.

4. NODAL FORCES AS REAL FORCES

The nodal force where a yield line meets a free edge is the shear force in the

edge strip. It is determined by the twisting moment on faces parallel to and normal to the edge. The twisting moment is readily calculated from the conditions that $M_x = 0$ on the edge and that the normal and twisting moments on the yield line are defined by the failure criterion to be :

$$M_{xy} = - M^x \cot \alpha \qquad (11)$$

The problem of a yield line intersecting an internal step change in mesh strength was posed and explored by Jones [6]. If the yield line makes an angle α with the internal boundary on which M^x steel normal to the boundary is reduced from M^x_1 to M^x_2 the conditions for satisfaction of the failure criterion on both sides of the change may be obtained in the fashion of equation (11) and are :-

$$(M_{xy_1} - M_{xy_2}) = - (M^x_1 - M^x_2) \cot \alpha \qquad (12)$$

The band of vertical shear is this time just inside the stronger zone and runs parallel to the boundary between the zones. The magnitude of the shear force is equal to the change in twisting moments and at a yield line becomes the nodal force determined by (12). A practical implication of the above conclusions are that such bands of shear should be included in the reinforcement design considerations.

5. INVALID AND BREAKDOWN CASES

The author has not been able to find further rigorous examples of nodal forces and has separated other pseudo nodal forces into invalid cases, which superficially appear to obey the Johannsen rules, and breakdown cases, which are neither rigorous nor obey the Johannsen rules for their determination.

5.1. Invalid nodal force. This is the intersection of sagging and hogging yield lines. It is possible to devise failure mechanisms which are kinematically admissible and appear to satisfy the failure criterion on all yield lines but fail to satisfy equilibrium at their intersection. The angle of intersection must be such that the failure moments also satisfy the transformation of axes (equilibrium) equation. For example, for isotropic reinforcement this requires orthogonality. For isotropic cases where non-orthogonal intersections are used the interpretation of Johannsen's rules which is widely accepted suggests a nodal force of

$$k = - (M - \bar{M}) \cot \alpha \qquad (13)$$

Similarities between this and (12) are deceptive because in this case neither yield line represents a strength discontinuity at which a step change in twisting moment can validly be invoked. Efforts by the author to produce solutions with artificial shear along one yield line led to the conclusion that this merely removes the violation of the yield condition by an amount Δx from the yield line since M_n would not change significantly over a small distance. The assumed nodal force is thus seen as a device which superficially localises the fundamental violation of statics at the intersection but also removes it an infinitesimal amount to one side of one yield line.

The conclusion is that the lack of rigour is implicit in both the equilibrium and the work method. In part this results from the exclusion of Fox's zones of finite curvature from the repertoire of mechanisms available in yield line theory.

5.2. Breakdown cases. These occur where the mechanism is overconstrained [6], and may or may not include invalid intersection angles of yield lines. The overconstraint leads to the necessity for twisting moments and shears on yield lines independently of the angle of intersection problem and thus to apparent forces which do not even superficially appear to satisfy Johannsen's rules.

Of the particular classes of problem which have been explored the following are

the three most important :

5.2.1 The re-entrant free edge. Because a free edge is involved at one end of the yield line this is the problem about which most meaningful observations can be made. While real nodal forces are the closure shear flows associated with twisting moments immediately inside a free edge it may readily be shown that an angular discontinuity in a free boundary no twisting moment may exist if all internal moments are required to be continuous. Hence no nodal force may exist at the re-entrant corner of a free boundary. Symmetrical cases show zero apparent nodal force and are the rigorous case of a yield line passing through a re-entrant corner of a free edge.

5.2.2. The re-entrant support. This generates a kinematic requirement for an intersection of a hogging with a sagging yield line which, in general, does not even superficially obey Johannsen's rules and hence goes beyond the case proved above to be invalid. It becomes an overconstrained case for which force transfer between segments is required in order to give the appearance of reconciliation.

5.2.3. The Maltese-Cross failure pattern for a square slab. Wood [6] attributes the posing of the problem to Nylander. This time the penalty of overconstraint is a twisting moment along the yield line associated with extremised solution. The comments under 5.1. above apply with respect to shifting the violation of the failure criterion an infinitesimal distance from the yield line if nodal forces at the centre are postulated as the mode of rectifying the unbalance. The extremised work solution thus cannot be considered as a valid one.

6. CONCLUSIONS

In order to understand the nature of nodal forces it has been necessary to introduce a more comprehensive analysis of boundary conditions than the standard Thomson-Tait one of statical equivalence. As a result it is concluded :

6.1. An internal shear force exists in a narrow strip parallel to a free or simply supported edge which is numerically equal to the twisting moment immediately inside the edge on faces parallel to and normal to the edge.

6.2. A shear force exists in a strip parallel to an internal strength discontinuity which is numerically equal to the step change across the discontinuity of the twisting moment on faces parallel to and normal to the discontinuity.

6.3. At the intersection of a yield line with an edge or internal strength discontinuity the shear force is known as a nodal force.

6.4. Various other cases including the intersection of sagging and hogging yield lines, re-entrant free edges, re-entrant supported edges and the Maltese-Cross failure mechanism for square slabs give rise to false nodal forces due to deficiencies in the posing of the problems.

6.5. Reinforcement requirements at free and simply supported edges and strength discontinuities will need to be re-examined in the light of the existence of the shear face demonstrated in this paper.

7. NOTATION

a	Constant, value of x
h	Slab thickness
n,t,z	Local co-ordinates normal and tangential to section
x,y,z	Cartesian co-ordinates

M Basic symbol for moments per unit length with the following variants :-

M	Isotropic yield moment (sagging)
$\overline{M}$	Isotropic yield moment (hogging)
M_x, M_y, M_{xy}	Applied moments in Cartesian co-ordinates stress resultants of σ_x, σ_y, τ_{xy} respectively.
M_n, M_t, M_{nt}	Applied moments in local co-ordinates.
M^x, M^y	Yield moments in Cartesian co-ordinates (sagging)
$\overline{M}^x, \overline{M}^y$	Yield moments in Cartesian co-ordinates (hogging)
M^n	Yield moment referred to normal co-ordinates

P A concentrated force

Z_y The vertical stress resultant of τ_{yz}

α Yield line orientation relative to M^x yield line

θ Slab parameter

8. REFERENCES

1. JOHANNSEN, K.W. Yield-line Theory. Doctoral Thesis Danmarks Tekniske Hojskole. 1943. English translation, Cement and Concrete Assoc.London 1962.

2. FOX, E.N. Limit analysis for plates: a simple loading problem involving a complex exact solution. Phil.Trans.Roy.Soc.,Vol.272 A.,1972, pp.1057-1073.

3. FOX, E.N. Limit analysis for plates: the exact solution for a clamped square plate of isotropic homogeneous material obeying the square yield criterion and loaded by uniform pressure. Phil.Trans.Roy.Soc.,Vol.277 A., 1974, pp.121-155.

4. WOOD, R.H. Some controversial and curious developments in the plastic theory of structures. Engineering Plasticity, ed.Heyman,J. and Leckie,F.A., Cambridge, 1978.

5. NIELSEN, M.P. The theory of plasticity for reinforced concrete slabs. Introductory Report,IABSE Colloquium on Plasticity in Reinforced Concrete, Copenhagen, 1979 . pp.93-114.

6. Recent Advances in Yield Line Theory. Special Publication of Magazine of Concrete Research, Cement and Concrete Assoc., London, 1965.

7. THOMSON, W. and TAIT, P.G. Natural Philosophy . 1883. Vol.1. Part 2.

8. POPOV, E.P. Kelvin's solution of the torsion problem. Journal of the Engineering Mechanics Div. Proc. of the Am.Soc. of Civ. Engineers. Vol.96, No.EM6 Dec. 1970. pp.1005-1012.

9. MOFFLIN, D. Nodal Forces in Yield Line Theory. Honours Thesis, University of Western Australia, 1978.

III

Punching Shear Failure of Hollow Concrete Spheres

Poinçonnement d'une coque sphérique en béton

Durchstanzversagen von Kugelschalen aus Beton

C.T. MORLEY
Lecturer
University of Cambridge
Cambridge, England

SUMMARY
The paper extends the plastic theory of punching shear failure to treat hollow concrete spheres. Graphs showing the theoretical predictions are presented, and some comparisons are made with experimental results for cylinders under concentrated radial loads.

RESUME
L'analyse plastique du poinçonnement est appliquée à une coque sphérique. Les résultats théoriques sont présentés graphiquement et quelques comparaisons sont faites avec des résultats expérimentaux obtenus pour des cylindres soumis à une force concentrée radiale.

ZUSAMMENFASSUNG
Die plastische Berechnung des Durchstanzversagens wird auf den Fall von Kugelschalen aus Beton ausgedehnt. Die theoretischen Voraussagen werden in graphischer Form dargestellt. Einige Vergleiche werden gemacht mit Ergebnissen von Versuchen an Zylindern, die durch in radialer Richtung wirkende Einzellasten belastet wurden.

1. INTRODUCTION

The purpose of this brief note is to extend to hollow concrete spheres the plastic theory of punching shear failure presented by Braestrup [1] for flat slabs. In slabs with zero tensile strength the optimum failure surface extends right out to the support, giving low failure loads, and it is necessary to introduce a small non-zero tensile strength in order to confine the failure surface and produce reasonable results. In a spherical shell under a radial point load the curvature of the shell will tend to confine the failure surface in punching shear, and the plastic theory should predict reasonable failure loads even if the concrete is assigned zero tensile strength. In what follows the extended theory is presented, using Braestrup's notation as far as possible, and some experimental results on cylinders are reported.

2. BASIC ASSUMPTIONS

A concrete spherical shell or dome of thickness h and internal radius R is assumed to be loaded by an inward radial force P applied to a rigid disc of diameter d_o, as shown in Fig.1. The shell is supported well away from the region of interest. In a punching shear failure a rigid axisymmetric plug of concrete defined by a 'failure surface' with generatrix AB is assumed to move inwards along the axis of P relative to the rest of the shell. The concrete is taken to be a rigid perfectly plastic material whose yield condition is the modified Coulomb failure criterion with angle of internal friction ϕ and zero tensile strength. Deformations are governed by the associated flow rule of plasticity theory (the normality condition).

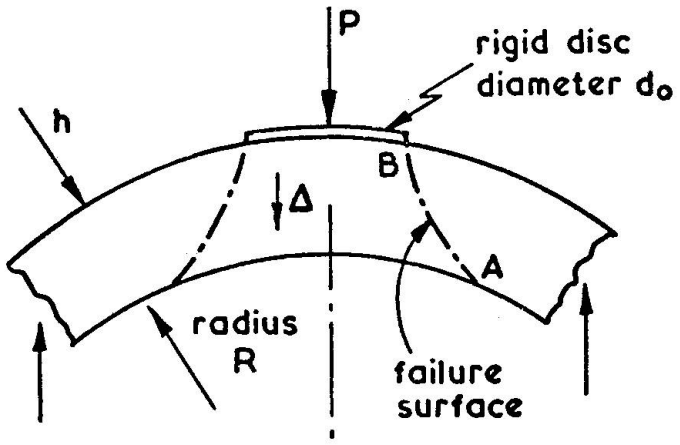

Fig. 1 A punching shear failure.

Following Braestrup, an upper bound on the failure value of P is found by writing the work equation for failure on an assumed surface, and the optimum failure surface giving the least upper bound is found by the calculus of variations. Since displacement is along the P axis hoop strains are zero everywhere and the concrete is in plane strain in planes containing the P axis: the appropriate yield locus is Fig.5(b) of Braestrup's paper, with $f_t = 0$. All deformation is assumed to occur in a narrow zone at the failure surface, which is a surface of revolution defined by the generatrix r = r(x), Fig.2.

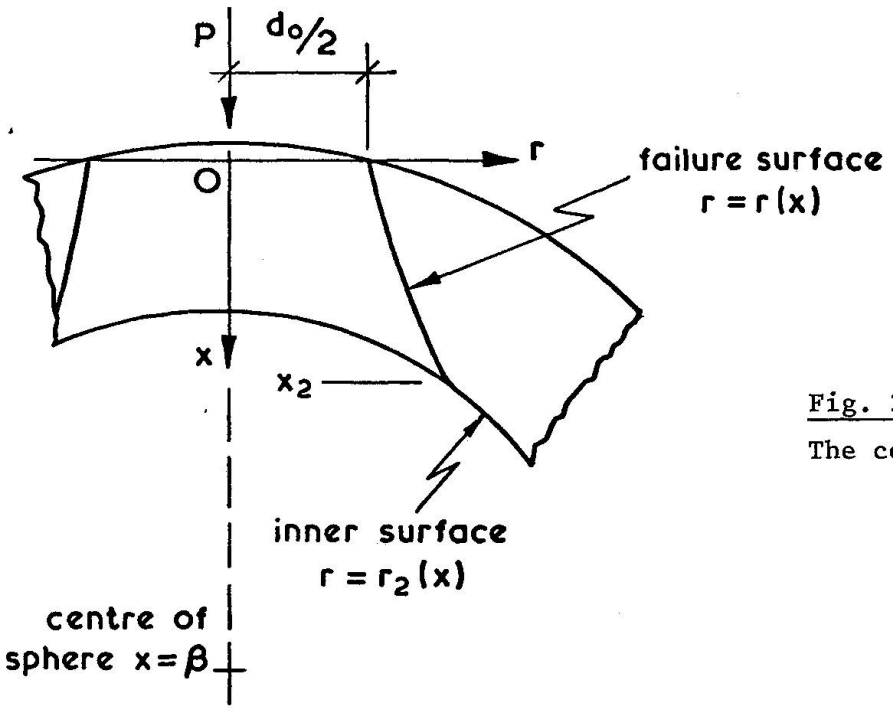

Fig. 2
The co-ordinate system.

On writing the work equation, the upper bound on the failure load is given by the equivalent of Braestrup's equation (9),

$$P = \pi f_c \int_o^{x_2} r(\sqrt{1 + (r')^2} - r')\, dx \qquad (1)$$

where a dash indicates differentiation with respect to x. In contrast to the situation in flat slabs, reinforcement running parallel to the curved shell surfaces will be compressed in such a failure, and therefore contribute to the energy dissipation. Here we ignore the contribution of such reinforcement, so that equation (1) only gives the failure load for an unreinforced shell.

3. THE OPTIMUM FAILURE SURFACE

The problem now is to find the function r(x) which minimises the load P in equation (1), subject to the condition dictated by the plane-strain yield locus that

$$r' \geq \tan\phi \qquad (2)$$

The additional difficulty in the case of spheres is that the upper limit of integration x_2 is itself variable because of the curvature of the inner shell surface.

We consider first the case when the minimising curve always has a slope greater than $\tan\phi$. The minimising curve presumably has r continuous, but discontinuities in slope r' would seem to be permissible on physical grounds. However, the Weierstrass-Erdmann corner conditions (ref. 2. p.33) show that the minimising curve for (1) will have continuous slope. According to the calculus of variations (see eg Pars [2] or Irving and Mullineux [3], the minimising curve r = r(x) will then satisfy the appropriate Euler equation, which for a functional of the form $\int F(x,r,r')dx$ can be written

$$\frac{\partial F}{\partial r} - \frac{d}{dx}\left(\frac{\partial F}{\partial r'}\right) = 0 \qquad (3)$$

On substituting from (1) this reduces to

$$1 + (r')^2 - r.r'' = 0 \qquad (4)$$

whose solution may be written

$$r = a \cosh\left(\frac{x}{a} + b\right) \qquad (5)$$

where a and b are constants.

The upper limit of integration x_2 is variable but the failure surface must end on the inner shell surface $r = r_2(x)$. In these circumstances the optimising function r(x) must satisfy the so-called 'transversality condition'.

$$F + (r_2' - r')\frac{\partial F}{\partial r'} = 0 \qquad (6)$$

at the upper limit $x = x_2$ (ref.2 p.96, ref. 3 p.362). From (1) and (6)

$$r_2' = r' + \sqrt{1 + (r')^2} \qquad (7)$$

which reduces, using (5), to

$$r_2' = \exp\left(\frac{x}{a} + b\right) \qquad (8)$$

at $x = x_2$.

It turns out that in many cases the catenary curve satisfying (5) and (8) and passing through the edge $(0, d_o/2)$ of the loaded area violates condition (2) near x = 0. The portion of the optimising generatrix near x = 0 will then be a straight line of slope $\tan\phi$, so that part of the failure surface is conical. Consideration of a series of catenaries satisfying (5) and (8) and passing through different points on this straight line then shows that the optimising generatrix is tangent at some point $x = x_1$ to this line. This may be confirmed by considering an analogy with a heavy string, and a numerical investigation shows that the stationary value found for the integral (1) is indeed a minimum.

We then obtain, independently of R/h, if a is positive,

$$x_1 = a\,\mathrm{cosec}\phi - \frac{d_o}{2}\cot\phi \qquad (9)$$

and

$$b = \sinh^{-1}(\tan\phi) - x_1/a \qquad (10)$$

The equation $r = r_2(x)$ for the inner circle may be written

$$r_2^2 = R^2 - (\beta - x_2)^2 \qquad (11)$$

where β is a known constant. This may be combined with (5) and (8) to give

$$a = 2(\beta - x_2)\left[1 - (\beta - x_2)^2/R^2\right] \qquad (12)$$

Equations (9), (10) and (12) give the important parameters x_1, b and a in terms of the upper limit x_2, for which an equation can be found by combining these and the transversality condition (8) to give

$$\frac{\beta - x_2}{\sqrt{R^2 - (\beta - x_2)^2}} = \exp\{\sinh^{-1}(\tan\phi) - \operatorname{cosec}\phi + \frac{2x_2 + d_o \cot\phi}{4(\beta - x_2)[1 - (\beta - x_2)^2/R^2]}\} \quad (13)$$

This equation for x_2 may be solved by iteration or by a graphical method. The possibility of obtaining numerical solutions by this approach was pointed out to me by P. R. Hunter.

Once the optimal failure surface has been found the corresponding failure load is obtained from equation (1) which becomes

$$\frac{P}{\pi f c} = (\sec\phi - \tan\phi)\frac{x_1}{2}(d_o + x_1\tan\phi) + \frac{a}{2}(x_2 - x_1)$$

$$+ \frac{a^2}{4}\left[\exp\left(-2\left(\frac{x_1}{a} + b\right)\right) - \exp\left(-2\left(\frac{x_2}{a} + b\right)\right)\right] \quad (14)$$

4. SOME TYPICAL SOLUTIONS

The optimising curves r(x) for the case R = 6h and various punch diameters are plotted in Fig. 3, for the same angle of friction as used by Braestrup, $\tan\phi = 3/4$. Notice that an appreciable proportion of the failure surface is conical even for $d_o = 0$, and that this proportion increases as the punch diameter increases until the optimal failure surface becomes entirely conical for d_o/h greater than about 3.3.

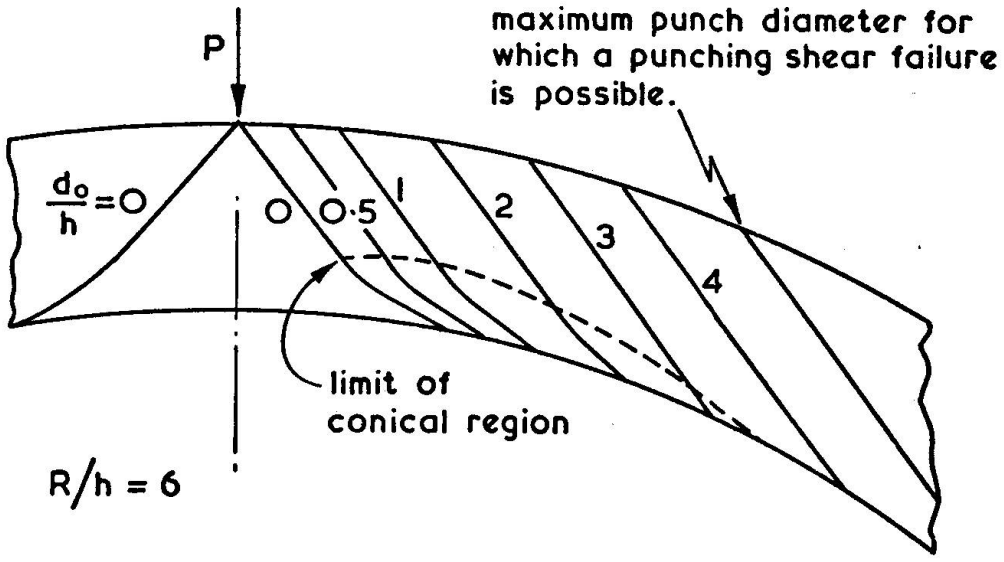

Fig. 3 Optimising curves for various punch diameters.

If the loaded area is large enough a punching shear failure is impossible because the cone with slope $\tan\phi = 3/4$ never intersects the inner surface of the shell. In these circumstances some other failure mode must intervene, presumably some form of bending failure. For punch diameters of practical interest, if the shell curvature is less marked, say R/h greater than about 10, the proportion of the optimal failure surface which is conical reduces as d_o/h increases, as in Braestrup's Fig. 8.

Some calculated failure loads are plotted in Fig. 4, which shows the dimensionless measure of failure load $P/\pi f_c h(d_o + 2h)$ used by Braestrup as a function of the shell curvature R/h for different punch diameters d_o/h. The increase of punching shear strength with shell curvature is clear.

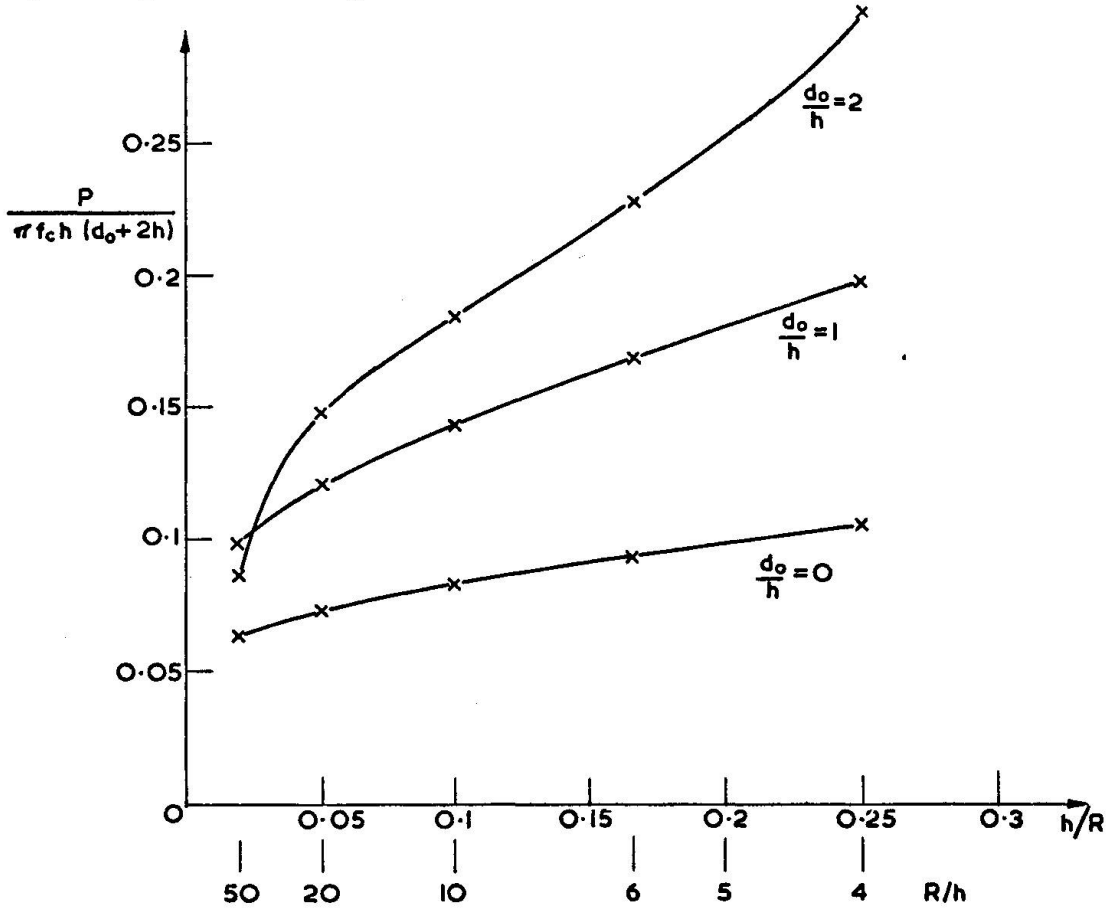

Fig.4 Theoretical failure load against curvature for a spherical shell.

5. SOME EXPERIMENTAL RESULTS ON CYLINDERS.

Some preliminary tests on concrete cylinders under concentrated radial load have recently been carried out in Cambridge by P. R. Hunter. The specimens were lengths of commercial spun-concrete sewer pipe, which were provided with diaphragms cast in situ and were supported on the laboratory floor all along a generator. The wall thickness was approximately 40 mm and the internal radius approximately 150 mm. The pipes had only nominal reinforcement, and small diameter cores drilled from them gave mean estimated cube strengths of 70.5 N/mm^2 for pipe 1, 57.5 N/mm^2 for pipe 2.

The pipes were loaded radially inwards through square steel plates cemented on to the concrete surface. Plates of various sizes were used, and in some cases pipes were retested with larger plates placed over the hole left by a previous test to failure. Various bending cracks developed during the tests, but in all cases failure occurred by punching out of a plug of concrete, square at the outer surface to match the steel loading plate. In the longitudinal cylinder direction the failure pieces were elongated as shown in Braestrup's Fig. 9, with the failure surface in some cases reaching to the nearest diaphragm. The failure pieces were much shorter in the hoop direction, as the present theory predicts, often with a steep failure surface close to the loading plate, corresponding to the predicted conical part of the failure surface.

Since the tests were on bought-in specimens the results were inevitably rather scattered, but some dimensionless failure loads are plotted in Fig. 5 against equivalent punch diameter. Also shown is the curve for a flat slab ($R/h \to \infty$) of concrete with a tensile strength f_t of $f_c/400$, from Braestrup's Fig. 10. The upper theoretical curves in Fig. 5 show the prediction of the theory for spherical shells having $f_t = 0$ and $R/h = 4$ and $R/h = 6$ respectively. For all the theoretical curves the yield strength f_c in compression is taken as 0.6 times the measured cube strength f_{cu}.

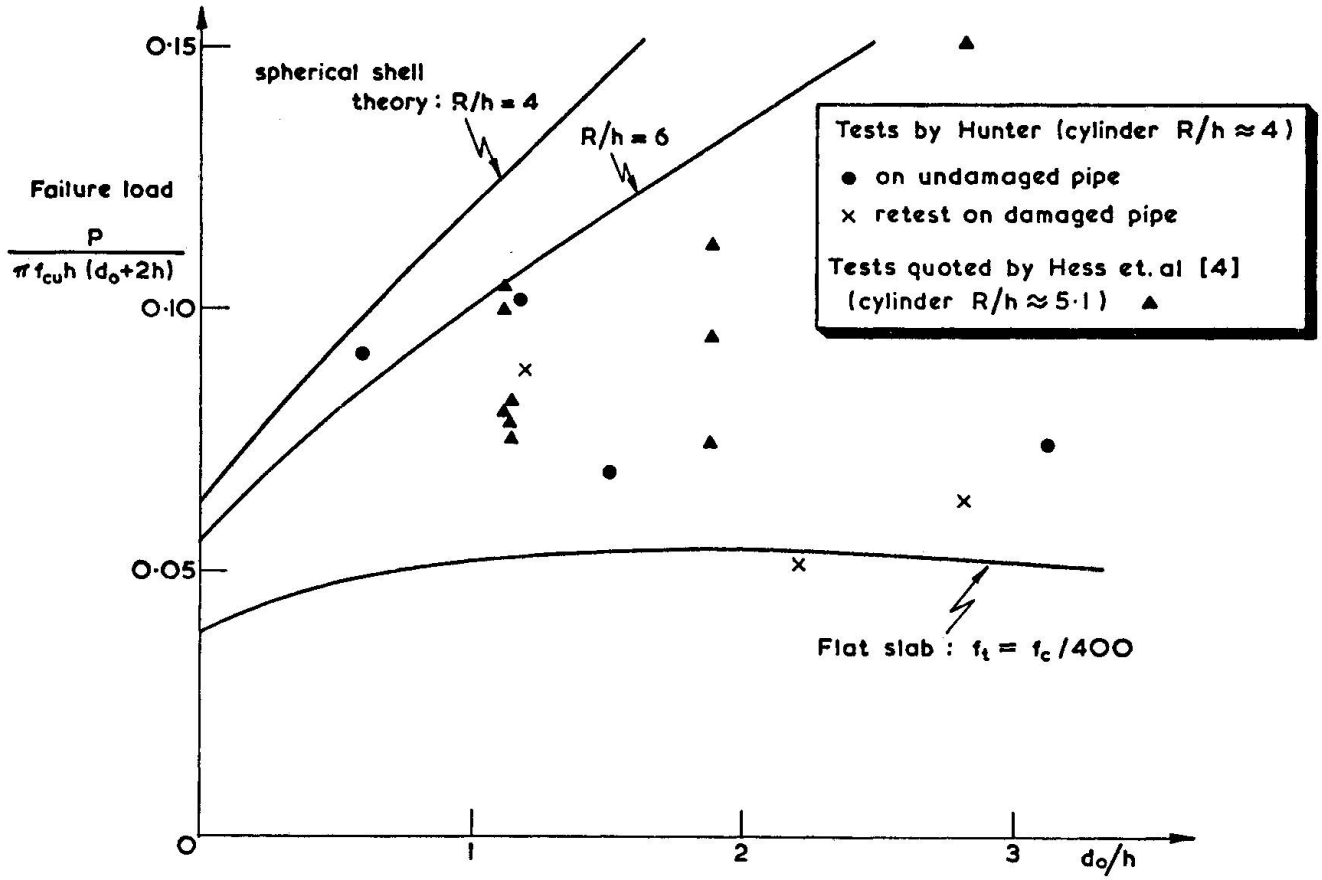

Fig. 5 Experimental results on cylinders in punching shear.

Also shown on the figure are some experimental results quoted by Hess [4] for cylinders with $R/h \approx 5.1$, taking the measured cylinder strength as 80% of the cube strength. These shells had about 1.6% of steel in the hoop direction.

One would expect the test results for cylinders to lie between the predictions for a sphere and a flat plate. This seems to be roughly true for small punch diameters, but the Cambridge results for larger punch diameters seem rather to follow the flat-plate predictions. Perhaps the large lateral compressive forces which should accompany the theoretical localised punching failure cannot easily be provided in a cylinder for large punch diameters, so that the failure mode is not pure punching but involves some bending. Clearly, more extended comparison of the theory with test results for spheres and cylinders is desirable.

6. CONCLUSIONS

A simple extension has been made to Braestrup's plastic theory of punching shear in flat slabs,to enable spherical shells with zero tensile strength to be treated. The theory predicts a substantial increase in failure load with shell curvature, but this increase is not very apparent in the results of the preliminary tests on cylindrical shells.

ACKNOWLEDGEMENT

I have had some very fruitful discussions with Dr. E. N. Fox, particularly about the application of the calculus of variations to this problem.

REFERENCES

1. Braestrup, M. W. Punching shear in concrete slabs. IABSE Colloquium on Plasticity in Reinforced Concrete, Copenhagen 1979, Introductory Report p. 115-136.

2. Pars, L. A. An introduction to the calculus of variations, Heinemann, London, 1962. 350 pp.

3. Irving, J. and Mullineux, N. Mathematics in physics and engineering. Academic Press, New York and London, 1959. 883 pp.

4. Hess, U. et. al. Gennemloking af jernbetonplader. Structural Research Laboratory, Technical University of Denmark, Report No. R 90, 1978, 63 pp.

III

Collapse of Reinforced Concrete Voided Slabs

La ruine de dalles en béton armé avec des ouvertures

Versagen von Stahlbetonhohlplatten

L.A. CLARK
Lecturer
University of Birmingham
Birmingham, England

SUMMARY
The paper derives an upper bound to the collapse load of a circular voided slab bridge simply supported along two opposite edges and loaded symmetrically. The critical mechanism involves flexural yield lines in combination with lines of shear failure.

RESUME
Une valeur supérieure est obtenue pour la charge ultime d'un pont-dalle avec des trous circulaires, appuyé simplement le long de deux bords opposés et chargé symétriquement. Le mécanisme critique implique des lignes de rupture causées par la flexion combinées avec des lignes de rupture causées par la flexion combinées avec des lignes de rupture causées par le cisaillement.

ZUSAMMENFASSUNG
Ein oberer Grenzwert für die Traglast einer symmetrisch belasteten, entlang zweier gegenüberliegender Seiten frei drehbar gelagerten Hohlplattenbrücke mit kreiszylindrischen Aussparungen wird hergeleitet. Der massgebende Mechanismus ist durch eine Kombination von Fliessgelenklinien und Schubbruchlinien gekennzeichnet.

1. INTRODUCTION

A reinforced concrete voided slab bridge tested at the Cement and Concrete Association [1] collapsed by the formation of a mechanism which involved lines of shear failure in addition to conventional flexural yield lines. The slab had a depth of void ratio of 0.786 and was loaded to collapse by means of a 16-wheel vehicle positioned centrally. The maximum load attained was 455 kN but this fell instantly to 414 kN. This load was held until longitudinal shear cracks formed near to the outer wheels of the vehicle when the load fell to 373 kN. On attempting to apply further load, longitudinal top and bottom flexural yield lines developed together with transverse hogging yield lines near to the supports. The central strip of slab, bounded by the longitudinal shear/flexural yield lines, then continued to rotate about the transverse hogging yield lines with distortion of two voids occurring. A theoretical analysis of such a collapse mechanism is considered in this paper.

2. UPPER BOUND ANALYSIS

2.1 Assumptions

It is assumed that the concrete is rigid-perfectly plastic, has a modified Coulomb yield criterion, zero tensile strength, compressive strength given by $f_e = \nu f_c$ where ν is an effectiveness factor and f_c is the cylinder strength which is assumed to be 80% of the cube strength, and the normality rule of plastic flow obtains. The reinforcement is assumed to be rigid-perfectly plastic and to carry only axial stresses.

2.2 Initial collapse

A general circular voided slab loaded symmetrically with respect to its centre is considered. The proposed initial collapse mechanism is shown in Fig. 1. The displacement rate ($\dot{\delta}$) is taken to be normal to the plane of the slab since the restraint of the rigid material each side of the shear failure lines is likely to prevent any outward movement of this material relative to the central portion of the slab.

If q is the ultimate shear per unit length measured in the span direction, m and αm are the sagging and hogging longitudinal moments of resistance respectively, P is the total applied load and w is the self weight of the slab per unit area, then the work equation is

$$P = \frac{2}{(2\ell-c-2d)} \left\{4m\,(b_b + \alpha b_t) + \left[2q - w\,(b_t + b_b)\right] (\ell^2-d^2)\right\} \qquad (1)$$

The minimum value of P is obtained when

$$\ell = \frac{c+2d}{2} + \sqrt{\frac{c^2+4cd}{4} + \frac{4m\,(b_b+\alpha b_t)}{2q - w\,(b_t+b_t)}} \qquad (2)$$

2.3 Value of q.

The value of q is obtained by considering the dissipation rate per unit length, measured in the span direction, of the concrete and of any vertical stirrups crossed by the shear failure line. The dissipation rate in the concrete is given by [2]

$$\dot{D}_c = 0.5 f_e \ell_e (1-\cos\theta)\dot{\delta}_x$$

where ℓ_e is the length of concrete in the failure line and δ_x is the displacement rate at a particular section x.

The dissipation rate in the stirrups is given by

$$\dot{D}_s = n A_{ss} f_{ys} \dot{\delta}_x$$

Where n is the number of rows of stirrups crossed by the failure line, A_{ss} is the area per unit length measured in the span direction of the stirrups and f_{ys} is the yield stress of the stirrup reinforcement.

Hence $$q = 0.5 f_e \ell_e (1-\cos\theta) + n A_{ss} f_{ys} \quad (3)$$

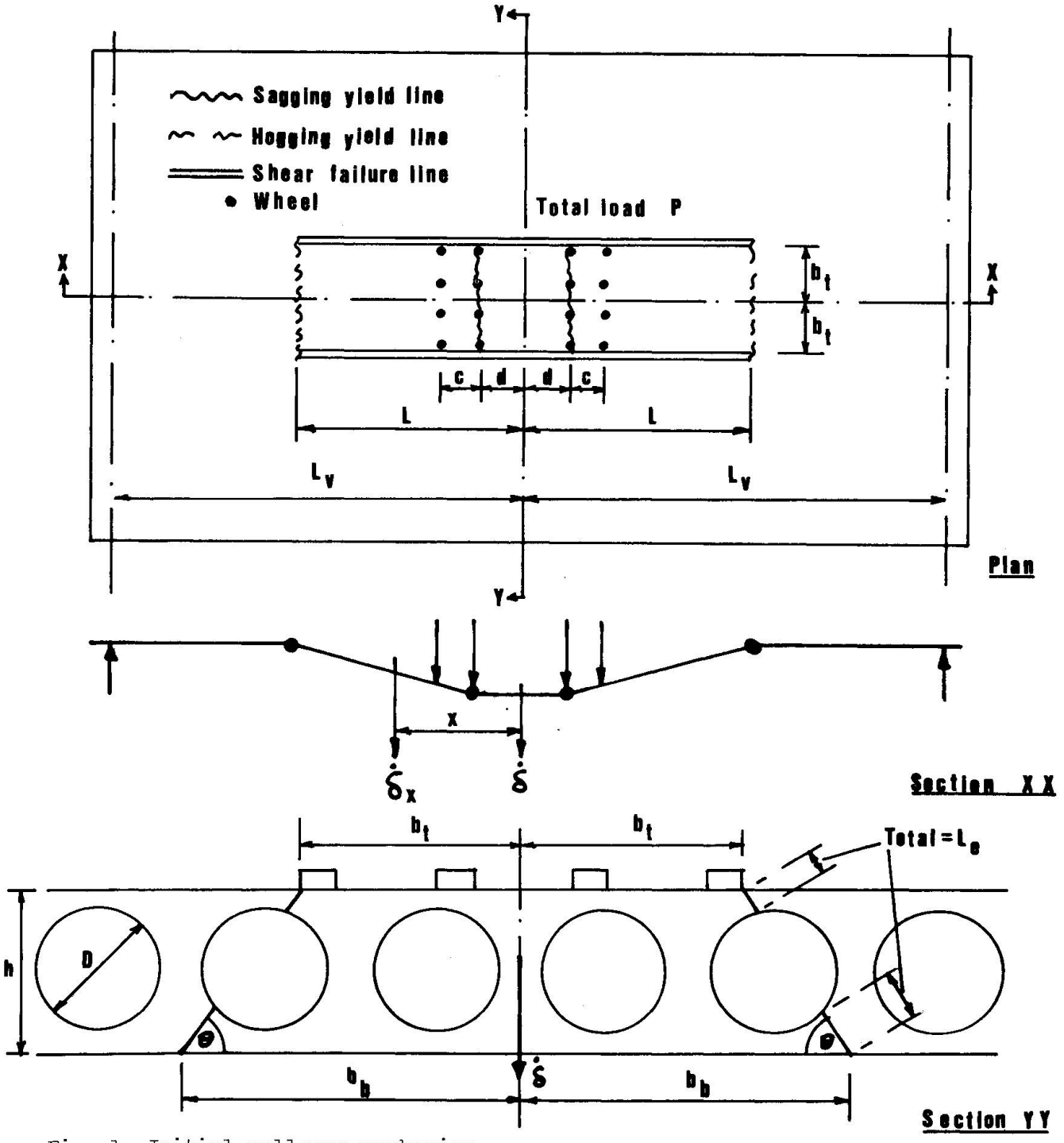

Fig. 1 Initial collapse mechanism

2.4 Value of ν

The effectiveness factor (ν) reflects the ductility of the concrete in compression and depends upon the concrete strength and the conditions under which the the concrete is stressed. However very little experimental evidence is available for voided slabs although ASTER [3] has tested a transverse strip of a slab with a depth of void ratio of 0.75 and having no shear reinforcement. An analysis indicates that ν = 0.13 which is small because of the flexibility of the cross-section of a voided slab and of the discontinuous failure surface.

2.5 Subsequent mechanism

It is proposed that after initial failure in accordance with the above mechanism, a subsequent mechanism involving distortion of the failed cells takes place as shown in Fig. 2.

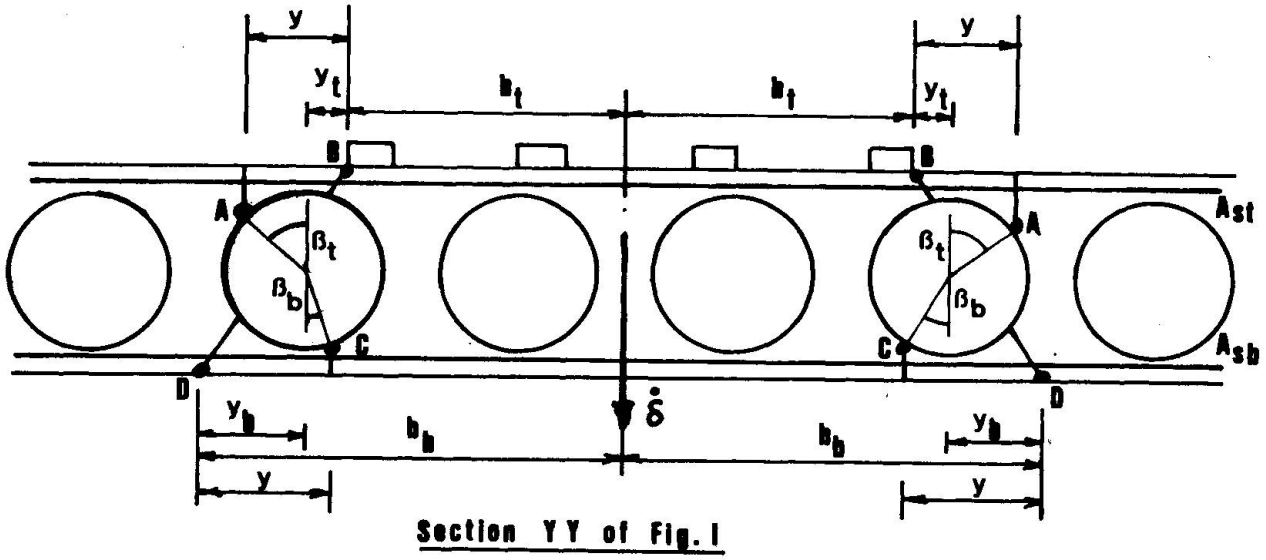

Fig. 2 Subsequent collapse mechanism

The positions of the centres of rotation B and D in Fig. 2 are determined by the initial shear failure and, of A and C, by minimising the load with the constraint that

$$y_t + \frac{D}{2} \sin \beta_t = y_b + \frac{D}{2} \sin \beta_b = y \qquad (4)$$

Assuming that, compared with the initial mechanism, the reduction in the rate of work of the self weight of the bottom flange is compensated by the increase of that of the top flange then the total rate of external work is unchanged. The dissipation rate in the mechanism is given by

$$\dot{D} = \dot{\delta} \left\{ 2m \frac{[(2b_b - y) + \alpha (2b_t + y)]}{\ell - d} + \frac{\zeta f_{yt} [A_{st} (h - D \cos \beta_t) + A_{sb} (h - D \cos \beta_b)] (\ell + D)}{y} \right\} \qquad (5)$$

where ζ is a membrane enhancement factor and f_{yt} is the yield stress of the transverse reinforcement in the flanges.

In general an analytical solution for a minimum P is unobtainable. However, if $y(1-\alpha)$ is small compared with $2(b_b + \alpha b_t)$ and $y_t \simeq y_b = \bar{y}$ so that $\beta_t \simeq \beta_b = \bar{\beta}$ then a minimum P is found for

$$\ell = \frac{c+2d}{2} + \sqrt{\frac{c^2+4cd}{4} + \frac{4m(b_b+\alpha b_t)}{\zeta\eta - w(b_t+b_b)}} \qquad (6)$$

where

$$\eta = \frac{f_{yt}\,(A_{st}+A_{sb})(h-D\cos\bar{\beta})}{\bar{y}+0.5\,D\sin\bar{\beta}} \qquad (7)$$

and

$$\tan\bar{\beta}/2 = \frac{h-D}{2y + \sqrt{4\bar{y}^2 + h^2 - D^2}} \qquad (8)$$

3. COMPARISON WITH TEST DATA

3.1 Initial failure

Dimensions relating to the failure line were observed to be $\theta = 48.4^\circ$ $\ell_e = 151$ mm, $y_t = 122$ mm, $y_b = 126$ mm, $2b_t = 596$ mm, $2b_b = 1092$ mm and $n = 0$.

The concrete cube strength was 52.3 N/mm^2 and if ν is taken to be the value derived from the analysis of Aster's strip then $f_e = 5.44$ N/mm^2. Equation 4 then gives, with $n = o$, $q = 0.138$ kN/mm

The sagging and hogging longitudinal moments of resistance are respectively 137 and 21.5 kNm/m; thus $\alpha = 0.157$. The other relevant data are $\ell_v = 2650$ mm, $c = 450$ mm, $d = 225$ mm and $w = 3.46$ kN/m^2.

From equation 2, $\ell = 1608$ mm whereas the observed value was 2370 mm; and, from equation 1, P = 878 kN which is much greater than the peak load of 455 kN attained or the load of 414 kN at which the slab 'yielded' in shear.

An explanation of this gross overestimate of the collapse load could be that when the slab first fails in shear only the concrete in the immediate vicinity of the load is deformed sufficiently to 'yield' in shear and that once the slab commences to 'yield' in shear the deformations in the vicinity of the load are too large for aggregate interlock to occur across the shear crack and the dissipation rate in the vicinity of the load falls to zero. It might thus be more appropriate to ignore the dissipation rate in those parts of the lines of shear failure which extend beyond the loading vehicle when calculating the peak load, and to ignore the dissipation rate in those parts of the lines of shear failure within the length of loading vehicle when calculating the lower load at which 'yield' of the slab in shear occurs.

3.2 Estimate of peak load

Neglecting the dissipation rate in those parts of the shear failure lines beyond the loading vehicle, the peak load is given by

$$P = \frac{2}{2\ell-c-2d}\left\{4m(b_b+\alpha b_t) + 2q\left[2(c+d)(\ell-d)-c^2\right] - w(b_t+b_b)(\ell^2-d^2)\right\} \qquad (9)$$

For a minimum P, it is found that $\ell = \ell_v$ and thus the peak load is estimated to be 523 kN which should be compared with the observed peak load of 455 kN.

3.3 Estimate of shear yield load.

Neglecting the dissipation rate in those parts of the shear failure lines within the loading vehicle, the yield load is given by

$$P = \frac{2}{2\ell-c-2d}\left[4m(b_b+\alpha b_t) + 2q(\ell-c-d)^2 - w(b_t+b_b)(\ell^2-d^2)\right] \quad (10)$$

For a minimum P, it is found that

$$\ell = \frac{c+2d}{2} + \sqrt{\frac{c^2+4cd}{4} + \frac{4m\,(b_b+\alpha b_t)-2qcd}{2q - w(b_b+b_t)}} \quad (11)$$

from which ℓ = 1563 mm and the yield load, from equation 10, is 481 kN which should be compared with the observed yield load of 414 kN.

3.4 Subsequent mechanism

ζ is taken to be 2. It is reasonable to take $\bar{y}$ as the mean of y_t and y_b and thus $\bar{y}$ = 124 mm. Then from equation 9, $\bar{\beta}$ = 12.4°; from equation 8, η = 0.0499; from equation 7, ℓ = 2322 mm; and P = 425 kN. The observed values of $\bar{\beta}$, ℓ and P were 14°, 2370 mm and 373 kN. The calculated load exceeds the observed value by 14%.

4. CONCLUSIONS

Upper bounds to the collapse load of a circular voided reinforced concrete slab bridge loaded symmetrically have been presented. The analysis overestimates the peak, shear and distortional yield loads by 15%, 16% and 14% respectively. However, a number of simplifications and, in some cases, somewhat arbitrary assumptions have been made in the analysis.

REFERENCES

1. ELLIOT, G., CLARK, L.A. and SYMMONS, R.M. Test of a quarter scale reinforced concrete voided slab bridge. London, Cement and Concrete Association. Technical Report 42.527 to be published.

2. NIELSEN, M.P. and BRAESTRUP, M.W. Plastic shear strength of reinforced concrete beams. Bygningsstatiske Meddelelser. Vol. 46, No. 3 September 1975. pp 61-99.

3. ASTER, H. The analysis of rectangular hollow reinforced concrete slabs supported on four sides. Ph.D. Thesis, University of Stuttgart. April 1968.

5. APPENDIX

5.1 Membrane enhancement factor

The mechanism shown in Fig. 2 neglects any membrane action in the flanges although such action must take place. In order to allow for membrane action, the enhancement factor (ζ) is introduced in equation 5.

If full lateral restraint is assumed, the enhancement factor can be assessed by considering the transverse section of a flange as a beam.

Since full restraint will not occur, and in the absence of a complete analysis of the membrane effects, ζ is estimated in this paper to be 50% of the full restraint value.

III

Application of the Yield-Line Theory for Reinforced Concrete Slabs allowing for Membrane Effects

Application de la théorie des lignes de rupture aux dalles en béton armé en considérant les effets de membrane

Anwendung der Fliessgelenklinientheorie bei Stahlbetonplatten mit Berücksichtigung der Wirkung von Membrankräften

D. KLEIN
Institut für Massivbau
Technische Hochschule
Darmstadt, Fed. Rep. of Germany

G. MEHLHORN
Institut für Massivbau
Technische Hochschule
Darmstadt, Fed. Rep. of Germany

SUMMARY
The paper presents two methods for calculating the influence of in-plane forces on the load bearing capacity of reinforced concrete slabs. The results are examined by a finite element analysis of an example.

RESUME
On présente deux méthodes pour calculer l'influence des effets de membrane sur la charge ultime des dalles en béton armé. Les résultats sont comparés avec ceux d'une analyse utilisant la méthode des éléments finis, dans un cas concret.

ZUSAMMENFASSUNG
Es werden zwei Methoden zur Untersuchung des Einflusses von Normalkräften auf die Traglast von Stahlbetonplatten vorgestellt. Die Ergebnisse werden an einem Beispiel durch eine Vergleichsrechnung nach der Finite Elemente Methode überprüft.

1. INTRODUCTION

The load bearing capacity of reinforced concrete slabs with restrained edges is higher than predicted by the conventional yield-line theory. The prevention of the outward expansion causes an in-plane compressive force within the slab which provides a higher moment capacity than is assumed by the yield-line theory. In the presented paper the solution of several research workers (for example Morley [1]), who have extended the yield-line theory by including the in-plane forces as generalized stresses for the assumption of a rigid perfectly - plastic material, is compared to a more realistic solution in which the condition of the inextensibility of the slab parts is deleted. It is assumed that the slab will behave elastically within its plane. An approach is developed to estimate the in-plane forces due to constraints which are induced by the reduction of the strains and cracking during slab deflection.

The results of the extended yield-line theory including in-plane forces are examined by a finite element analysis of reinforced concrete slabs. With a program system that was developed in Darmstadt [2], [3], the realistic behaviour of reinforced concrete slabs can be calculated by considering material and geometrical nonlinearities. The computational methods are demonstrated by a rectangular slab under uniform load, supported along three edges. In Fig. 1 the system and the idealization of the slab into elements is shown.

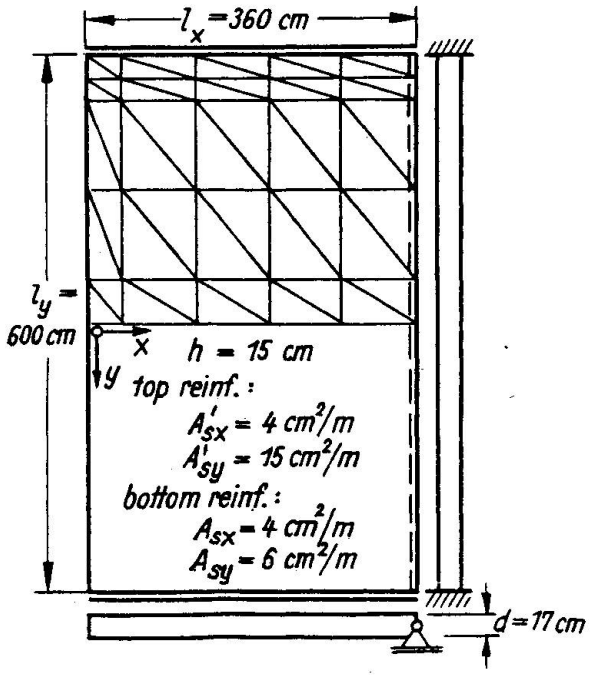

Fig. 1 System and Finite Element Idealization

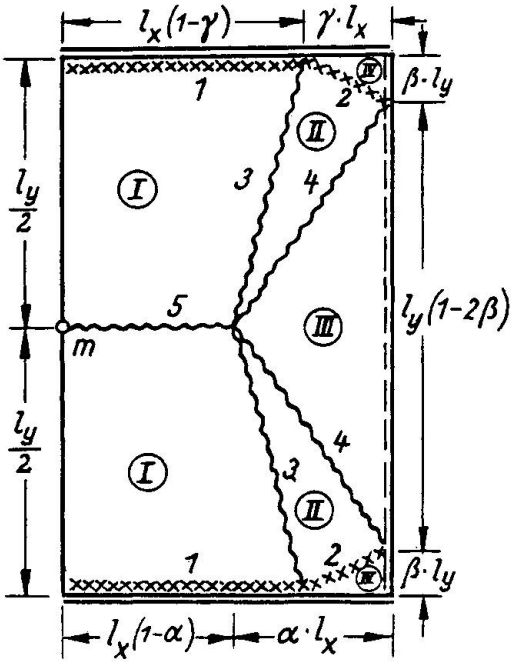

Fig. 2 Yield-Line Pattern with Three Parameters

2. LOAD BEARING CAPACITY INCL. INPLANE FORCES ASSUMING IDEAL-PLASTIC BEHAVIOUR

For the general case of a transversely loaded thin slab the failure will start in a flexural mode. The in-plane forces induced as a secondary effect have only little influence on the failure mode, so that the yield line pattern of the conventional yield line theory for pure bending can be used as a failure mechanism. In Fig. 2 the chosen three-parameter yield-line pattern is shown. With the dimensions indicated in Fig. 1, the yield strength of reinforcement, β_S = 420 N/mm^2 and the characteristic strength of the concrete, β_R = 25 N/mm^2, the lowest upper bound for the ultimate load is by application of the conventional yield-line theory p_o = 40,6 kN/m^2 with the inherent parameters α = 0,556, β = 0,094 and γ = 0,188.

In extension of the conventional yield-line theory, not only the bending moments but also the resulting in-plane forces normal to the yield lines are used as generalized stresses. By applying the principale of virtual work, the energy dissipated by the in-plane forces along the yield lines must be added to the dissipation density per unit length of the yield line

$$d_i = m \cdot \dot{\Theta} + n \cdot \dot{\Delta} \tag{1}$$

The moments m and forces n are connected by a moment-force-interaction as yield-condition. With a stress-distribution as shown in Fig. 3 the resulting moments and forces normal to the yield line are

$$m_{nn} = A_{sx}\beta_s e_x \cos^2\varphi + A_{sy}\beta_s e_y \sin^2\varphi + \beta_R a\left(b_o - \frac{1}{2}a\right) \tag{2}$$

$$n_{nn} = A_{sx}\beta_s \cos^2\varphi + A_{sy}\beta_s \sin^2\varphi - \beta_R \cdot a \tag{3}$$

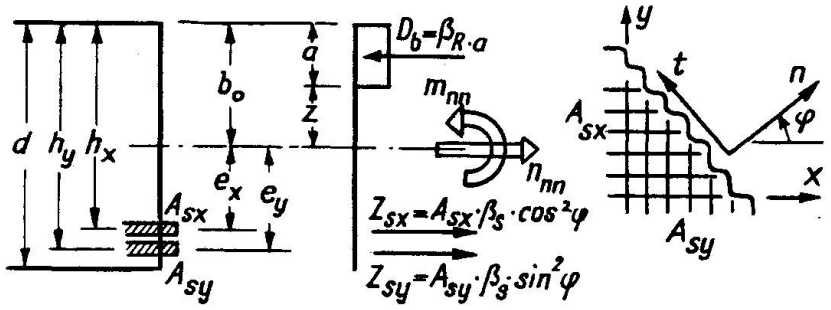

Fig. 3 Stress-Distribution Normal to Yield-Line

By elimination the depth a of the compression zone, the yield criterion becomes

$$F(m_{nn}, n_{nn}) \equiv m_{nn} + \left(b_o - A_{sx}\frac{\beta_S}{\beta_R}\cos^2\varphi - A_{sy}\frac{\beta_S}{\beta_R}\sin^2\varphi\right) n_{nn} + \frac{n_{nn}^2}{2\beta_R} = m_{nnF} \qquad (4)$$

where m_{nnF} stands for the yield-moment of the conventional yield-line theory. By application of the flow rule (normality law), a relation between the rate of rotation and the rate of deformation within the reference plane as an internal compatibility condition in the yield line is developed

$$\frac{\dot{\Delta}}{\dot{\Theta}} = b_o - a = z \qquad (5)$$

This condition states that the relative rotation axis between two slab parts is identical with the neutral axis. A rotation of the rigid slab parts is only possible, if the rotation axes are horizontal, so that the height of each of the relative rotation axis during the actual deflection under developed failure mechanism can be defined by one parameter, for example the depth of the compression zone a at any point of the yield-line. In Fig. 4 the failure mechanism is shown in the elevation and the rates of displacements of the relative rotation axes by a virtual rate of deflection $\dot{w}_m$ are indicated.

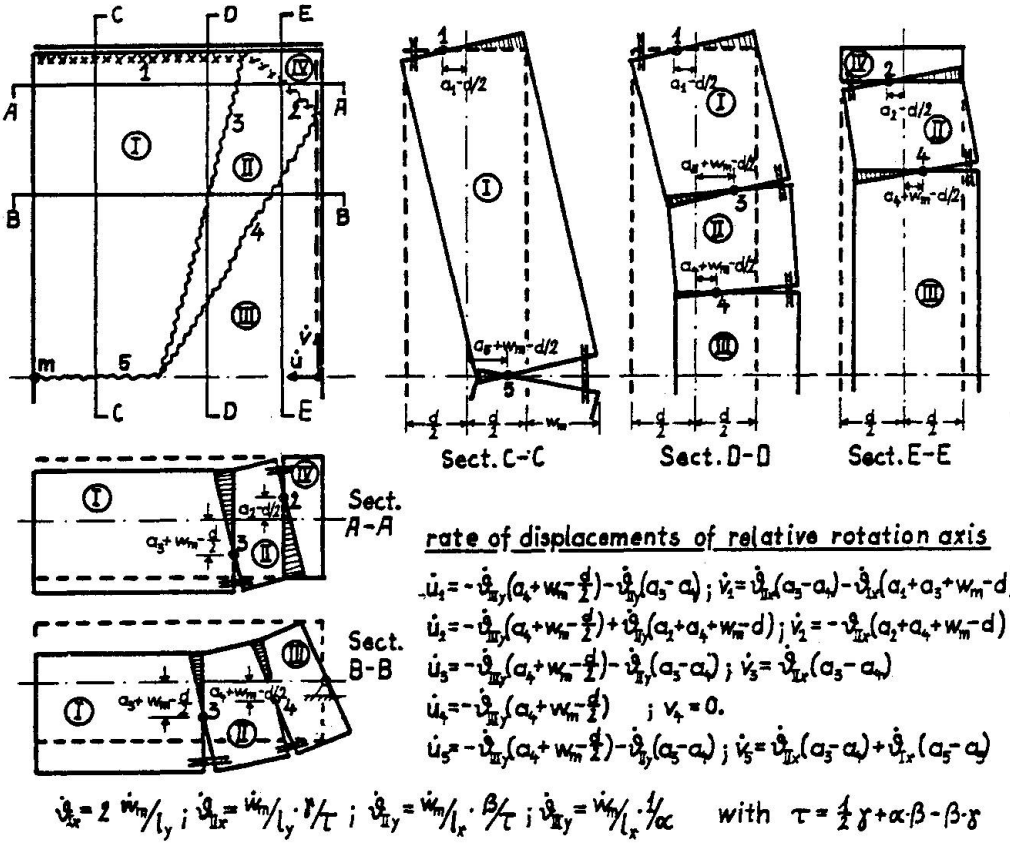

Fig. 4 Failure Mechanism in the Elevation

Eqs. (1), (2), (3) and (5) define the internal energy that is dissipated per unit length of a yield-line during a virtual rate of plastic rotation

$$d_i = \left[A_{sx}\beta_s(h_x-a)\cos^2\varphi + A_{sy}\beta_s(h_y-a)\sin^2\varphi + \frac{1}{2}a^2\beta_R\right]\cdot\dot{\Theta} \tag{6}$$

By equating the total internal and external virtual work, the depth of the compression zones of the five yield-lines, a_1 to a_5, remain unknown. If the clamped edges are fixed in their plane, the rate of displacements of yield-lines nr. 1 and 2 and because of symmetry also of nr. 5 must be zero. By the three conditions $\dot{v}_1 = 0$, $\dot{v}_2 = 0$ and $\dot{v}_5 = 0$ ($\dot{v}$ see Fig. 4) three parameters can be eliminated. The remaining two parameters must be computed by minimizing the ultimate load. This results in a failure load dependent on the actual deflection

$$p_1\left[\frac{kN}{m^2}\right] = 84{,}7 - 3{,}8\ w_m + 0{,}16\ w_m^2 \tag{7}$$

3. ESTIMATION OF THE SELF-INDUCED IN-PLANE FORCES FOR ELASTIC PLATE STRETCHING

The derivation in the preceeding section assumes that the stress-strain-relation of the concrete as well as the reinforcement is ideally-plastic. In reality, however, the stresses of the concrete in the compression zone remain in the elastic range. The flexural response of the slab is well represented by plastic behaviour as soon as the yield point of the reinforcement is exceeded. The in-plane forces, however, are transferred across the yield line mainly by the concrete, so that even in the plastic range of the reinforcement, the plate is deformed elastically in its plane.

To compute the in-plane forces which are induced prior to failure the cracked slab is considered to be an elastic orthotropic panel. It is assumed that the concrete only transfers compression stresses and that shear stresses are possible only in the uncracked zone. Poisson's effect is neglected. If the cross-section remains plane after deflection, the relations between the resultant stresses and the strains within the reference plane are:

$$n_{xx} = K_{xx}\left[\varepsilon_{xx} - \left(b_o - b_{sx}\right)\left|\frac{\partial^2 w}{\partial x^2}\right|\right];\quad n_{yy} = K_{yy}\left[\varepsilon_{yy} - \left(b_o - b_{sy}\right)\left|\frac{\partial^2 w}{\partial y^2}\right|\right]$$
$$n_{xy} = \frac{1}{2}a_{xy}E_b\left[\varepsilon_{xy} - \left(b_o - \frac{1}{2}a_{xy}\right)\left|\frac{\partial^2 w}{\partial x\,\partial y}\right|\right] \tag{8}$$

with $$K_{xx} = \left(A_{sx} + A'_{sx}\right)E_s + a_{xx}E_b\ ;\quad K_{yy} = \left(A_{sy} + A'_{sy}\right)E_s + a_{yy}E_b \tag{9}$$

and the distance of the elastic centroid from the compression side of the slab

$$b_{sx}=\frac{1}{K_{xx}}\left[E_s\left(A_{sx}h_x+A'_{sx}h'_x\right)+\frac{1}{2}E_b a_{xx}^2\right];\ b_{sy}=\frac{1}{K_{yy}}\left[E_s\left(A_{sy}h_y+A'_{sy}h'_y\right)+\frac{1}{2}E_b a_{yy}^2\right] \quad (10)$$

It is assumed that the deflection surface w(x,y) is known and that the in-plane forces do not influence the deflection. Then eqs. (8) to (10), together with the equilibrium conditions and the strain deformation relations within the reference plane

$$\varepsilon_{xx}=\frac{\partial u}{\partial x}+\frac{1}{2}\left(\frac{\partial w}{\partial x}\right)^2;\ \varepsilon_{yy}=\frac{\partial v}{\partial y}+\frac{1}{2}\left(\frac{\partial w}{\partial y}\right)^2;\ \varepsilon_{xy}=\frac{\partial u}{\partial y}+\frac{\partial v}{\partial x}+\frac{1}{2}\frac{\partial w}{\partial x}\cdot\frac{\partial w}{\partial y} \quad (11)$$

form a complete system of equations to resolve the planar problem. An exact solution of the problem, however, is impossible as the depth of the compression zone varies over the slab region and is a function of the induced in-plane forces. As an approximation for the active part of the section of the concrete, the compression zone of the cross-section under uniaxial, elastic bending and normal forces is chosen

$$a_{xx}=-\left(A_{sx}+A'_{sx}\right)\frac{E_s}{E_b}+\sqrt{\left(A_{sx}+A'_{sx}\right)^2\frac{E_s^2}{E_b^2}+2\left(A_{sx}h_x+A'_{sx}h'_x\right)\frac{E_s}{E_b}-\frac{2n_{xx}}{E_b\left|\frac{\partial^2 w}{\partial x^2}\right|}} \quad (12)$$

To estimate the membrane forces along the yield-lines, further assumptions are necessary. If a horizontal movement of only the clamped edges is prevented and the slab is able to deform freely in the x-direction, the in-plane forces in this direction may be neglected, $n_{xx} = 0$, and n_{yy} may be constant in the y-direction.

As boundary condition, the elongation of the slab in the y-direction must be zero, so that the integration yields

$$\int_{l_y}\frac{\partial v}{\partial y}dy=0=n_{yy}\cdot\int_{l_y}\frac{dy}{K_{yy}}-\frac{1}{2}\int_{l_y}\left(\frac{\partial w}{\partial y}\right)^2dy+\int_{l_y}\left(b_o-b_{sy}\right)\left|\frac{\partial^2 w}{\partial y^2}\right|dy \quad (13)$$

With a deflection surface $w=w_m\cdot\left(1-2\frac{x^3}{l_x^3}+\frac{x^4}{l_x^4}\right)\cdot\left(1-8\frac{y^2}{l_y^2}+16\frac{y^4}{l_y^4}\right)$, (14)

the in-plane forces are determined by eq. (13). The solution of eq. (13) is possible only by an iterative process resulting in

$$n_{yy}\left[kN/cm\right]=0{,}21\,w_m^2\left(1-2\frac{x^3}{l_x^3}+\frac{x^4}{l_x^4}\right)^2-3{,}6\,w_m\left(1-2\frac{x^3}{l_x^3}+\frac{x^4}{l_x^4}\right) \quad (15)$$

Now the load bearing capacity of the slab can be calculated by conventional yield-line theory with a yield moment m_{nn} that is related to the in-plane force $n_{nn} = n_{yy} \sin^2\varphi$ by eq. (4). The action of the in-plane forces at the deformed system is taken into account, if the variation of the position of the cross-section to the reference plane during the deflection (see Fig. 4) is considered. Numerical calculations result in

$$p_2 \left[kN/m^2\right] = 40{,}6 + 9{,}57\, w_m - 1{,}83\, w_m^2 + 0{,}112\, w_m^3 - 0{,}0022\, w_m^4 \qquad (16)$$

4. COMPARISON OF YIELD-LINE SOLUTION WITH THE RESULTS OF FINITE ELEMENT COMP.

To demonstrate the influence of edgerestraint on the load-bearing capacity, in Fig. 5 the strain distributions of the elements along the free edge are shown and compared with the freely movable system at the same load stage. In Fig. 6 the variation of the in-plane forces with increasing deflection are shown. The agreement of the approximation with the results of the FEM is sufficient. Fig. 7 shows the non-dimensionalized load-deflection curves. Although the assumption of elastic plate stretching yields better results than by rigid ideal-plastic behaviour, the ultimate load is overestimated. In the finite element approach failure is reached when the compression stresses of the concrete violate a failure criterion in the biaxial stress state. This happens for the slab with fixed edges before a flexural failure in the plastic range is evident. In [4] the assumptions of the extended yield-line theory are described in detail together with further examples.

5. REFERENCES

[1] MORLEY, C. T.: Yield line theory for reinforced concrete slabs at moderately large deflections, Magazine of Concrete Research, Vol. 19, No. 61, Dec. 1967, pp. 212 - 222.

[2] KLEIN, D./KRISTJANSSON, R./LINK, J./MEHLHORN, G./SCHÄFER, H./SCHNEIDER, K.: Zur Berechnung von dünnen Stahlbetonplatten bei Berücksichtigung eines wirklichkeitsnahen Werkstoffverhaltens. Forschungsberichte aus dem Institut für Massivbau der TH Darmstadt, Heft Nr. 32, 1976.

[3] KRISTJANSSON, R.: Physikalisch und geometrisch nichtlineare Berechnung von Stahlbetonplatten mit Hilfe Finiter Elemente. Dissertation Darmstadt 1977.

[4] KLEIN, D.: Anwendung der Fließgelenklinientheorie zur Berechnung von Stahlbetonplatten unter Berücksichtigung der Membrankräfte, Dissertation Darmstadt, 1979.

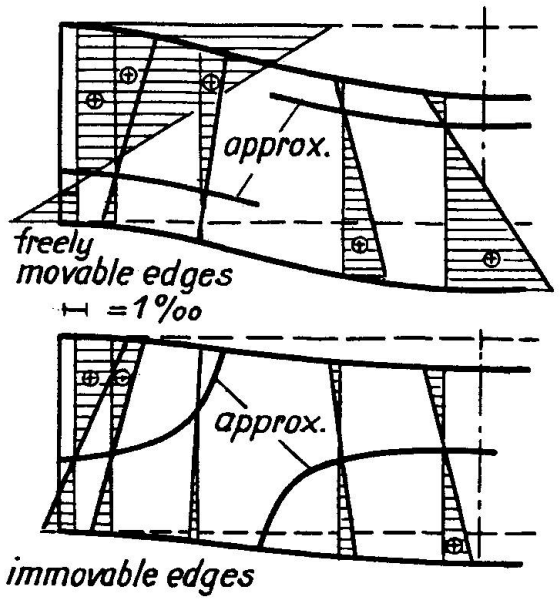

Fig. 5 Strain-Distribution and Assumed Compression Zones

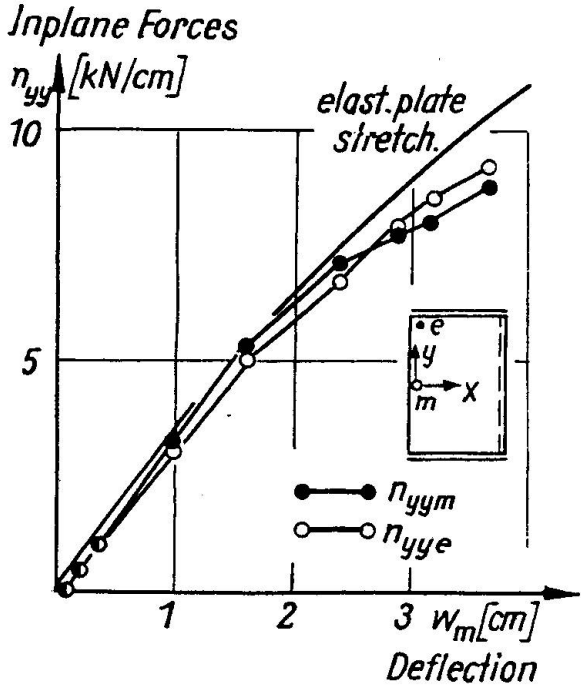

Fig. 6 Development of In-Plane Forces

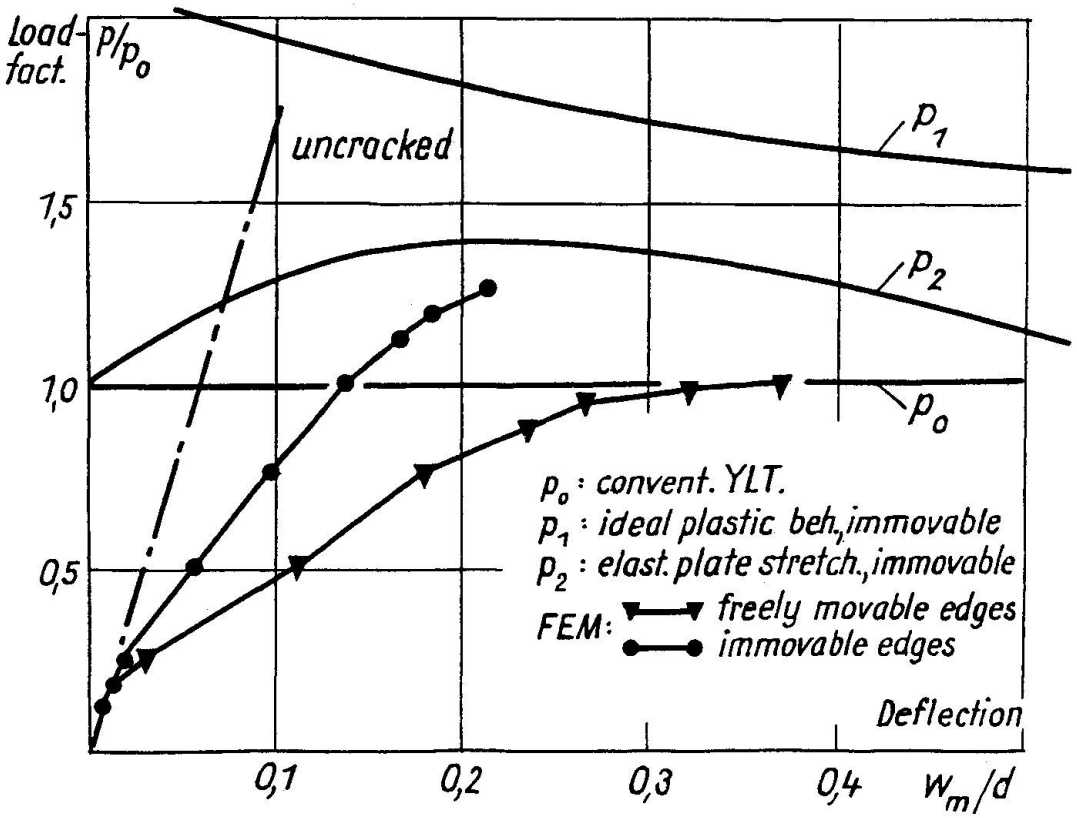

Fig. 7 Load-Deflection Relations

III

Computer Aided Optimum Design of Concrete Slabs

Minimalisation de l'armature des dalles à l'aide de l'ordinateur

Computerunterstützte optimale Bemessung der Armierung von Platten

E. ANDERHEGGEN
Professor of Applied Computer Science
Swiss Federal Institute of Technology
Zurich, Switzerland

J. THEILER
Research Associate
Swiss Federal Institute of Technology
Zurich, Switzerland

SUMMARY

A computer based optimum design procedure satisfying various practical design constraints is presented for finding the minimum weight reinforcement distribution for concrete slabs. The procedure uses finite element analysis and is derived from the shake-down theorem of the theory of plasticity. The approach used represents a combination of automatic optimum design and interactive computer aided design methods.

RESUME

Le rapport présente une méthode servant à minimaliser le volume d'armature des dalles en béton armé tout en tenant compte de certaines conditions dictées par la pratique. Le procédé utilise la méthode des éléments finis et est basé sur le théorème fondamental de la théorie de la plasticité. Le programme de dimensionnement offre à l'utilisateur la possibilité de modifier les données pendant le déroulement du programme.

ZUSAMMENFASSUNG

Es wird eine den praktischen Gegebenheiten angepasste Methode zur optimalen Bemessung der Armierung von Platten beschrieben. Das Verfahren benützt die Methode der Finiten Elemente und basiert auf dem Einspielsatz der Plastizitätstheorie.
Es ist ein computerunterstütztes interaktives Bemessungsverfahren mit automatischen Optimierungsalgorithmen.

1. INTRODUCTION

This paper reports on a research project presently in progress. While the main ideas on which the project is based seem today to be well understood, the development of the complex computer program needed for practical applications has not yet reached the stage where numerical results can be obtained. Therefore general conclusions concerning the applicability of the suggested design method can not be drawn yet. Experience also shows that the final system might look considerably different as it is planed today.

The aim of the project is the development of a computer based design procedure for finding the minimum weight reinforcement for concrete slabs of given geometry subjected to any kind of dead- and life-loads taking into account different kinds of practical design restrictions. Only the plate-bending action of the slabs shall be considered.

Most practically oriented civil engineers are rather sceptical towards automatic optimum design procedures. They feel - with good reasons - that the process of designing real-life structures involves too much personal experience, feeling and imagination to be left to a computer program developed by some stranger. Today much more attention is paid to interactive computer aided design methods, where the computer only checks given designs while the task of finding an "optimum", whatever that means, is left to the designer. The main problem of this approach is to make man - machine - communication so easy and to have the computer answering so quickly that some kind of a dialog between the designer sitting in front of a terminal and the computer becomes possible.

The procedure discussed here represents a combination of both approaches: while the designer is still expected (at least in the final stages of the design process) to interact with the computer sitting in front of a terminal, the computer, whenever requested, will have to perform optimality search by linear programming methods and show his results quickly and clearly. In fact, the chances that such an approach will prove useful for real-life problems rely on the facts that today's computers (a DEC-10 is used for this project) are powerful enough for performing complex calculations without keeping the user waiting too long, that man - machine communication, specially due to computer graphics, has become easy and also that the problem considered while of considerable practical significance, is one of the best suited for optimum design procedures based on the theory of plasticity.

2. THEORETICAL BACKGROUND AND OVERVIEW OF THE DESIGN METHOD

The design method suggested here is based on the shake-down theorem of the plasticity theory and was first used for framed structures by one of the co-authors in 1965 (see [1,2]). When applied to plate-bending problems the shake-down theorem says that if it is possible to find any distribution of residual moments (i.e. any homogeneous stress state) which, combined with the ideal-elastic moment distribution for every possible loading case, nowhere violates the plasticity conditions, then the structure will eventually stabilize or "shake-down" for any possible loading cycle.

With the usual assumption that reinforcement has no influence on the elastic behaviour of concrete structures, the moment distributions due to external loads can be obtained by linear-elastic finite element analysis. By prescribing as additional unit load cases different initial curvature distributions any number of residual homogeneous moment distributions can also be obtained by finite element analysis. The design problem can then be stated as follows:

A linear combination of these unit load cases leading to an optimum residual homogeneous moment distribution has to be found and added to the linear-elastic moment envelopes due to the external loads. Optimality is achieved when the weight of the reinforcement needed for the combined moment envelopes is minimal. According to the shake-down theorem, this procedure will result in the design of a structure where plastic deformations may only occur during the first load cycles, which is certainly an appropriate design criterion for reinforced concrete slabs.

Assuming that the plastic resistances needed to satisfy the plasticity conditions for the combined moment envelopes throughout the slab are linear functions of the amount of reinforcement in a number of chosen "check-points", the optimum design problem stated above can be formulated as a linear program for minimizing the total steel weight. The unknown parameters to be determined are the cross-sectional areas A_1 to A_{NG} of NG predefined groups of steel bars as well as the amplitude-factors X_1 to X_{NH} multiplying each of the NH homogeneous load cases considered.

The user of this computer-based design procedure will have to specify length, position and direction of different groups of steel bars (possibly of several alternative groups among which the linear program algorithm will look for a minimum weight solution) as well as a number of homogeneous unit load cases to be used for optimization. These will be specified by introducing a constant unit initial curvature in a given direction in one or more elements of the linear-elastic finite element model.

All static calculations, both for the external loads and for the initial curvature loads are performed by linear-elastic finite element analysis. The hybrid model with triangular and quadrilateral linear-moment plate-bending elements described in [3] and [4] is used for this purpose. Shear deformations are not be taken into account. Column-supports and elastic foundations are treated by means of "elastically" supported elements.

3. DERIVATION OF THE LINEAR PROGRAM

The total steel weight or the total steel volume V of NG predefined groups of steel bars is to be minimized. Each of these groups covers a rectangular or a parallelogram-shaped portion of the slab of length L_g (g = 1 to NG) and is positioned near the top or the bottom surface of the slab for providing negative or positive bending resistance. If A_g denotes the total cross-sectional area of all bars of given length L_g belonging to the g-th bar group, the design optimality criterion can be expressed in scalar or matrix notation as follows:

$$V = \sum_{g=1}^{NG} L_g \cdot A_g = \{L\}^T\{A\} \quad \rightarrow \quad \text{Minimum} \qquad (1)$$

The plasticity conditions will be checked in a sufficiently large number NC of "check-points" chosen in such a way that no violation will occur elsewhere in the slab. This is done by using the following well-known plasticity conditions valid for relatively low degrees of reinforcement:

$$-n_\varphi \leq m_\varphi \leq p_\varphi \qquad (2)$$

where n_φ, p_φ and m_φ represent the negative and positive bending resistances and the bending moment in any direction φ. As suggested by Wolfensberger [5] the angle φ can be eliminated and the non-linear conditions Eq. (2) can be linearized by introducing eight linear inequality constraints for the bending and twisting moments m_x, m_y, and m_{xy} in two orthogonal coordinate directions x and y. In matrix

notation these eight inequalities for a check-point c (c = 1 to NC) are given by:

$$\begin{aligned} \{m_c\}_{max} &\leq \{p_c\} \\ -\{m_c\}_{max} &\leq \{n_c\} \end{aligned} \tag{3}$$

where the moment-envelope vectors $\{m_c\}_{max}$ and $\{m_c\}_{min}$ and the positive and negative resistance vectors $\{p_c\}$ and $\{n_c\}$ are defined by:

$$\{p_c\} = \begin{Bmatrix} P_x + P_{xy} \\ P_x - P_{xy} \\ P_y + P_{xy} \\ P_y - P_{xy} \end{Bmatrix} \text{at c} \qquad \{n_c\} = \begin{Bmatrix} N_x + N_{xy} \\ N_x - N_{xy} \\ N_y + N_{xy} \\ N_y - N_{xy} \end{Bmatrix} \text{at c} \qquad \{m_c\} = \begin{Bmatrix} m_x + m_{xy} \\ m_x - m_{xy} \\ m_y + m_{xy} \\ m_y - m_{xy} \end{Bmatrix} \text{at c} \tag{4}$$

A detailed derivation of the positive and negative plastic bending resistance coefficients P_x, P_y, P_{xy}, N_x, N_y and N_{xy} for orthogonal and non-orthogonal reinforcement can be found in [5].

If the reinforcement is relatively low it is reasonable to assume, at least for practical design purposes, that the plastic resistance vary linearly with the reinforcement, implying that this has no influence on the lever-arm of the internal forces. The resistance coefficients of the vectors $\{p_c\}$ and $\{n_c\}$ can then be expressed by linear functions of the reinforcement areas A_1 to A_{NG} as follows:

$$\begin{aligned} \{p_c\} &= [P_c]\{A\} \\ \{n_c\} &= [N_c]\{A\} \end{aligned} \tag{5}$$

where the coefficients of the 4xNG matrices $[P_c]$ and $[N_c]$ represent the resistance contributions due to a unit reinforcement area $A_g = 1$ provided that the c-th check-point lies within the surface of the slab covered by the g-th steel bar group.

The maximum and minimum moment-envelope vectors $\{m_c\}_{max}$ and $\{m_c\}_{min}$ introduced in Eq. (3) result, as explained earlier, from the superposition of the linear-elastic moment-envelopes $\{m_c^{ext}\}_{max}$ and $\{m_c^{ext}\}_{min}$ due to the external loads and the corresponding vector $\{m_c^{hom}\}$ due to NH homogeneous load cases of unknown amplitudes X_1 to X_{NH}. This leads to:

$$\begin{aligned} \{m_c\}_{max} &= \{m_c^{ext}\}_{max} + \{m_c^{hom}\} = \{m_c^{ext}\}_{max} + [H_c]\{X\} \\ \{m_c\}_{min} &= \{m_c^{ext}\}_{min} + \{m_c^{hom}\} = \{m_c^{ext}\}_{min} + [H_c]\{X\} \end{aligned} \tag{6}$$

the coefficients of the 4xNH matrix $[H_c]$ (as well as those of the vectors $\{m_c^{ext}\}_{max}$ and $\{m_c^{ext}\}_{min}$) being found by linear-elastic finite element analysis.

Introducing Eqs. (5) and (6) in Eq. (3) the eight plasticity conditions at a check-point c can be written as follows:

$$\begin{aligned} \{m_c^{ext}\}_{max} + [H_c]\{X\} &\leq [P_c]\{A\} \\ -\{m_c^{ext}\}_{min} - [H_c]\{X\} &\leq [N_c]\{A\} \end{aligned} \tag{7}$$

Design constraints formulated as maximum or minimum allowable reinforcement areas can also be introduced:

$$\{A_{min}\} \leq \{A\} \leq \{A_{max}\} \tag{8}$$

From Eqs. (1), (7) and (8) the following linear program for the unknowns X_1 to X_{NH} and A_1 to A_{NG} (see also Fig. 1) is obtained:

$$
\left.
\begin{aligned}
&V = \{L\}^T \{A\} \quad \rightarrow \quad \text{Minimum} \\
&0 \leq -\{m_c^{ext}\}_{max} - [H_c]\{X\} + [P_c]\{A\} \qquad (c = 1 \text{ to } N_c) \\
&0 \leq \{m_c^{ext}\}_{min} + [H_c]\{X\} + [N_c]\{A\} \qquad (c = 1 \text{ to } N_c) \\
&0 \leq -\{A_{min}\} + \{A\} \\
&0 \leq \{A_{max}\} - \{A\}
\end{aligned}
\right\} \qquad (9)
$$

This linear program can be considerably simplified. The minimum reinforcement inequalities can be immediately eliminated by introducing as design variables, instead of the A_g's, non-negative $\overline{A}_g$ parameters defined by:

$$\{\overline{A}\} = \{A\} - \{A_{min}\} \geq 0 \qquad (10)$$

Also, it will certainly not be necessary to formulate all eight linear plasticity conditions in all check-points. The values of the moment envelopes due to the external loads will show that many plasticity checks are most probably not necessary (e.g. positive moment checks over a column support) thus allowing a great reduction in the number of inequalities to be considered. Maximum reinforcement inequalities will also, in many cases, not be introduced for all bar groups.

The linear program (9), simplified as explained, will be solved in core by the simplex algorithm. It should also be noted, that the designer, as explained later, will be able during the design process to introduce or to delete any A- or X-variable and any linear inequality constraint he wishes. The computer will then have to solve each time the modified linear program starting from the previous solution.

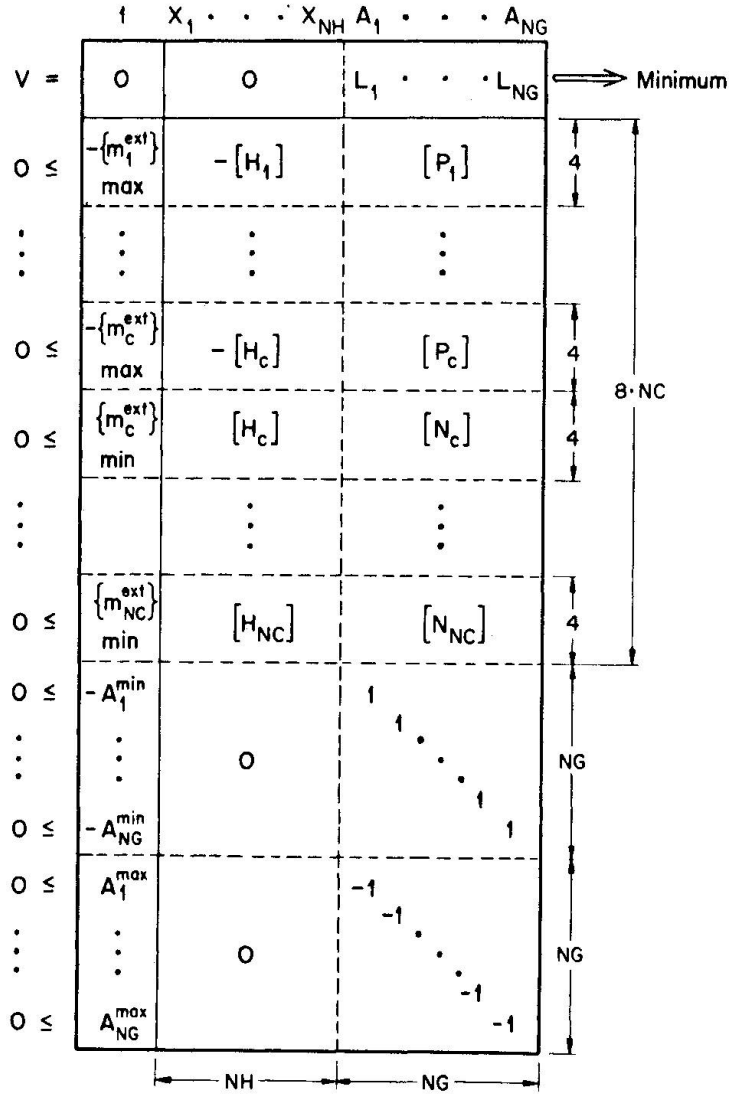

Fig. 1: Tableau form of the linear program (9)

4. INTERACTIVE DESIGN PROCEDURE

In a first step the designer has to specify, as usual in finite element analysis, all structural and load data necessary to determine the moment-envelopes in all possible check-points, i.e. in all joints and in the center of all elements. These values as well as the data needed for analysing the additional homogeneous load cases to be specified later (local load vectors for three unit initial curvatures within each element, triangular half-inverse of the global stiffness matrix, etc.) are then saved on secondary storage.

In a second step the following design data have to be specified or, whenever possible, automatically determined by the program:

a) Lengths,positions and directions of all groups of reinforcement steel bars covering rectangular or parallelogram-shaped portions of the slab. Net reinforcements with steel bars in two orthogonal directions as well as bar groups of identical cross-sectional area but covering two or more distinct portions of the slab can also be specified.
b) Minimum and maximum allowable reinforcement for any bar group.
c) Criteria for determining which of the eight possible linear plasticity conditions have to be considered in any check-point. In most cases the program will be able to determine these automatically by examining the values of the moment-envelopes due to the external loads.
d) Homogeneous load case informations concerning the direction of unit initial curvatures in one or more elements. If no such load is specified, the slab will be designed assuming no plastic moment redistribution.

With these data the program will be able to determine the linear-elastic moment distributions for the homogeneous load cases, set up the coefficient matrix of the linear program and solve this in core by the simplex algorithm. At the end of this step (as well as at the end of all subsequent steps) the program will check all linear plasticity conditions originally ignored. If any of these is found to be violated, the corresponding inequalities are introduced into the linear program and a modified optimum solution is found.

As these two steps will generally require a considerable amount of computing time, the corresponding program sections will not allow direct interaction with the designer. However, input preparation is made easy by the use of a simple problem-oriented input language described by few easily understandable syntax diagrams (see also [3] and [4]).

Full line by line interaction based on a command language also described by syntax diagrams will be possible in the subsequent design steps. Within each of these the designer will be able to request anyone of the following actions:

a) introduce a new reinforcement bar group or delete an existing one
b) change, add or delete a minimum or maximum reinforcement constraint
c) require a reinforcement area to assume a given value. This may be desirable when the designer choses to use a certain number of steel bars of standard diameter corresponding to a total cross-sectional area not identical to the optimum value found by the linear program.
d) introduce new homogeneous load cases hoping that these will help to further reduce the total steel weight.

Each of these steps implies the addition or the deletion of some variables or some inequality constraints requiring the previous solution to be modified, which, in general, can be done with a relatively little computational effort. The designer can then be informed on the effects of the action he took (change in total steel weight, changes in single reinforcements, plasticity conditions becoming

active, i.e. exactly fulfilled, or inactive, etc.) in order to be able to plane his next design step.

In fact, if the program has to interact in real time with a designer changing at each step his design specifications until a satisfactory and in all respects practicable reinforcement distribution is found, the problem of man - machine communication becomes of crucial importance. Certainly extensive graphical output and possibly some graphical input capabilities have to be incorporated into the program. The designer should be able to see at a glance which parts of the slab are more heavily stressed and which are not. This will help him finding the most favourable position and shape of each reinforcement bar group and also tell him how to assume the homogeneous load cases. These will probably lead to the most favourable moment redistribution when initial curvatures are introduced in the directions and in the elements where moments are large.

It is too early to discuss these points in detail. It should only be mentioned that the graphical capabilities of a storage-tube Tektronix 4014 terminal connected with a DEC-10 computer appear to be adequate for this project.

5. OUTLOOK

Optimum design and interactive computer aided design procedures have attracted and continue to attract much attention and much research work. It is a fact, however, that at least in civil engineering such procedures are today very seldom used for practical purposes. In awareness of this it would be illusory to expect that procedures similar to the one described here will very soon become standard tools of practicing structural engineers. The main scope of our project, which is nevertheless quite an ambitious one, is therefore to assess as clearly as possible for a well defined and actually relatively simple practical optimum design problem the feasibility of the approach.

References

[1] E. Anderheggen, "Optimale Bemessung von Stabtragwerken", Dissertation No. 3710, ETH Zürich, 1966

[2] E. Anderheggen, B. Thürlimann, "Optimum Design using Linear Programming", Abhandlungen IVBH, Vol. 26, 1966.

[3] U. Walder, "Beitrag zur Berechnung von Flächentragwerken nach der Methode der finiten Elemente", Dissertation No. 5961, ETH Zürich, 1977.

[4] E. Anderheggen, D. Green, U. Walder, "Das Computerprogramm FLASH", Abhandlungen IVBH, Band 36-II, 1976.

[5] R. Wolfensberger, "Traglast und optimale Bemessung von Platten", Dissertation No. 3451, ETH Zürich, 1964.

Leere Seite
Blank page
Page vide

III

Finite Element Approach to Optimization of Slab Reinforcement

Optimalisation de l'armature des dalles au moyen de la méthode des éléments finis

Optimierung der Plattenbewehrung mittels finiter Elemente

A. BORKOWSKI
Dr.-Ing.
Institute of Fundamental Technological Research
Warsaw, Poland

SUMMARY
A numerical procedure is presented which enables an optimization of reinforcement to be carried out in the preliminary design of concrete slabs. The method is based upon discretization of the slab by means of triangular finite elements. A rigid-plastic behaviour of the slab is assumed. The reinforcement volume is minimized by linear programming taking into account technological constraints where necessary.

RESUME
La méthode exposée permet d'optimaliser l'armature des dalles en béton dans une phase préliminaire du projet. La méthode s'appuie sur la discrétisation des dalles en éléments finis triangulaires et suppose que le comportement des dalles est rigide-plastique. Le volume de l'armature est minimisé par programmation linéaire en tenant compte, si nécessaire, des contraintes d'exécution pour les variables du projet.

ZUSAMMENFASSUNG
Es wird ein numerisches Verfahren beschrieben, durch welches es möglich ist, die Armierung von Betonplatten an einem vorläufigen Entwurf zu optimieren. Die Methode stützt sich auf die Diskretisierung der Betonplatte mit Hilfe von dreieckigen finiten Elementen unter der Annahme von starr-plastischem Verhalten. Das Volumen der Armierung wird durch lineare Programmierung minimiert, wobei herstellungsbedingte Schranken für die Entwurfsvariablen, soweit nötig, in Betracht gezogen werden.

1. INTRODUCTION

The yield-line theory [1] belongs to the most widely used tools of the plastic design. Despite its purely kinematical nature, this method provides, when properly used, a conservative estimate of the reinforcement of concrete slabs. This is due to such effects neglected in the yield-line theory as the steel hardening, arching and membrane action. Each of them is favourable to the safety of design.

It is rather simple to find an adequate collapse mode for a conventionally shaped and loaded plate of an uniform reinforcement. However the primary task of an engineer is rather to look for the most efficient reinforcement pattern than to analyse a given slab. This can be accomplished by means of the finite element method and linear programming as shown in a paper [2]. The aim of the present article is to recall the main features of such approach. As far as discretization is concerned the present method is similar to those proposed by Anderheggen, Knöpfel [3] and Kawai [4].

2. OPTIMUM PLASTIC DESIGN AS LINEAR PROGRAMMING PROBLEM

It is well known that linear programming (LP) is far more numerically efficient than any other method of constrained optimization. Therefore it is natural to try to convert an engineering optimization problem into the shape of the LP-problem. Considering design of reinforced concrete slabs on the ground of the ultimate load theory one has to introduce two main assumptions in order to achieve this goal:

1) the minimized volume of reinforcement should be a linear function of the principal yield moments,

2) the yield surface should be piecewise-linear.

The first assumption means that dependence of the arm of stress couple acting in the yielded cross-section upon the area of reinforcement is neglected. The second one can be regarded as numerical approximation of the true convex yield surface. Of course the consequences of such an approximation for the collapse mechanism must be taken into account.

Let an arbitrary structure be discretized in such a way that its mechanical behaviour is represented by the following vectors: a stress $\underline{s} \in E^m$, strain $\underline{q} \in E^m$, load $\underline{p} \in E^n$, displacement $\underline{w} \in E^n$ and plastic modulus $\underline{c} \in E^k$. Taking into account two basic assumptions listed above one can formulate the optimum design problem as follows:

a) a static approach -

minimize $V = \underline{l}^t \underline{c}$,

subject to:

$$\underline{C}^t \underline{s} = \underline{p}, \qquad (1)$$
$$\underline{G}^t \underline{c} - \underline{N}^t \underline{s} \geqslant \underline{0},$$
$$\underline{c} \geqslant \underline{0};$$

b) a kinematic approach -

maximize $\dot{W} = \underline{p}^t \dot{\underline{w}}$,

subject to:

$$\underline{C}\, \dot{\underline{w}} - \underline{N}\, \dot{\underline{\lambda}} = \underline{0}, \qquad (2)$$
$$\underline{G}\, \dot{\underline{\lambda}} \leqslant \underline{l},$$
$$\dot{\underline{\lambda}} \geqslant \underline{0}.$$

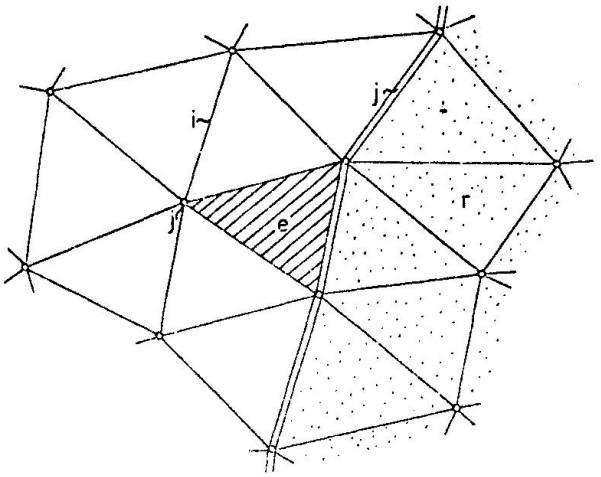

Fig. 1 Finite-element Mesh

A cost function of the primal problem (1) expresses the minimized volume of reinforcement. Here $\underline{l} \in E^k$ is a constant vector of the cost factors. The first constraint in the static approach is the equilibrium equation that relates the stress $\underline{s}$ to the given ultimate load $\underline{p}$. The second one describes a convex polyhedron of admissible stresses. The dual problem (2) reads as a search of the maximum external power over a set of the collapse mechanisms kinematically compatible with the strain rate $\dot{\underline{q}}$ that follows from the associated flow rule:

$$\dot{\underline{q}} = \underline{N}\, \dot{\underline{\lambda}} \,. \qquad (3)$$

The second constraint in (2) is the optimality condition relating the plastic multipliers $\dot{\underline{\lambda}}$ to the cost factors $\underline{l}$. For practical purposes it is advisable to replace the last constraint in (1) by

$$\underline{c}^- \leqslant \underline{c} \leqslant \underline{c}^+ \qquad (4)$$

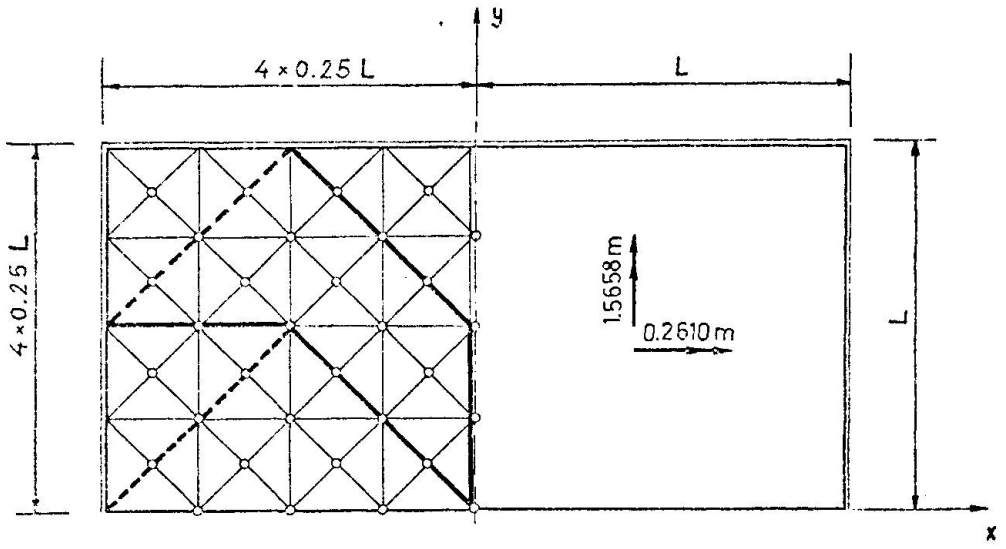

Fig. 2 Rectangular Slab with Free Edge - Optimal Solution for Single Bottom Reinforcement Grid

where $\underline{c}^-$, $\underline{c}^+$ are fixed bounds for the design variable $\underline{c}$. Since the dual problems (1)-(2) are equivalent one can use any one of them as an input for the simplex routine which provides the solution $\underline{c}^*$, $\underline{s}^*$ and $\dot{\underline{w}}^*$, $\dot{\underline{\lambda}}^*$.

3. DISCRETE MODEL OF REINFORCED SLAB

A mesh of triangular finite elements as shown in Figure 1 was chosen for discretization. It was assumed that $\dot{w}$ is linear while the moments M_x, M_y, M_{xy} are constant over an element. The slope discontinuities $\dot{\theta}_j$ along the edges of each triangle are collected into the strain rate vector $\dot{\underline{q}}$. The nodal deflection rates $\dot{w}_j$ enter the vector $\dot{\underline{w}}$. Rational technology requires the reinforcement to be composed from a small number of grids, each of them having a constant mesh and constant diameter of steel rods. Therefore prior to optimization the area of the slab should be divided into a small number of regions of constant principal yield moments. Theoretically a region can include single element but usually there are many elements in it. The adjacent regions are connected via the narrow strips that can rotate independently about their longitudinal axes. The rates of such rotations $\dot{\psi}_j$ are included into $\dot{\underline{w}}$.

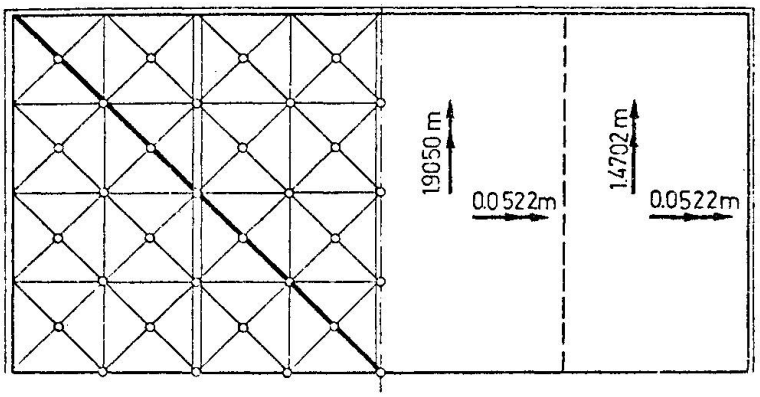

Fig. 3 Rectangular Slab with Free Edge - Optimal Solution for Two Bottom Reinforcing Grids

These connectors provide a continuous slope of the slab along the lines of discontinuity of the yield moment.

In the static description of the slab the entries of $\underline{s}$ are the bending moments M_i acting normal to the edges of triangles. The components of $\underline{p}$ are the nodal forces and the external moments attached to the connecting strips. The vector of design variables $\underline{c}$ collects the principal yield moments for each region. Denoting by x and y the orthogonal directions of reinforcing bars, common for the entire slab, one has four design parameters for a region: the yield moments m_x, m_y for positive bending (bottom reinforcement) and the yield moments m'_x, m'_y for negative bending (top reinforcement). The yield criterion for this discrete model reads: i-th line of the mesh is at the yield when (a) the positive bending moment M_i reaches the ultimate value

$$m_i = m_x \sin^2 \alpha_i + m_y \cos^2 \alpha_i, \qquad (5)$$

or (b) the negative moment reaches the value

$$m'_i = m'_x \sin^2 \alpha_i + m'_y \cos^2 \alpha_i. \qquad (6)$$

Here α_i denotes the angle between i-th line and the x-axis.

The cost factors l_k result from the expression of the reinforcement volume as the linear function of the principal yield moments. Usually these factors are taken proportional to the areas of regions with constant reinforcement. A detailed derivation can be found in [2] as well as the modifications of the model (1)-(2) for the cases of prescribed orthotropy and/or asymmetry of reinforcement.

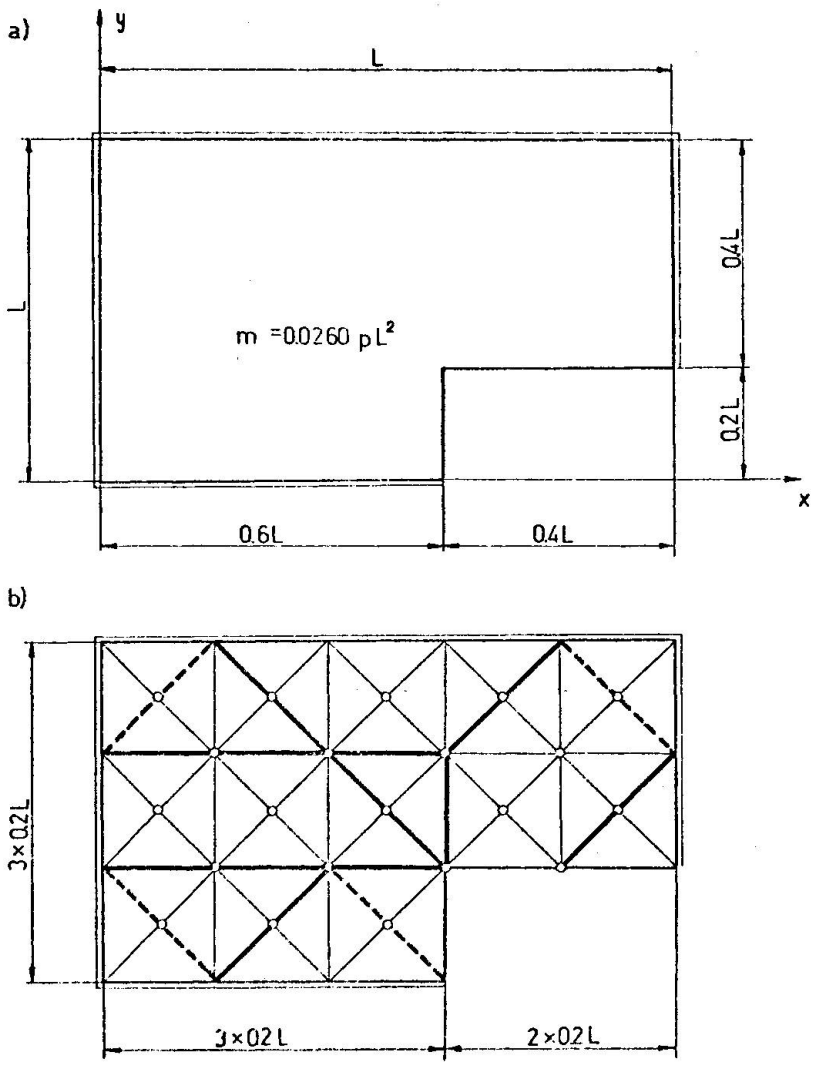

Fig. 4 Simply Supported Slab with Cut-off - Isotropic Reinforcement: a) Dimensions and Yield Moment, b) Discretization Mesh and Collapse Mechanism.

4. NUMERICAL EXAMPLES

The first example (Figure 2) concerns the rectangular slab with three edges simply supported and the fourth edge free. The following optimum values of the principal yield moments were obtained for a single bottom reinforcement grid:

$$m_x^* = 0.30\ pL^2 \qquad m_y^* = 0.05\ pL^2 \qquad (7)$$

Here p denotes the transversal pressure and L is the length of the shorter edge of the slab. The optimum orthotropy factor is

$$\mu^* = m_y^*/m_x^* = 0.1667 \qquad (8)$$

The volume of reinforcement for this design is 8 % less as compared to the isotropic plate.

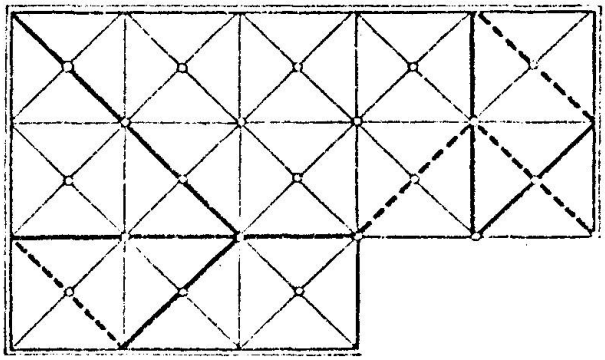

Fig. 5 Simply Supported Slab with Cut-off - Discretization Mesh and Collapse Mechanism for Optimum Orthotropy

The second example (Figure 3) shows the optimum solution for the same slab but having two reinforcement grids. It was assumed additionally that for technological reasons the yield moment should not be less than $0.01\ pL^2$. The optimum values of the principal yield moments are:

for the central region: $m_x^* = 0.365\ pL^2$, $m_y^* = 0.01\ pL^2$ (9)

for the outer region: $m_x^* = 0.282\ pL^2$, $m_y^* = 0.01\ pL^2$ (10)

This solution reduces the reinforcement volume by 13 % in comparison to the isotropic case. Finally Figures 4 and 5 show the results for a slab with cut-off. The solution for isotropic case is depicted in Figure 4 while the optimum values

$$m_x^* = 0.667 \times 10^{-2}\ pL^2, \quad m_y^* = 3.85 \times 10^{-2}\ pL^2 \qquad (11)$$

correspond to the collapse mechanism shown in Figure 5.

5. CONCLUSIONS

The computer based version of the yield-line method offers a cheap tool for preliminary design of slabs. Computational effectiveness of the algorithm makes it possible to run several trial optimizations with differently chosen reinforcement patterns. After a final choice has been made on the ground of the rigid-plastic approach, one has to check whether other requirements, such as a sufficient stiffness and crack resistance, are met. The final design can be recalculated by the present method in order to establish its safety factor against plastic collapse.

ACKNOWLEDGMENT

Present research was conducted partly during the stay at the Institute of Statics and Dynamics of Aeronautical and Space Structures, the University of Stuttgart under the sponsorship of the Alexander von Humboldt Foundation which is gratefully acknowledged.

REFERENCES

1. JOHANSEN, K.W.: Yield-line Theory, Cement and Concrete Association, 1962

2. BORKOWSKI, A.: Optimization of Slab Reinforcement by Linear Programming, Comp. Meths. Appl. Mech. Engng., 12 (1977) 1-17

3. ANDERHEGGEN, E. and KNÖPFEL, H.: Finite Element Limit Analysis Using Linear Programming, Int. J. Sols. Structs., 8 (1972) 1413 -1431

4. KAWAI, T.: New Discrete Structural Models and Generalization of the Method of Limit Analysis, Proc. Int. Conf. on Finite Elements in Non-linear Solid and Structural Mechanics, Geilo, Norway, 1977

On the Load-Carrying Capacity of Concrete Pavements

Jiang Da-hua

(Tong Ji University, Shanghai)

The load-carrying capacity of concrete pavement under central load is investigated. The pavement is treated as a rigid-plastic slab of infinitely large size resting on an elastic subgrade. Under the action of a concentrated load over a small circular area the subgrade reaction is represented by a conical diagram and its variation with displacement is neglected. The same problem was solved by G. G. Meyerhof in the early 60's when he was studying the carrying capacity of concrete pavement under wheel loads. His formulae for central loads are actually upper bound solutions. The exact solution under the above mentioned assumptions is obtained in which the position of the circular yield line is somewhere inside the circle of zero subgrade reaction.

The ultimate load can be expressed as follows

$$P_0 = \frac{4\pi M_0}{1 - \frac{2}{3}\frac{a}{b}\left(\frac{b}{c}\right) - \left(\frac{c}{b}\right)^2 + \frac{1}{2}\left(\frac{c}{b}\right)^3}$$

in which the value of $\frac{c}{b}$ can be determined from the equation

$$4\frac{a}{b} - 12\left(\frac{c}{b}\right)^3 + 9\left(\frac{c}{b}\right)^4 = 0$$

M_0 is the ultimate moment of the slab section, a, b and c being the radius of the circle of the loaded area, of zero subgrade reaction and of the circular yield line respectively.

Ultimate loads for dual, triple and quadriple circular loads and a strip load are also investigated.

The moment curvature relation of a plain concrete section is deduced by considering the existance of horizontal axial thrust in the slab and the gradual cracking of the section. It is interesting to note that the moment curvature relation thus obtained is practically of elasto-plastic type.

The theoretical analysis is simple, and it explains why full redistribution of internal forces to form a collapse mechanism is possible in a large plain concrete pavement as has been observed in the experiments carried out in China in recent years.

DEFORMATION CAPACITY IN REINFORCED CONCRETE SLABS

Peter Lenkei Hungarian Institute for Building Science (ÉTI) Budapest

Summary

In reinforced concrete slabs at yielding not only the load bearing capacity but the deformations and the cracking process too are greatly influenced by the level of orthotropy and by the divergence in the principal directions of the resistance of the slab and of the external moments. The theoretical and experimental investigations proved that this fact should in some cases be taken into account.

Experimental investigations

Rectangular slabs with fixed corners and with different levels of orthotropy were tested in the Laboratory of the Hungarian Institute for Building Science (ÉTI, Budapest). The details of the test specimens are given in Fig. 3.

The difference in the amounts of reinforcement and in the level of orthotropy altered the load bearing capacity and the yield pattern in the corners of the slabs. Of course in the middle part of the slabs the angle Ψ was equal to zero, but in the corners Ψ differed considerably from zero.

Due to these differences, the behaviour of the slabs during the transition process, the deformations and the crack pattern at the maximum load (at yielding) were different (Fig. 4).

References

1. Sawczuk A., Jeager Th.: Grenztragfähigkeitstheorie der Platten. Springer, Berlin. 1963.

2. Gvozdev A.A.: On the question of limit conditions (yield conditions) of orthotropic solids and reinforced concrete slabs. (In Russian) Anniversary Collection of papers in honour of the 80th birthday of Prof. J.M. Rabinovich, Moscow 1966. Pp. 208-212.

3. Lenkei P.: On the yield condition for reinforced concrete slabs. Archiwum Inzynierii Ladovej, T. XIII. Fasc 1/1967, pp. 5-11.

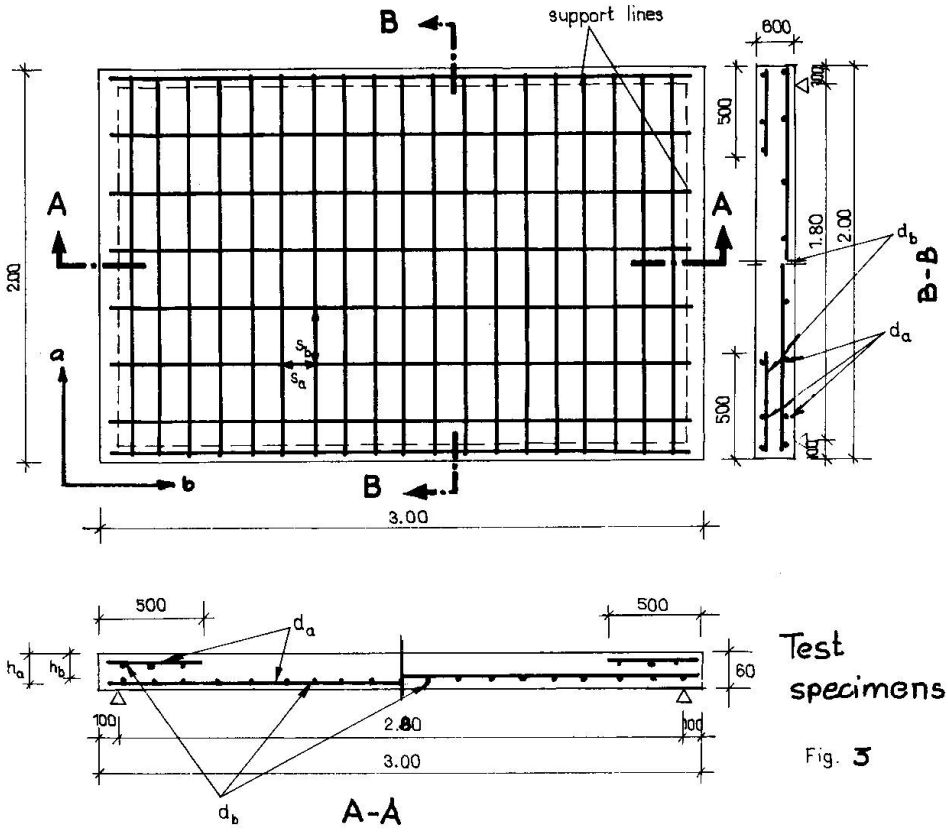

Test specimens

Fig. 3

Reinforcement data (design values)

Slab type and number		s_a mm	s_b mm	d_a mm	d_b mm	A_a mm²/m	A_b mm²/m	h_a mm	h_b mm	ϱ_a %	ϱ_b %	$\frac{\varrho_a}{\varrho_b}\lambda^2$
1	1/1	150	200	4.2	4.2	69	92	47.9	43.7	0,144	0.210	0.686
	1/2											
2	2/1	150	300	4.2	4.2	46	92	47.9	43.7	0.096	0.210	0.457
	2/3							43.7	47.9	0.158	0.144	1.097
3	3/1	200	200	4.2	4.2	69	69	47.9	43.7	0.144	0.158	0.911
	3/2											
	3/3											
4	4/2	100	300	4.2	7.6	46	454	40.3	46.2	0.114	0.987	0.116
5	5/1	100	150	4.2	7.6	92	454	40.3	46.2	0.228	0.987	0.231
	5/2											
	5/3											

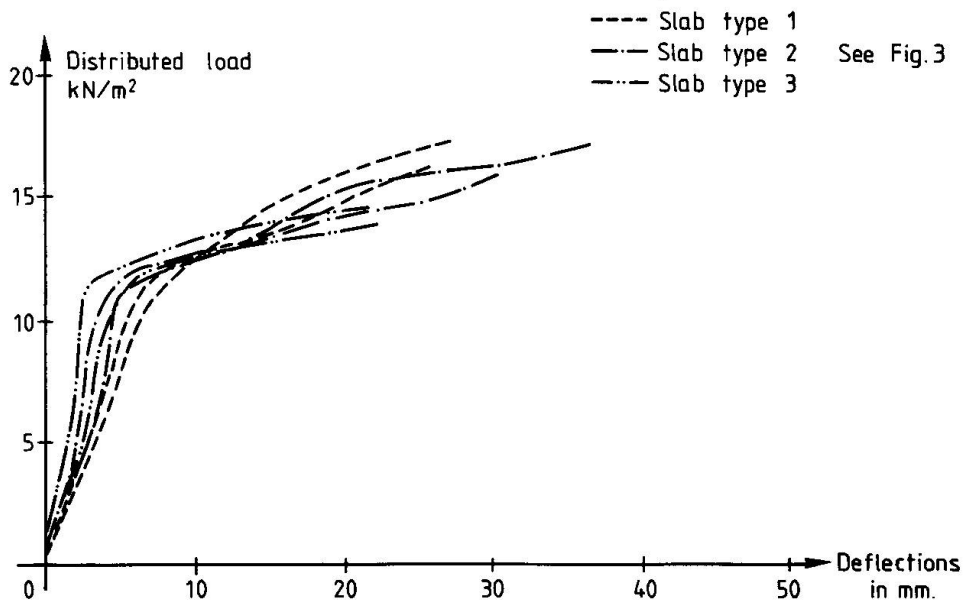

Fig. 4. Deformations of Slabs

Punching of Slabs subjected to In-plane Biaxial Tension

R.P. JOHNSON, University of Warwick, England

The punching shear strength of slabs subjected to in-plane biaxial tension is of interest to designers, because this situation can occur in continuous composite steel-concrete bridge decks in regions where a cantilever cross girder intersects a main girder near an internal support, and the neutral axes for bending of the two composite members lie many slab thicknesses below the deck.

Such a region has been studied at the University of Warwick in tests on cruciform specimens composed of two intersecting composite girders, supported at the centre of the cross and subjected to downwards point forces at the ends of the arms. Control of these forces enabled known biaxial tensile strains to be maintained at the top surface of the slab, which was 90 mm thick. There were four layers of reinforcement (8 and 12 mm bars at 150 or 200 mm pitch). The tensile strains at the underside of the slab were about 80% of those at the top surface.

Punching shear tests were done on three quadrants of the same cruciform slab, while the mean tensile strains in the top two layers of reinforcement were 0, 860 and 1730 microstrain, respectively. The corresponding punching loads were 164, 162, and 163 kN. The punch diameter was 120 mm, and the maximum diameter of the punched-out area was about 850 mm (limited by the flanges of the steel girders), giving a mean slope of 14° for the surfaces on which failure occurred.

These results confirm what can be deduced from the upper bound analysis presented by M.P. Braestrup: that membrane tensile strain in a slab has no effect on its strength in punching shear, in the range of strains likely to occur in practice.

DISCUSSION ON POST-PLASTIC BEHAVIOUR OF RESTRAINED SLABS

by I. KANITAKIS, Research Fellow, N.T.U.- Athens

Prof. T.P. Tassios and myself would like to present some very first results of a theoretical investigation related to the problem of post plastic behaviour of Reinforced Concrete slabs, rigidly connected at their ends.

Each span is assumed to be fixed-ended and without any lateral displacement. The slab has equal compression and tension reinforcement along its length. The gradual modification of the bearing mechanisms of the slab are considered qualitatively, through three consecutive models.

The first model is the conventional elastoplastic model. Here, moment redistribution is also considered and the values of the stiffness along the span are variable. There is no axial force in the slab.

The second model is the post plastic one (fig.1). The slab geometry has significantly changed (compressive membrane) contributing to a considerable increase of the ultimate load capacity of the slab. (Negative axial force N).

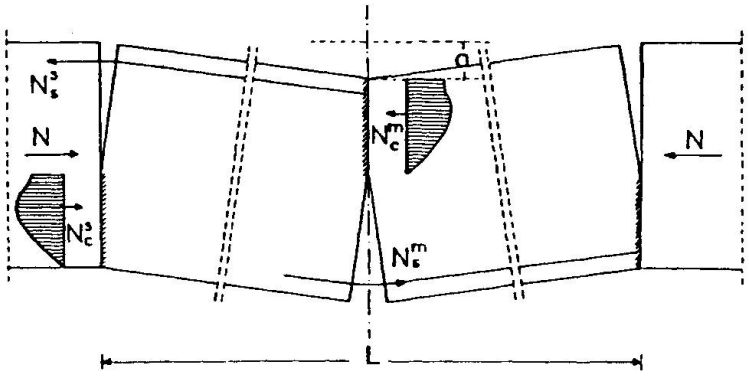

fig.1

The third model is the catenary one, where concrete in critical sections is destroyed and only the steel can carry some load. (Positive axial force N).

The load versus mid-span deflection curve for a slab 120 mm thick and with a percentage of reinforcement of 0.318% is shown in Fig.2. Branch OA is due to the elastoplastic model. Branch AB is due to the post plastic model and branch BC is due to the catenary model. The dotted line in fig.2 shows a more smooth transition curve which should be worked out and theoretically located.

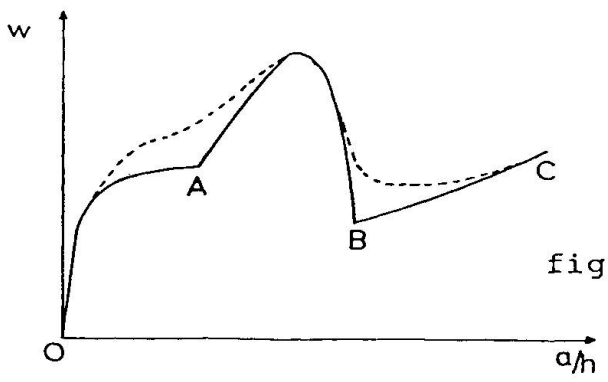

fig.2

Leere Seite
Blank page
Page vide

SUMMARY OF DISCUSSION - SESSION 3

Ch. Massonnet opened the discussion by questioning the validity of the square yield locus used by M.P. Nielsen for moments (Introductory Lecture, Fig. 3.3.2). He cited test results pointing to the effect of reinforcement kinking, leading to a concave yield locus with sharp corners.

M.P. Nielsen replied that he had never been convinced by the Liège tests, the reinforcement arrangement being rather complicated. He would study some of the other tests cited, which he had not previously come across. He pointed out that numerous Danish tests on slabs in pure torsion (upper left hand corner of Fig. 3.3.2) showed no increase in strength compared with biaxial bending. In the case of isotropic bending (upper right hand corner) there might be some strength enhancement due to biaxial compression of the concrete, but this is believed to be an effect of secondary importance.

Ch. Massonnet further remarked to D.H. Clyde that he found it hard to believe in the statical equivalence of twisting moments and shear forces.

D.H. Clyde pointed out that the sandhill analogy for pure torsion also predicts forces at the edges of the slabs.

Z. Sobotka presented a method of controlling the yield line pattern by varying the ratio between top and bottom reinforcement in such a way that excessive cracking in the service state is avoided.

P. Marti commented on D.H. Clyde's paper by citing a recent investigation of pure torsion in slabs and beams, using the modified contours criterion with zero tensile strength and an angle of friction of 37°. Lower bound solutions corresponding to statically admissible stress fields were derived, and matching kinematically admissible velocity fields found except for small corner regions. The analysis shows that:

- the concrete crushes in a compressed shell around the periphery of the cross-section
- the compressed shell separates from the stress-free control region
- if there are twisting moments at an edge of a slab, a vertical reinforcement is necessary to connect the top and bottom reinforcement along the edge.

A. Sawczuk asked M.P. Nielsen about needed research in connexion with membrane effects, and commented with regard to K. Sonoda's contribution that it was difficult for the computer to distinguish between elastic unloading and the falling branch of the stress-strain curve. He further requested more information from D.H. Jiang concerning the interaction between slab and subgrade.

M.P. Nielsen replied that he had mentioned the membrane effect mainly to stress its importance in practical applications, but that a theory is still lacking.

Da Hua Jiang explained that the response of the subgrade was measured by load cells, and the pressure subsequently idealized to a conical distribution, as indicated. In answer to a question from A. Losberg, Da Hua Jiang stressed that only unreinforced slabs were considered.

Most of the second discussion period was devoted to problems concerning punching shear.

R.P. Johnson mentioned that we would expect the punching strength to be considerably reduced in the presence of membrane forces, especially in the case of biaxial tension. However, tests carried out had shown no such effect. From the audience it was remarked that similar results had been obtained at Ithaca.

A. Losbey was surprised that the analyses presented by M.W. Braestrup did not take account of the main reinforcement, and he wanted to know if the dowel effect had been investigated.

M.W. Braestrup explained that the analysis only considered the strength in a proper punching failure, which is independent of any membrane forces or main reinforcement. Another point is that the likelihood of such a failure will be strongly affected by these factors. He did not believe there was any significant dowel effect; the reinforcement is of itself very flexible so the only source of dowel action is the tensile concrete strength, which is too small to measure.

M. Reiss remarked that in practical cases of punching, the load is often applied by a column, monolithically connected to the slabs. The boundary conditions at the edge of the column would then be different from those considered by M.W. Braestrup, the shear force being transferred at the tip of a wedge (cf. Fig. 4 of the Introductory Lecture). Therefore tests show that the failure surface generatrix starts perpendicularly in the slab and is not inclined as shown in Fig. 1.

H. Aschl claimed that we all know that tensile concrete stresses are necessary to carry shear loads. On the other hand, the paper presented on plastic analysis showed that good agreement with test results is only obtained assuming zero tensile strength. How do we reconcile these facts?

M.W. Braestrup replied that in most cases the shear failure is constrained by main reinforcement or by the surrounding structure, in such a way that failure cannot occur by separation only. Thus the deformation must include some sliding, in which case the compressive strength of the concrete is mobilised and a tensile strength is not necessary.

M.P. Nielsen showed how shear in beams and slabs may be carried by inclined compression without any need for tensile stresses.

M.W. BRAESTRUP